

1. Report No. FHWA/TX-90/1182-1		2. Government Accession No.		3. Recipient's Catalog No.	
4. Title and Subtitle Effects of Banded Post-Tensioning in a Prestressed Concrete Flat Slab				5. Report Date June 1990 REVISED	
				6. Performing Organization Code	
7. Author(s) Roschke, P.N., and Inoue, M.				8. Performing Organization Report No. Research Report 1182-1	
9. Performing Organization Name and Address Texas Transportation Institute The Texas A&M University System College Station, Texas 77843-3135				10. Work Unit No.	
				11. Contract or Grant No. Study No. 2-5-88-1182	
12. Sponsoring Agency Name and Address Texas State Department of Highways and Public Transportation: Transportation Planning Division P.O. Box 5051 Austin, Texas 78763				13. Type of Report and Period Covered Final - September 1987 June 1990	
				14. Sponsoring Agency Code	
15. Supplementary Notes Research performed in cooperation with DOT FHWA. Research Study Title: Evaluation of Factors Affecting Slabs Due to Localized Post-Tension Forces.					
16. Abstract <p>A new class of flat slab concrete bridges employs bidirectional post-tensioning. While longitudinal post-tensioning is uniform, transverse tendons are concentrated in the vicinity of column lines to act as bentcap-like supports. For multispan structures, transverse post-tensioning is limited to a series of narrow banded regions. This report, first in a series, documents displacement, strain, stress, and punch-through shear capacity of a 3/10ths scale model of a column and slab region of a prototype bridge. Concomitant efforts are underway on a large two-span laboratory bridge model, a field study of a full-size bridge, and a numerical simulation package.</p> <p>The current study investigates degree of validity of a design procedure for a column region of a prototype bridge. Construction, instrumentation, testing, and numerical simulation are described for the concrete model slab. A loading schedule enables stress distribution determination for a variety of tendon and load patterns. The number of stressed tendons varies from one to nine. Results of a large number of transducer readings and finite element simulations are presented via fringe plots, tables, and graphs. Finally, the slab is loaded by a specially fabricated load frame and the circular support column so as to impose punch-through shear failure. A brittle failure at 207 kips (923 kN) is followed by reserve capacity at 111 kips (496 kN) which collapsed the slab. Shear formulas recommended by the American Association of State Highway and Transportation Officials, American Concrete Institute, and other researchers are compared with experimental failure and reserve capacity loads.</p>					
17. Key Words Bridges, failure, finite elements, plate, prestressing, shear, slab, strain			18. Distribution Statement No restriction. This document is available to the public through the National Technical Information Service. 5285 Port Royal RD. Springfield, Virginia 22161		
19. Security Classif. (of this report) Unclassified		20. Security Classif. (of this page) Unclassified		21. No. of Pages 134	22. Price

**EFFECTS OF BANDED POST-TENSIONING
IN A PRESTRESSED CONCRETE FLAT SLAB**

by

Paul N. Roschke
Assistant Research Engineer

and

Masamichi Inoue
Graduate Research Assistant

Research Report 1182-1

on

Evaluation of Factors Affecting Slabs Due to Localized Post-Tension Forces

Research Study No. 2-5-88-1182

Sponsored by

Texas State Department of Highways and Public Transportation

in cooperation with

The United States Department of Transportation

Federal Highway Administration

June 1990

Texas Transportation Institute

The Texas A&M University System

College Station, Texas 77843-3135

METRIC (SI*) CONVERSION FACTORS

APPROXIMATE CONVERSIONS TO SI UNITS

Symbol	When You Know	Multiply By	To Find	Symbol
LENGTH				
in	inches	2.54	centimetres	cm
ft	feet	0.3048	metres	m
yd	yards	0.914	metres	m
mi	miles	1.61	kilometres	km

AREA				
in ²	square inches	645.2	centimetres squared	cm ²
ft ²	square feet	0.0929	metres squared	m ²
yd ²	square yards	0.836	metres squared	m ²
mi ²	square miles	2.59	kilometres squared	km ²
ac	acres	0.395	hectares	ha

MASS (weight)				
oz	ounces	28.35	grams	g
lb	pounds	0.454	kilograms	kg
T	short tons (2000 lb)	0.907	megagrams	Mg

VOLUME				
fl oz	fluid ounces	29.57	millilitres	mL
gal	gallons	3.785	litres	L
ft ³	cubic feet	0.0328	metres cubed	m ³
yd ³	cubic yards	0.0765	metres cubed	m ³

NOTE: Volumes greater than 1000 L shall be shown in m³.

TEMPERATURE (exact)

°F	Fahrenheit temperature	5/9 (after subtracting 32)	Celsius temperature	°C
----	------------------------	----------------------------	---------------------	----

APPROXIMATE CONVERSIONS TO SI UNITS

Symbol	When You Know	Multiply By	To Find	Symbol
LENGTH				
mm	millimetres	0.039	inches	in
m	metres	3.28	feet	ft
m	metres	1.09	yards	yd
km	kilometres	0.621	miles	mi

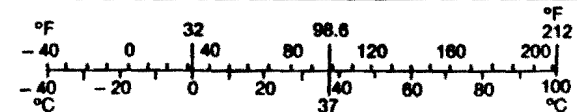
AREA				
mm ²	millimetres squared	0.0016	square inches	in ²
m ²	metres squared	10.764	square feet	ft ²
km ²	kilometres squared	0.39	square miles	mi ²
ha	hectares (10 000 m ²)	2.53	acres	ac

MASS (weight)				
g	grams	0.0353	ounces	oz
kg	kilograms	2.205	pounds	lb
Mg	megagrams (1 000 kg)	1.103	short tons	T

VOLUME				
mL	millilitres	0.034	fluid ounces	fl oz
L	litres	0.264	gallons	gal
m ³	metres cubed	35.315	cubic feet	ft ³
m ³	metres cubed	1.308	cubic yards	yd ³

TEMPERATURE (exact)

°C	Celsius temperature	9/5 (then add 32)	Fahrenheit temperature	°F
----	---------------------	-------------------	------------------------	----



These factors conform to the requirement of FHWA Order 5190.1A.

* SI is the symbol for the International System of Measurements

ABSTRACT

This study investigates strain distribution in regions immediately adjacent to the transverse post-tensioning bands in a new class of flat slab reinforced concrete bridges employing bidirectional post-tensioning. While longitudinal post-tensioning is uniform, transverse tendons are concentrated in the vicinity of column lines. The currently applied design assumes that the transverse post-tensioning effect spreads along straight lines at a specified angle.

Size of a laboratory model slab is chosen so that this assumption may be checked for validity. Strain in the model is measured by strain gages attached in pairs to reinforcement bars. With a known stress-strain relation of concrete, the pairing allows determination of internal force and moment resultants. Deflections and loading forces are measured by an array of linear variable differential transformers (LVDTs) and load cells, respectively. A load schedule is used to study strain distribution for a variety of tendon and load patterns. Three load patterns are applied for each tendon set in which the number of stressed tendons varies from one to nine. Effects of the number of tendons and loads on the strain is discussed, with emphasis on the distribution of the in-plane strain.

Each load case is simulated with a finite element analysis. Numerical strains are calculated and compared to actual data collected. Reasonably good correlation between laboratory data and the computer program allows increased confidence in numerical simulation. Predictions based on the current design method do not always match laboratory or numerical results. An equation based on theory of elasticity yields substantially better results than the current design method.

Following testing and analysis of elastic loads, the slab is loaded to impose a punch-through shear failure. A brittle failure mode at 207 kips (923 kN) is followed by a reserve capacity at 111 kips (496 kN), which collapsed the slab. Shear formulas recommended by the American Association of State Highway and Transportation Officials, American Concrete Institute, and other researchers are compared with experimental failure and reserve capacity loads.

DISCLAIMER

The contents of this report reflect the views of the authors who are responsible for the opinions, findings, and conclusions presented herein. The contents do not necessarily reflect the official views or policies of the Texas State Department of Highways and Public Transportation. This report does not constitute a standard, specification, or regulation.

KEY WORDS

Bridge, Column, Computer, Failure, Finite-Element, Plate, Prestressing, Shear, Slab, Strain, Stress

ACKNOWLEDGMENTS

This study was conducted as part of an ongoing research project under contract with the Texas State Department of Highways and Public Transportation. The opinions expressed herein are strictly those of the researcher, and do not necessarily reflect the official view, policy or opinions on the part of the Texas State Department of Highways and Public Transportation, Texas Transportation Institute, nor Texas A&M University.

IMPLEMENTATION STATEMENT

Results of this study are preliminary in that only a region of a bridge slab which surrounds a column has been tested. Interaction effects of multiple columns and structural effects from the entire slab are not included. A complementary study is in progress on a large laboratory model and a field study of a newly constructed bridge. While the current report is primarily concerned with localized behavior in the column region, the additional study components are expected to add important information related to overall bridge design and behavior.

TABLE OF CONTENTS

	<i>Page</i>
ABSTRACT	iv
DISCLAIMER	v
ACKNOWLEDGEMENTS	v
IMPLEMENTATION STATEMENT	vi
LIST OF FIGURES	ix
LIST OF TABLES	xi
I. INTRODUCTION	1
1.1 Current State of Art	4
1.2 Review of Literature	6
1.3 Problem Identification	9
II. MODEL ONE	11
2.1 Justification for Size and Three-Tenths Scale	11
2.2 Calculation of Ultimate Load	13
2.3 Scale Factors	16
2.4 Reinforcement Bars	18
2.5 Longitudinal Tendons	20
2.6 Transverse Tendons	23
2.7 Concrete	24
2.8 Pedestal	25
2.9 Pickup Points and Safety Cables	27
2.10 Construction Procedure	30
2.11 Instrumentation	32
2.12 Elastic Loading Procedures	37
III. COMPUTER SIMULATION	40
IV. RESULTS OF LINEAR ELASTIC LOAD TESTING	43
4.1 Deflection of Laboratory Model	43
4.2 Strains of Transverse Tendons and Elastic Loading	43
4.3 Internal Moment	51
4.4 Discussion of Computer Predictions and Laboratory Data	53
4.5 Elasticity Predictions	67

	<i>Page</i>
V. ULTIMATE LOAD TESTING	69
5.1 Model Location and Overhead Load Frame	70
5.2 Ultimate Loading	71
5.3 Discussion of Ultimate Load	74
VI. CONCLUSIONS	81
VII. REFERENCES	83
APPENDICES	85
I. - NOTATION	85
II. - ELASTICITY PROGRAM	87
III. - TABLES OF ELASTIC LOADING RESULTS	88
IV. - PARTIAL LIST OF SAMPLE INPUT FILE FOR NOPARC	108
V. - PARTIAL LIST OF SAMPLE OUTPUT FILE FOR NOPARC	112

LIST OF FIGURES

<i>Figure</i>		<i>Page</i>
1.	Slab Bridge Schematic	2
2.	Taft Boulevard Bridge	3
3.	Current Assumption of Effective Prestressing Region	5
4.	Critical Diameter of Two-Way Shear	6
5.	Model One	10
6.	Tendon Pattern	12
7.	Formwork for Model One	12
8.	Reinforcement Pattern	20
9.	Longitudinal Tendon Anchor	21
10.	Transverse Tendon Anchor	24
11.	Safety Cables	28
12.	Pickup Point	29
13.	Longitudinal Tendon Duct	30
14.	Result of Concrete Cylinder Tests	31
15.	Loading Square	33
16.	Transverse Tendon Jacking	34
17.	Installed Strain Gages	35
18.	Strain Gage Locations	35
19.	Installed LVDTs	36
20.	LVDT Locations	36
21.	Data Acquisition Schematic	38
22.	Elastic Loading Schedule	38
23.	Finite Element Model	41
24.	Strains with Longitudinal Tendons before Placement on Column	44
25.	Strains with No Transverse Tendon	45
26.	Strains with One Transverse Tendon	46
27.	Strains with Three Transverse Tendons	47
28.	Strains with Five Transverse Tendons	48
29.	Strains with Seven Transverse Tendons	49

<i>Figure</i>	<i>Page</i>
30. Strains with Nine Transverse Tendons	50
31. Stress Block for Moment Computation	51
32. Mid-Plane Transverse Strain with No Transverse Tendon	54
33. Mid-Plane Transverse Strain with One Transverse Tendon	55
34. Mid-Plane Transverse Strain with Three Transverse Tendons	56
35. Mid-Plane Transverse Strain with Five Transverse Tendons	57
36. Mid-Plane Transverse Strain with Seven Transverse Tendons	58
37. Mid-Plane Transverse Strain with Nine Transverse Tendons	59
38. Assumed Distribution Pattern of Transverse Strain along Center Line of Slab	61
39. Transverse Normal Strain Predictions at Center of Slab with Varying Number of Tendons	62
40. Comparison of SDHPT and NOPARC Transverse Strain Predictions	64
41. Transverse Strains	65
42. Percentage Difference between SDHPT Method and NOPARC Prediction	66
43. Loading Pattern for Elasticity Equation	68
44. Load Frame with Two Actuators	70
45. Load Frame with Four Actuators	71
46. Model Location below Two Beams	72
47. Loading Frame and Load Cells Approximating Circular Line Load	73
48. Differential Strains under 50-kip Load	73
49. Neoprene Pad at Column Capital	75
50. Crack Propagation	76
51. Failure Pattern of the Slab	77
52. Differential Strains during Ultimate Testing	78
53. Corner Displacement during Ultimate Testing	79

LIST OF TABLES

<i>Table</i>		<i>Page</i>
1.	Scale Factors	17
2.	Comparison of Prototype, True Model, and Model One	19
3.	SDHPT and NOPARC Predictions of Stress and Strain Distribution	62
4.	Comparison of Predicted Failure Loads	80
5.	Laboratory and Computer Predicted Strain and Moment before Hoisting	88
6.	Laboratory and Computer Predicted Strain and Moment under Load 0.1	89
7.	Laboratory and Computer Predicted Strain and Moment under Load 0.2	90
8.	Laboratory and Computer Predicted Strain and Moment under Load 0.3	91
9.	Laboratory and Computer Predicted Strain and Moment under Load 1.1	92
10.	Laboratory and Computer Predicted Strain and Moment under Load 1.2	93
11.	Laboratory and Computer Predicted Strain and Moment under Load 1.3	94
12.	Laboratory and Computer Predicted Strain and Moment under Load 3.1	95
13.	Laboratory and Computer Predicted Strain and Moment under Load 3.2	96
14.	Laboratory and Computer Predicted Strain and Moment under Load 3.3	97
15.	Laboratory and Computer Predicted Strain and Moment under Load 5.1	98
16.	Laboratory and Computer Predicted Strain and Moment under Load 5.2	99
17.	Laboratory and Computer Predicted Strain and Moment under Load 5.3	100
18.	Laboratory and Computer Predicted Strain and Moment under Load 7.1	101

<i>Table</i>	<i>Page</i>
19. Laboratory and Computer Predicted Strain and Moment under Load 7.2	102
20. Laboratory and Computer Predicted Strain and Moment under Load 7.3	103
21. Laboratory and Computer Predicted Strain and Moment under Load 9.1	104
22. Laboratory and Computer Predicted Strain and Moment under Load 9.2	105
23. Laboratory and Computer Predicted Strain and Moment under Load 9.3	106
24. Laboratory and Computer Predicted Differential Strain and Moment under 50-kip Load	107

I. INTRODUCTION

Overall thickness of today's low-profile concrete slab bridges is being reduced due to availability of higher strength concrete and demand for maximum overhead clearance. Elimination of concrete girders minimizes thickness of short-span highway structures, which adds to clearance for traffic below without increasing elevation of the overpass. Likewise, omission of girders necessitates alternate forms of design, such as longitudinal slab prestressing.

Prestressed concrete uses high-strength steel and concrete, thereby taking advantage of materials with superior qualities. Such design needs smaller quantities of materials than conventionally reinforced concrete. The lighter weight is attractive for long-span girders and bridges where the dead load is dominant. Although higher-strength material costs more than equivalent lower-strength quantities, benefits from increase in strength far exceed increase in cost.

In addition, the entire section of a prestressed concrete member resists bending moment, while only the smaller uncracked portion of a conventional reinforced concrete section is effective. Since prestressed concrete tends to close surface cracks, protection of steel against corrosion in aggressive environments is improved over that of conventional reinforced concrete. Finally, prestressed concrete has better shear resistance than reinforced concrete. This is due to the prestress compression which reduces diagonal tension. Thus prestressed members require fewer stirrups.

These attributes are appealing for highway bridge design. The Texas State Department of Highways and Public Transportation (SDHPT) has developed a new class of bridges which capitalize on these advantages. In post-tensioned slab bridges designed by SDHPT, prestressing allows a thinner, and therefore lighter, design that is aesthetically pleasing as well as effective in reducing dead load. This results in reduced material quantity and cost. Because of wider availability of high-strength concrete today, the cost increase associated with the use of such concrete is minimal. Protection against corrosion is an asset, since SDHPT design philosophy emphasizes the importance of preventing corrosion to such an extent that epoxy-coated re-bars are specified for the top mat of reinforcing steel (Cox 1985) in locations where de-icing salt may be used. Finally, effective control of deflection is a desirable trait to design engineers, since it improves driving comfort and maintains required vertical clearance.

Further reduction of overall thickness, simpler construction, and more effective use of prestressed concrete is possible through elimination of bent caps at the column line. Required flexural strength over columns is obtained by post-tensioning in the transverse direction. With such a bridge, the slab rests directly on columns and is not tied to them with extensive reinforcing steel. Only a single straight, dowel bar extends from the center of each column through a neoprene bearing pad and into the slab. No other steel reinforcement connects the slab and column.

Current design philosophy calls for increased strength in the transverse direction only near column lines. Post-tensioning is limited to these regions as shown in Fig. 1. In what follows, the term "banded post-tensioning" refers to prestressing in limited, band-shaped regions. Elimination of bent caps and concrete girders allows a simple architectural design, which is not only structurally effective but also aesthetically pleasing (Figs. 1, 2) and also economical for certain span lengths. This approach forgoes several construction phases and details associated with bent caps and facilitates simpler and more rapid construction.

Due to concrete compression, diagonal tension is reduced, and the tendency of a punch-through shear failure for a slab-on-column structure is lessened (Naaman 1982). In fact, by current design, these bridges lack stirrups and rely entirely on slab thickness for shear capacity. One of the most common failure modes of plate

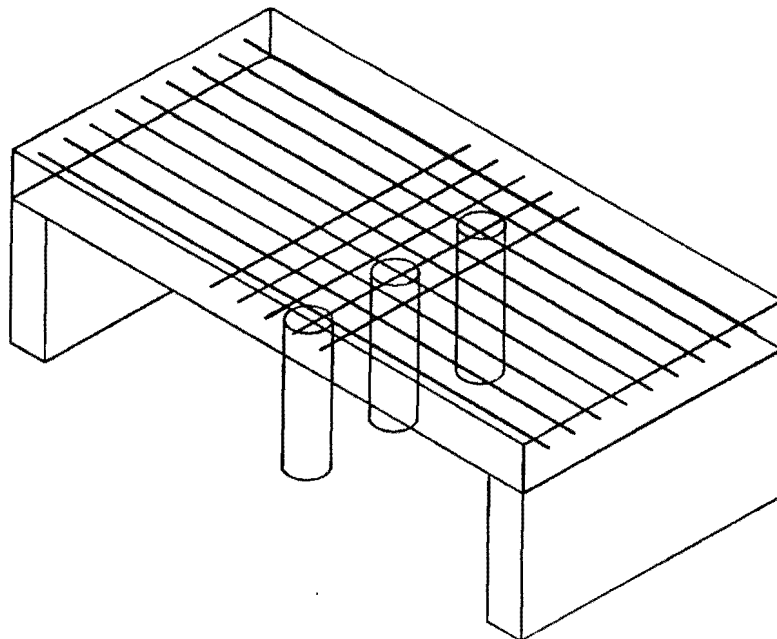
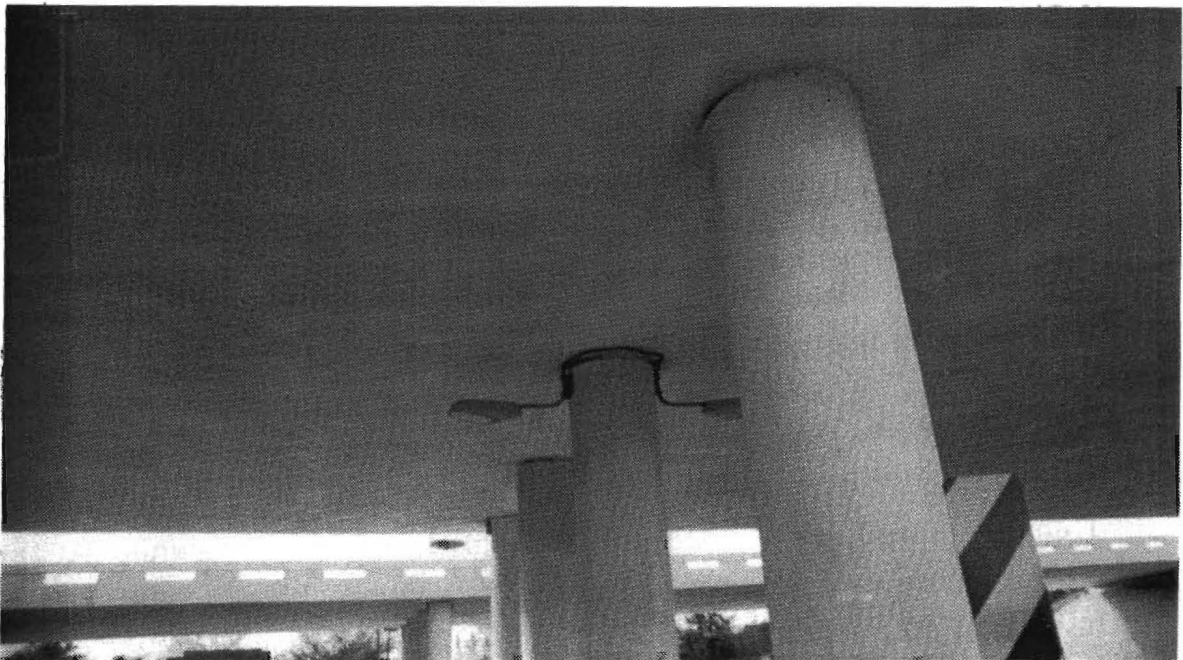


FIG. 1. Slab Bridge Schematic



(a)



(b)

FIG. 2. Taft Boulevard Bridge. (a) Overview; (b) Column Line

structures, however, is two-way shear, which has been studied extensively for thin-slab floor structures (Burns and Hemakom 1977, 1985; Gerber and Burns 1971). Increasing use of post-tensioning in concrete bridge slabs leads to more economical use of materials, thinner slabs, and an increased risk of punch-through failure from concentrated column loads.

1.1 Current State of Art

Concrete under biaxial compression shows significant increase in virtually all aspects of strength. In an experimental study (Kupfer et al. 1969), up to 27 percent higher compressive capacity was recorded under biaxial compression than for uniaxial compression. Current design of bidirectionally prestressed slab bridges, as carried out by SDHPT, does not take into account increased strength of concrete under biaxial compression. The current method assumes a unidirectional narrow plate strip for analysis of longitudinal post-tensioning (Cox 1985). After longitudinal design has been completed, engineers design localized transverse post-tensioning independent of effects of longitudinal post-tensioning.

Although the effective area of localized transverse post-tensioning extends beyond the actual rectangular post-tensioning region of the tendons themselves, distribution and intensity of those stresses are assumed to vary linearly within the region shown in Fig. 3. This assumed distribution pattern is used to verify whether or not there is adequate compression in the slab. Also, design of the transverse tendons is based on extreme fiber stress of the slab due to in-plane and moment forces according to:

$$\frac{P}{A} + \frac{Mc}{I} < \sigma_{\max} \dots \dots \dots (1)$$

where σ_{\max} is the maximum allowable concrete stress, P is the total of all tendon forces, M is the internal moment, c is the distance from the neutral axis, A is a cross-sectional area along a given line of constant stress, as shown in Fig. 3, and I is the moment of inertia at the same cross-sectional location.

Design procedures of the American Association of State Highway and Transportation Officials (AASHTO) and American Concrete Institute (ACI) do not provide guidelines with regard to prestress distribution, although the Post-Tensioning Institute (PTI) gives some indirect criteria. The latter recommends an approach for calculating the effective flange width of a unidirectionally post-tensioned T-section (*Post-Tensioning* 1985). PTI states that effective width of a flange increases at an angle of 33° from the tendons.

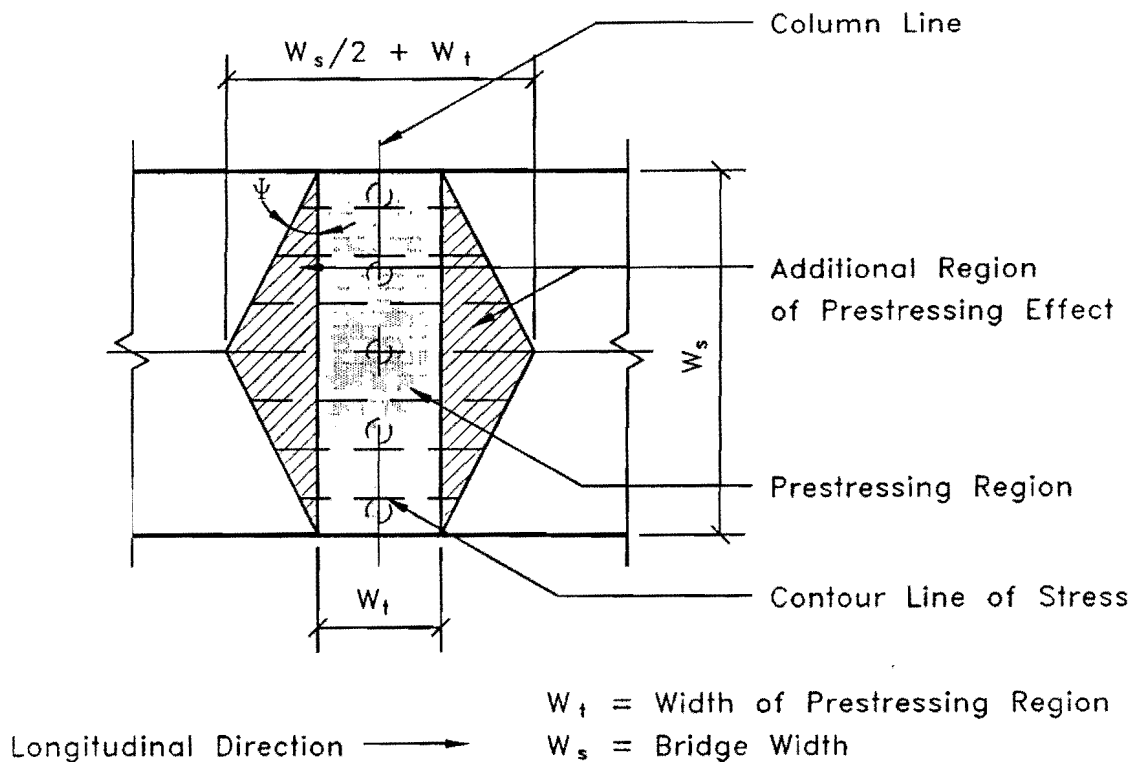


FIG. 3. Current Assumption of Effective Prestressing Region

Current design of these structures relies entirely on slab thickness for shear resistance (Cox 1985). Two-way shear capacity for service loads is calculated using the equation specified by the AASHTO code (*Standard* 1989), section 8.15.5.6.3. In this calculation, the critical section is taken to be at a distance equal to one-half the slab thickness away from the perimeter of a column (Fig. 4). Furthermore, the AASHTO equation used by SDHPT does not take prestressing into account.

Naaman (1982) states that prestressed concrete has higher shear capacity than conventional reinforced concrete. However, likelihood of shear failure increases as slab thickness decreases; prestressed slabs tend to be designed thinner than conventionally reinforced concrete due to their increased flexural capacity. In fact, tests conducted by Burns and Hemakom (1977, 1985) and Gerber and Burns (1971) showed that two-way shear was the dominant failure mode for bidirectionally post-tensioned flat slabs. Better knowledge of shear capacity, in combination with improved understanding of moment capacity, would allow designers freedom to construct a bridge with the thinnest and most efficient slab possible. This would yield a lighter structure and thereby further reduce dead load. It also gives more aesthetic

flexibility than a relatively thicker slab, and provides increased freedom in architectural design.

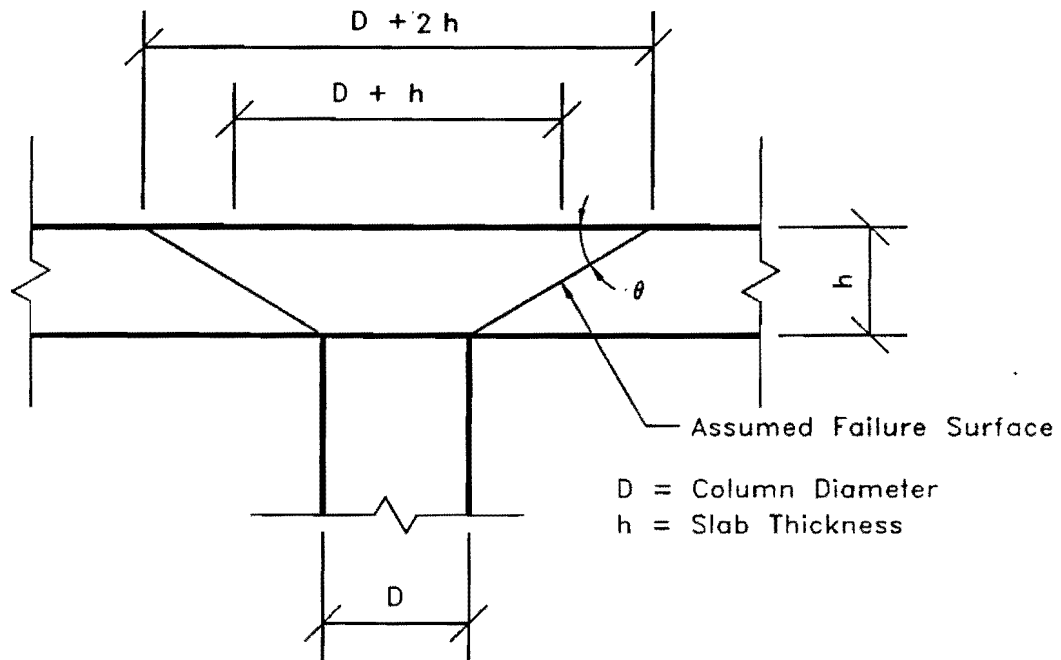


FIG. 4. Critical Diameter of Two-Way Shear

1.2 Review of Literature

ACI-ASCE ("Recommendations" 1983) publishes recommendations for prestressed concrete members with unbonded tendons, including two-way systems. The predominant and recommended method uses uniformly distributed tendons in one direction and banded tendons in the other, similar to the design under investigation in this study. Maximum tendon spacing is given as six to eight times the slab thickness, with a minimum average prestress in the concrete of 125 psi (860 kPa).

More recently, ACI-ASCE (*Analysis* 1988) suggests use of post-tensioned slab bridges for short spans of up to 80 ft (24 m). According to the committee, advantages for this bridge type are neat and simple appearance, shortest construction time of any cast-in-place system, and little required maintenance. The committee report refers to transverse prestressing as an optional reinforcement.

A system employing banded post-tensioning has been investigated for flat slab floor systems commonly used in building construction (Burns and Hemakom 1977, 1985; Gerber and Burns 1971). Testing was carried out on multi-column supports with a 2-3/4-in. (69.9-mm) slab. One test (Burns and Hemakom 1977) had symmetrical tendon size and spacing in two directions, with 4-1/4-in. (108-mm) tendon spacing in the column strip and 10-in. (254-mm) spacing in the middle strip. Design of the slab was done using an equivalent frame analysis (Naaman 1982). Other research conducted by Burns and Hemakom (1985) used a slab of the same dimensions with banded tendons, in which 23 tendons were uniformly spaced in the slab at 17.1 in. (434 mm) in one direction, and seven tendons were spaced at 3.6 in. (91.4 mm) over each column line in the other direction. In both experiments, researchers found higher punch-through shear capacity than predicted by AASHTO (*Standard* 1989) and ACI (*Building* 1989) codes. The failure surface in the specimens formed an 18° to 19° angle with the top surface, which was considerably shallower than the 45° assumed in conventional engineering practice (Fig. 4).

Earlier testing conducted by Gerber and Burns (1971) was for a single-column structure. The research was conducted on 10 slabs having a 7-in. (178-mm) thickness, four of which simulated cast-in-place slabs, and the remaining six slabs were constructed using a lift-slab technique. The research provided information on shear capacity, flexural capacity, reserve capacity, and effect of reinforcing steel configurations.

Lin, Scordelis, and May conducted experimental research on bidirectionally prestressed lift slabs (1957). The specimens studied were 6-ft (1.83-m) square with thicknesses of 6, 8, and 10 in. (152, 203, and 254 mm), and made of either 3,000-psi (20.7-MPa) or 4,500-psi (31.0-MPa) concrete with average initial prestress of 250 to 500 psi (1.72 to 3.45 MPa) in the concrete. The slabs were supported along the perimeter, and loaded at the center. Prominent failure mode was punching of a cone out of the slab, which occurred at an angle of 18° to 25° with the slab surface instead of at 45° as conventionally assumed. Researchers developed an empirical formula to predict the failure load for this class of prestressed slabs.

Elstner and Hognestad (1956) conducted experimental research on 39 conventionally reinforced concrete slabs which were 6-ft (1.83-m) square and 6-in. (152-mm) thick. Design strength of concrete varied from 2,000 to 7,000 psi (13.8 to 48.2 MPa) with tension and compression reinforcement ratios varying from 0.5 to 3.7 percent and 0 to 1.0 percent, respectively. Thirty-four specimens failed by the column punching through the slab, most of them failing after initial yielding of reinforcement

in the column region. Researchers also found that mild steel compression reinforcement had a negligible effect on ultimate shear capacity. Also, an analysis using a beam strip approach did not always lead to correct prediction of the failure mode.

Bazant and Cao (1987) conducted extensive punch-through shear testing on nonprestressed circular slabs. Research included effect of thickness of a specimen on its behavior at failure load. Thicknesses of the specimens were 1 in. (25.4 mm), 2 in. (50.8 mm), and 4 in. (102 mm). Typically, thinner slabs were found to have more ductility than thicker slabs. The researchers found brittle failure for slabs without shear reinforcement. Also their published literature review indicates such enormous scatter in data that their proposed formula is neither contradicted nor validated.

Scordelis, Lin and Itaya (1959) conducted tests on a 3-in. (76.2-mm) slab resting on nine columns. The slab was post-tensioned in both directions using 1/4-in. (6.4-mm) high-strength steel wire spaced 15 in. (381 mm) on center. Researchers found that a theoretical prediction using beam theory was reasonably accurate when compared with the experimental result, but prediction obtained by elastic plate theory was more accurate.

Kupfer, Hilsdorf, and Rusch (1969) conducted extensive research on concrete under biaxial compression. Concrete specimens were loaded in two directions at various load ratios to study increase in ultimate load capacity over compressive strength of uniaxially loaded concrete. As mentioned before, the researchers found that concrete under biaxial compression exhibited up to 27 percent increase in strength over concrete under uniaxial compression.

Zia, White, and Vanhorn (1970) studied effects of scale factors in laboratory models. They investigated several types of distortion that may be expected from a scale model and ways to compensate for the problem. The paper states, however, that distortion increases significantly if the scale of a model becomes smaller than one-fourth.

Experimental research on a box-girder bridge model conducted at the University of California, Berkeley (Davis 1978), compensated for the effect of scale factor on dead load by placing blocks of concrete on the top surface of the model, thereby increasing the effective model dead load stress of the model to that of the prototype. This research report served as a primary reference in designing the current laboratory models.

Analytical research was also conducted at the University of California, Berkeley (Van Greunen 1979), on prestressed concrete flat slabs. Several computer

codes were combined by Van Greunen into a finite element analysis package for prestressed concrete slabs. The program, NOPARC (NOn-linear Prestressed And Reinforced Concrete), utilizes nonlinear plate bending theory to analyze stress and strain in each layer of an element, and determines displacements and nodal forces at each node. Prestressing force is converted to appropriate nodal force according to magnitude, direction, and location of the tendon. The program has an option of analyzing concrete in a non-linear mode in order to simulate behavior of concrete more accurately than by use of conventional linear theory. Numerical simulation using NOPARC shows excellent correlation with published experimental results.

1.3 Problem Identification

To test and verify adequacy of current procedures as well as to provide computer analysis and design aid software for this type of bridge, it is desirable to build, test, and analyze actual slabs with banded prestressing. For this purpose two laboratory models, denoted Model One and Model Two, are being constructed and tested, along with instrumentation and data acquisition of an actual bridge in Wichita Falls, Texas. Model One is a column and slab portion of a bridge (Fig. 5). The slab size of the model is 9 ft (2.74 m) wide by 9 ft (2.74 m) long by 9 in. (229 mm) thick. Scale of Model One was chosen to be 3/10ths. Model Two is a two-span laboratory approximation of a three-span bridge in Wichita Falls, Texas. Its overall length is 54 ft (16.5 m). At 17.5 ft (5.33 m), width of the slab is approximately twice that of Model One. Each of the two span lengths of Model Two is 27 ft (8.25 m), which is the equivalent of a 90-ft (27.4-m) span in the prototype bridge. The actual bridge to be studied under another phase of this research contract with SDHPT is Brook Avenue overpass, which is also located in Wichita Falls, Texas.

The computer program, NOPARC (Van Greunen 1979), is used to analyze the two models and the Brook Avenue bridge. In this report, numerical simulation is reported only for Model One. NOPARC uses three-node triangular elements, with uniform strain and finite thickness. The program has the ability to analyze time-dependent behavior of concrete, such as creep and shrinkage. Correlation between computer analysis and laboratory results serves to enhance confidence in accuracy of the computer program. If the degree of correlation is acceptable, analysis of the structure may be based almost entirely on the numerical simulation, which is easier, faster, and less expensive than field and laboratory investigation. One of the final

objectives for this research study is to produce a user-friendly software package to analyze such a slab.



FIG. 5. Model One

II. MODEL ONE

The purpose of the single-column laboratory model (hereafter termed Model One) is to determine the effects of localized transverse post-tensioning due to a variable number of tendons in the banded direction, and to test for punch-through shear capacity. To this end, the model simulates a square portion of a bridge deck removed from a three-tenths scale bridge model. Model One is tested for effects of localized post-tensioning under dead load and symmetrical live load. Additionally, the Model One experiment serves to calibrate, if necessary, computer analysis and data acquisition procedures as well as to verify planned construction, instrumentation, and data acquisition of Model Two. Finally, the model is tested for a punch-through shear failure to determine ultimate and reserve shear capacity, as well as slab behavior at failure load in a bidirectionally post-tensioned region of a slab. The primary objective of the failure loading is to determine how accurately shear capacity of the post-tensioned slab specimen is predicted by published equations.

Model One differs from the prototype in several ways. First, it has only one column interacting with the slab, while in the prototype bridge interaction effects from multiple columns appear in the slab. Also, free edges of the small slab do not duplicate internal resultant forces and moments in the prototype structure.

In order to maintain consistency with the actual bridge and Model Two, the direction parallel to the uniformly spaced tendons is called the "longitudinal" direction. The direction parallel with the banded tendons is called the "transverse" direction as shown in Fig. 6.

2.1 Justification for Size and Three-Tenths Scale

Aside from similitude to Model Two as mentioned above, weight of the slab was considered when the size of Model One was designed. In order to simplify formwork involved in fabrication, the slab was cast on the floor using plywood sheets resting on top of seven 2-in. x 10-in. (38.1-mm x 235-mm) timbers (Fig. 7). This technique eliminated erection of scaffolding, but imposed a constraint on size such that the slab needed to be light enough to be hoisted to the top of the column with the existing 20-ton (178-kN) capacity overhead crane. Several preliminary designs were discarded due to their excessive weight, until the size of 9 ft x 9 ft x 9 in. (2.74 m x 2.74 m x 229 mm) was proposed. Assuming 150 lb/ft³ (2,400 kg/m³) for density of

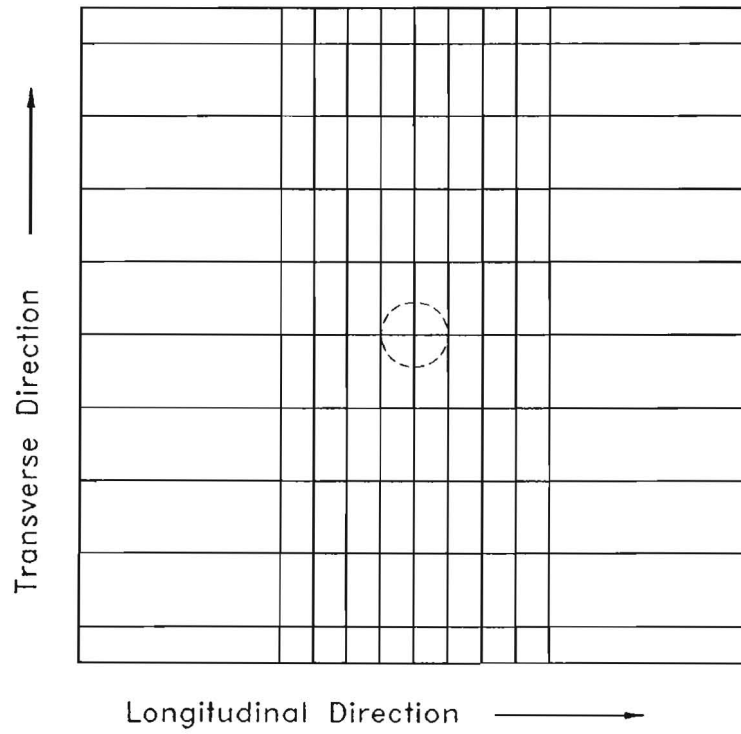


FIG. 6. Tendon Pattern

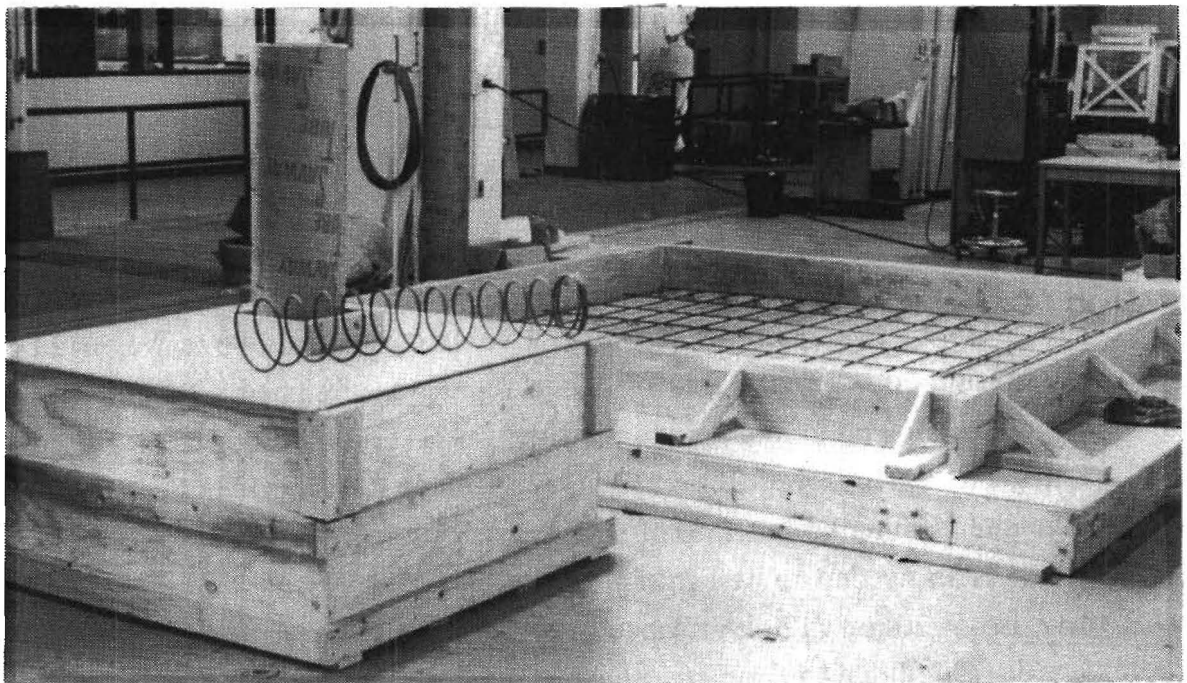


FIG. 7. Formwork for Model One

reinforced concrete, weight of the slab of the final design was 9 ft x 9 ft x 9 in. x 150 lb/ft³ = 4.6 tons (40.9 kN), which was well within limits of the crane.

SDHPT design procedure for this type of bridge assumes that compression due to in-plane transverse tendons is distributed in a hexagonal region surrounding the tendons (Fig. 3). Edges of the hexagonal area lie at an angle of two to one, or $\psi = 26.6^\circ$, from a parallel to the column line. To verify this assumption, the test slab of width W_s must have a minimum length of $W_s/2 + W_t$. The 3/10ths scale model had W_s of 9 ft (2.74 m) and W_t of 3.6 ft (1.10 m), which called for a minimum length of 8.1 ft (2.47 m). Therefore, the constructed 9-ft (2.74-m) length was sufficient to enclose the assumed prestressing envelope.

2.2 Calculation of Ultimate Load

Ultimate load capacity for punch-through shear, which also affected design size of the slab, can be calculated according to several different predictive models. SDHPT design follows AASHTO specifications for highway bridges (*Standard* 1989), section 8.16.6.6.2, which does not take prestressing effects into account for estimating the ultimate shear load. In this provision shear stress, v , is calculated by:

$$v = \frac{V}{b_o d} \dots \dots \dots (2)$$

where b_o is the perimeter of a critical section, d is the average depth of tensile reinforcement, and v is the shear force. Critical section for b_o is defined as the smallest perimeter of the concentrated load or reaction area, which is at least $d/2$ away from its load point or area. For a circular column of diameter D , the perimeter of the critical section has a length of $(D + d)\pi$. For Model One, with a column diameter of 10 in. (254 mm) as explained in a later section, this value is 17.875π in. (454π mm). The average depth of tensile reinforcement is calculated by subtracting concrete cover and one-half of the reinforcing bar mat thickness from the slab thickness, or:

$$\begin{aligned} d &= 9 \text{ in.} - 0.75 \text{ in.} - 0.375 \text{ in.} \\ &= 7.875 \text{ in. (200 mm)} \dots \dots \dots (3) \end{aligned}$$

Maximum shear stress under the AASHTO provision (sec. 8.16.6.6.2) is given by:

$$v_c = \left(2 + \frac{4}{\beta_c}\right)\sqrt{f'_c} \leq 4\sqrt{f'_c} \quad \dots \dots \dots (4)$$

where β_c is the ratio of long side to short side of a concentrated load or reaction area, and f'_c is the compressive capacity of concrete in pounds per square inch. Combining Eqs. 2 and 4, shear force may be calculated as:

$$V = \left(2 + \frac{4}{\beta_c}\right)b_o d \sqrt{f'_c} \leq 4b_o d \sqrt{f'_c} \quad \dots \dots \dots (5)$$

For 5,000-psi (34.5-MPa) concrete and a circular reaction area, Eq. 5 becomes:

$$\begin{aligned} V &= (2 + 4)(17.875\pi)(7.875)\sqrt{5,000} \\ &= 187.6 \text{ kips (835 kN)} \quad \dots \dots \dots (6) \end{aligned}$$

with an upper limit of:

$$\begin{aligned} V &= 4(17.875\pi)(7.875)\sqrt{5,000} \\ &= 125.1 \text{ kips (555 kN)} \quad \dots \dots \dots (7) \end{aligned}$$

which is the predicted ultimate shear capacity of the model slab without prestressing. This value, 125.1 kips (555 kN), may be considered to be a lower bound for the failure load.

From calculations in accordance with the ACI code (*Building* 1989), section 11.12.2.2, the slab is predicted to fail by punch-through shear under a column reaction force of:

$$V_c = [3.5\sqrt{f'_c} + 0.3f_{pc}]b_o d + V_p \quad \dots \dots \dots (8)$$

where f'_c is the ultimate compressive strength of concrete in pounds per square inch; f_{pc} is the average of concrete stresses induced by longitudinal and transverse prestressing in pounds per square inch, which must lie between 125 and 500 psi (861 and 3,450 kPa); b_o is the perimeter of the critical failure surface in inches; d is the depth of tensile reinforcement in inches; and V_p is the vertical component of effective prestress force along the failure perimeter in pounds.

For Model One, the design concrete compressive strength was 5,000 psi (34.5 MPa). The longitudinal tendons exerted 780 psi (5.37 MPa) of compressive stress on the concrete while the transverse tendons exerted compressive stress somewhere between 352 psi (2.43 MPa) and 780 psi (5.37 MPa), as described in a later section for tendons. Therefore, f_{pc} was taken to be 500 psi (3.45 MPa) because of the limitation described earlier.

If a 45° failure surface is assumed for diagonal tension in accordance with conventional engineering practice, the diameter of the critical surface may be taken as the sum of slab thickness and the column diameter. As calculated earlier, the depth of tensile reinforcement for Model One is 7.875 in. (454 mm), and b_o is 17.875π in. (1,426 mm). v_p is zero, because the tendons are straight and parallel to the slab surface. Therefore, v_c may be evaluated as follows:

$$v_c = [3.5\sqrt{5,000} + 0.3(500)](17.875\pi)(7.875) \\ = 176 \text{ kips (782 kN)} \dots \dots \dots (9)$$

In contrast, Gerber and Burns (1971) refer to an empirical formula derived by Lin, Scordelis, and May (1957) which predicts failure of a two-way prestressed slab at:

$$v_c = f'_c b d (0.175 - 0.0000242 f'_c + 0.000020 \frac{F_{ps}}{S}) \dots \dots \dots (10)$$

where v_c is the ultimate shear force, f'_c is the strength of concrete in pounds per square inch, d is the distance of post-tensioning tendons from the top surface of the column in inches, b is the perimeter of a lifting collar, column, or column capital in inches, F_{ps} is the post-tensioning force in pounds, and s is the tendon spacing in inches. Since longitudinal tendons in Model One were designed with an eccentricity of 0.6 in. (15.2 mm) and transverse tendons had no eccentricity, the average distance to tendons was 4.2 in. (107 mm). According to the Eq. 10 and these values, Model One is predicted to fail at:

$$v_c = 5,000(10\pi)(4.2) \left[0.175 - 0.0000242(5,000) \right. \\ \left. + 0.000020 \left(\frac{84,000}{12} \right) \right] \dots \dots \dots (11)$$

or:

$$v_c = 128 \text{ kips (571 kN)} \dots \dots \dots (12)$$

Gerber and Burns, however, found an average capacity 1.5 times greater than predicted by Eq. 10 and a maximum of 1.82 times this capacity for one of their specimens. Applying these factors to the prediction for Model One, the slab is expected to fail at 192 kips (854 kN) and 233 kips (1,037 kN), respectively, which are both within available actuator capacity. Neither Eq. 8 nor Eq. 10 takes ordinary reinforcement into account.

Shear capacity of a two-way slab, however, tends to be unpredictable. Bazant and Cao (1987), for example, found wide distributions from calculated values of punch-through shear capacity of slabs. Also, since actual concrete strengths vary widely, the above calculations only predict a statistical failure load, which may be significantly different from the actual failure load.

In experiments conducted by Gerber and Burns (1971), no tendons broke when two-way shear failure occurred. After failure, the load was removed and subsequently reapplied until tendons started to break. This procedure is called reserve load testing. The failure of tendons, or the reserve capacity load, occurred at a lower load than the primary failure magnitude. Tendons usually broke at sharp bends, above columns or column collars, and not at anchorages. Reserve load capacity for bridges serves to prevent sudden catastrophic collapse, thereby providing additional safety for occupants of vehicles on the structure.

2.3 Scale Factors

In order to study a prototype bridge using a scaled laboratory model, adequate knowledge of scale factors is necessary to understand the extent of direct correlation between model results and prototype results. In this research, scaling information is taken from an ACI study conducted by Zia, White, and Vanhorn (1970). Calculation of scale factors in the current application is based on the requirement that stress applied to a member remains constant regardless of the geometric scale factor. Expression of scale factors are based on the following notation:

- S_1 - Linear scale factor, required;
- SF - Actual scale factor for quantity under consideration; for a length quantity, $SF = S_1$;
- F - Force quantity;
- L - Length quantity.

Using this notation, FL^{-2} must remain unchanged for a scale model in order to have model stresses match those of the prototype. This approach leads to relationships shown in Table 1. According to the table, pressure, line, or concentrated loads may be adjusted according to the corresponding scale factor. For example, a concentrated load applied to the prototype must be multiplied by S_1^2 for application on the model structure.

The effect of dead load, however, does not follow as easily since dead load is controlled by density and material quantity (Table 1). If the same material is used in

TABLE 1. Scale Factors

Dimension	Quantity Examples	Scale Factor
L ²	Area	S ₁ ²
L	Length	S ₁
FL ⁻³	Density	S ₁ ⁻¹
FL ⁻²	Stress, Pressure	1
FL ⁻¹	Line Load	S ₁
F	Point Load, Shear	S ₁ ²
FL	Moment	S ₁ ³

L = Length unit, F = Force unit,
S₁ = Linear scale factor

the model and the prototype, as is the case for Model One and Model Two, density of the material stays constant, whereas from a pressure loading standpoint, dead load needs to be scaled by S₁⁻¹. Therefore, dead load per unit area must be increased through an alternative means in order to account for the reduced dead load stress of the scale model.

Because of this requirement, shear due to dead load becomes:

$$V = DL \times S_1^{-1} \times A \dots \dots \dots (13)$$

in which the dead load per unit area (DL) is multiplied by the scale factor, S₁⁻¹, and then by the cross-sectional area, A, to obtain the shear load on the model slab. Replacing these terms by their corresponding scale factors, the shear scale factor becomes:

$$\begin{aligned} SF_V &= S_1 \times S_1^{-1} \times S_1^2 \\ &= S_1^2 \dots \dots \dots (14) \end{aligned}$$

By the same approach, dead load moment becomes:

$$\begin{aligned} SF_M &= DL \times S_1^{-1} \times A \times L_M \\ &= S_1 \times S_1^{-1} \times S_1^2 \times S_1 \\ &= S_1^3 \dots \dots \dots (15) \end{aligned}$$

where L_M is the moment arm. The resultant scale factors are the same as those required by Table 1.

Scale factor considerations were taken into account for the preliminary design of Model Two, which in turn dictated design of Model One. In Model One, however, dead load was not artificially increased, because one of the objectives for Model One was to study the behavior of a slab and the construction technique in preparation for construction and observation of Model Two. Relationships between the prototype bridge, a true model, and Model One are summarized in Table 2.

2.4 Reinforcement Bars

In order to maintain a 3/10ths scaling factor, reinforcement bars were chosen so that the ratio of cross-sectional steel area to cross-sectional concrete area, ρ , would be the same as that of the full-size bridge. The Taft Boulevard bridge shown in Fig. 2., on which the two laboratory models are based, have No. 5 (15.9 mm) bars in both longitudinal and transverse directions. Longitudinal re-bars are placed 12 in. (305 mm) on center whereas transverse re-bars are placed 6 in. (152 mm) on center. Mild steel in this bridge type is included by SDHPT designers to guard against uncertainty in design and to control temperature and shrinkage effects. In order to maintain the same stress in the concrete of the model as in the Taft Boulevard bridge, the scaled steel area in a model with a linear scale of s_1 must be s_1^2 (Zia et al. 1970). For Model One this area scale becomes the square of 3/10ths or 9/100. When the steel area of all re-bars normal to a given cross-sectional area is divided by the width of the slab, the resulting thickness may be considered to be an equivalent, distributed steel layer thickness. In computer analyses which use plate theory to treat composite material, the reinforcing steel is converted to multiple anisotropic layers, in which stiffness of each layer is limited to one direction. Anisotropic layers simulate reinforcement bars that resist force only in one direction. In designing a scale model, the ratio of this equivalent steel thickness to the total slab thickness must remain unchanged so that properties of elements are the same for the model and the prototype.

In designing both laboratory models, No. 3 (9.53-mm) bars were used in both directions for the final model design since they were more readily available than smaller No. 2 (6.35-mm) or metric-unit bars. Use of No. 3 (9.53-mm) bars, however, somewhat restricted freedom of spacing for strain gage installation. In order to keep the 3/10ths linear scale factor according to the computation described above, reinforcement bars were placed 14.3 in. (363 mm) and 7.2 in. (183 mm) on center in the longitudinal and transverse directions, respectively (Fig. 8). The reinforcement

TABLE 2. Comparison of Prototype, True Model, and Model One

Properties (1)	Prototype (2)	True Model (3)	Model One (4)
Scale	1	3/10	3/10
Dimension (ft)	300 x 60	90 x 18	9 x 9
Span (ft)	100	30	—
Thickness (in.)	30	9	9.25
No. of Columns	5 x 2	5 x 2	1
Column Size (in.)	36	10.8	10
Column Height (ft)	16	4.8	3
No. of Tendons			
Longitudinal	40	40	9
Transverse	7 x 2	7 x 2	1-9
Tendon Type	Bonded	Bonded	Unbonded
Tendon Shape			
Longitudinal	Draped	Draped	Straight
Transverse	Straight	Straight	Straight
Tendon Sizes (in.)			
Longitudinal	0.5 x 19	0.15 x 19	0.5 x 4
Transverse	0.5 x 19	0.15 x 19	0.6 x 1
Tendon Spacings (in.)			
Longitudinal	18	5.4	12
Transverse	18	5.4	5.4
Elastic Modulus of Tendons (ksi)	28,000	28,000	28,000
Duct Sizes (in.)			
Longitudinal	3.5	1.05	1.25
Transverse	3.5	1.05	0.75
Re-bar Sizes			
Longitudinal	No. 5	4.8 mm	No. 3
Transverse	No. 5	4.8 mm	No. 3
Re-bar Spacings (in.)			
Longitudinal	12.0	3.6	14.3
Transverse	6.0	1.8	7.2
Minimum Re-bar Cover(in.)	2.0	0.6	0.75
Live Load			20 kips
Dead Load (psf)	375	375	113
f'c at 28 days (psi)	5,000	5,000	4,800
Aggregate Size (in.)	1.5	0.45	0.75
Slump (in.)	7	7	6
Longitudinal P/A (psi)	780	780	780
f _y (ksi)	60	60	60
f _{pu} (ksi)	270	270	270

1 in. = 25.4 mm, 1 ft = 304.8 mm, 1 kip = 4.45 kN,
1 psi = 6.89 kPa

bar cover was 3/4 in. (19.1 mm) to maintain the bond between reinforcement bars and concrete (*Building* 1989).

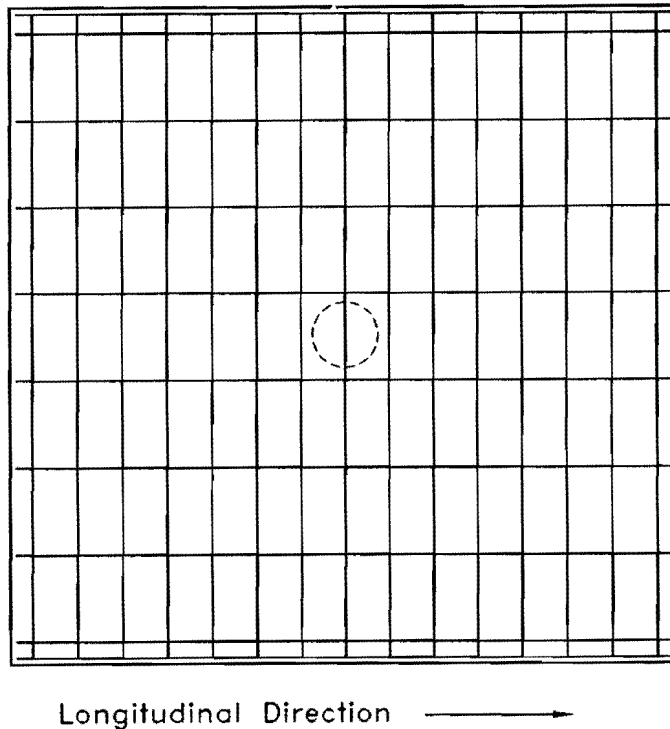


FIG. 8. Reinforcement Pattern

2.5 Longitudinal Tendons

Post-tensioning tendons were placed in the model so as to induce an amount of compressive stress in the concrete that was equivalent to the stress in its counterpart material in the prototype bridge. Since the investigation for Model One was not primarily concerned with effects of longitudinal post-tensioning, tendon size and spacing in this direction were chosen for convenience and availability. High-strength steel, supplied by VSL Corporation, was 270-ksi (1.86-GPa) 7-wire strand that meets American Society for Testing and Materials, ASTM A416 specifications. Estimated ultimate force is 41.3 kips (184 kN) for a 1/2-in. (12.7-mm) strand and 58.6 kips (261 kN) for a 0.6-in. (15.2-mm) strand (Post-Tensioning 1985). Yield force is 35.1 kips (156 kN) for a 1/2-in. (12.7-mm) strand and 41.0 kips (183 kN) for a 0.6-in. (15.2-mm) strand. Elastic moduli for both types of tendons are 28,000 ksi (193 GPa).

Because of a limitation in availability of anchor sizes as well as ease of construction, longitudinal tendons were placed 12 in. (305 mm) on center. This allowed enough space to place a series of VSL EC 5-7 anchorages, as shown in Fig. 9, which measure 7 in. x 7 in. (178 mm x 178 mm) and have the capability of anchoring seven 1/2-in. (12.7-mm) strands (Post-Tensioning 1985). EC-type anchors use a smaller bearing area than comparable anchors, which is a desirable trait for use in a 9-in. (229-mm) slab in which the bearing area is quite limited when compared to available area in the 30-in. (762-mm) prototype slab. To induce a longitudinal compressive stress of 780 psi (5.4 kPa) in the concrete of Model One, as is the case with the actual bridge, each tendon must exert a total force of 84 kips (374 kN) to its resisting 9 in. x 12 in. (229 mm x 305 mm) concrete area. To accommodate this force without exceeding AASHTO and ACI prescribed stress limits of the steel, four 1/2-in. (12.7-mm) strands were used for each tendon. AASHTO, section 9.15.1, and ACI, section 18.5.1(c), limit the tendon stress at anchorages to 70 percent of the ultimate tendon stress, or f_{pu} , after prestress transfer and 90 and 85 percent, respectively, of f_{pu} during jacking; for a 270-ksi (1.86-GPa) strand, the tendon force after stressing and the jacking limit are $0.70 \times 270 = 189.0$ ksi (1.23 GPa) and $0.85 \times 270 = 215.7$ ksi (1.49 GPa), respectively. Longitudinal tendons are placed with an eccentricity of 0.6 in. (15.2 mm) below the neutral plane to avoid spatial conflict with the transverse tendon ducts and to simulate a small negative moment at the column support. The average distance of the tendon steel from the top of the column is 4.2 in. (107 mm).

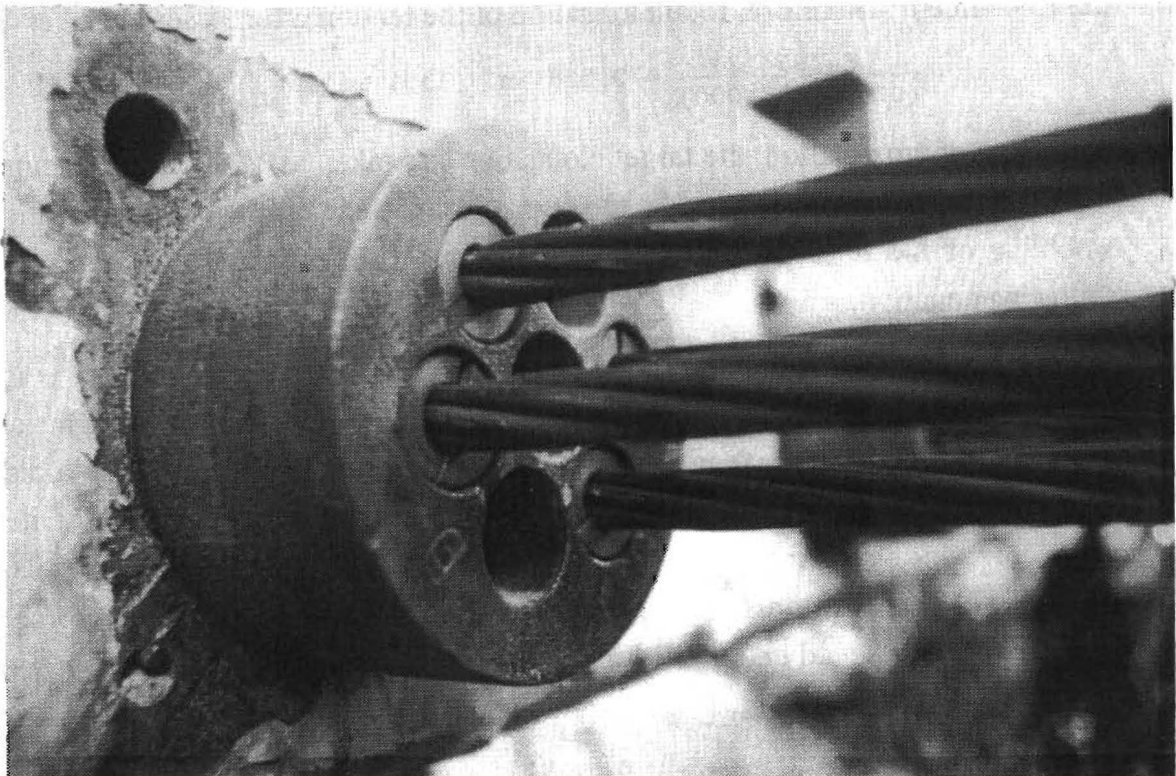


FIG. 9. Longitudinal Tendon Anchor

During construction each tendon was pulled until a small amount of stress was shown on a pressure gage attached to a tendon jack. At this load level the anchors at the dead end were set. The jacking force was released to near zero and a mark was made on the tendon at a given distance from the anchor head. Then the tendon was pulled until the required stress was recorded on the pressure gage. Residual elongation was measured using the mark made after the anchor wedges set. To compensate for anchor set loss at the jacking end, the tendons were stressed again. The jack was set against a chair, and shims of required thickness were placed so that the tendons would have the desired final elongation and, therefore, maintain the desired stress.

The relationship between tendon force and elongation may be obtained by the equation:

$$\frac{F_{ps} L_t}{A_t E} = \Delta L_t \dots \dots \dots (16)$$

where F_{ps} is the axial force of the tendon, L_t is the tendon length, A_t is the cross-sectional area, and E is the modulus of elasticity. VSL Corporation, which supplied the post-tensioning tendons, rates the elastic modulus at 28,000 ksi (193 GPa). Area of a tendon is four times the area of a 1/2-in. (12.7 mm) strand, or $4 \times 0.153 = 0.612$ in² (395 mm²). Therefore, total elongation of the tendon after losses must be:

$$\frac{84(9)(12)}{(0.612)(28,000)} = 0.529 \text{ in. (13.4 mm)} \dots \dots \dots (17)$$

As a close approximation, the target elongation was taken as 17/32 in. (13.5 mm).

Since the tendons in Model One were straight, the only friction loss came from wobbling of the tendons. Tendon force after friction loss is calculated from the following equation:

$$F_{ps}(x) = F_j e^{-(\mu\alpha + Kx)} \dots \dots \dots (18)$$

where μ is the friction coefficient, which is assumed to be zero for a straight tendon; α is a change in angle between the force at the anchorage and the force at a distance x in radians; K is the wobble coefficient; $F_{ps}(x)$ is the tendon force at a given distance x ; and F_j is the jacking force (Naaman 1982). If K is taken to be 0.001 as a reasonable assumption for the given conditions (Naaman 1982), the force after friction loss at the dead end of the tendon becomes:

$$84 \times e^{-0.001(9)} = 83.2 \text{ kips (370 kN)} \dots \dots \dots (19)$$

which deviates less than 1 percent from 84 kips (374 kN). Thus, friction loss may be ignored, even with a somewhat higher friction coefficient.

Unlike the prototype bridge, tendons in the model were left unbonded for practical reasons. Straight, unbonded tendons exert prestress force onto a concrete slab only at anchors, whereas bonded tendons exert force both at anchors and along the entire length of the tendons. This difference becomes substantial for a long tendon, especially over time as concrete undergoes time-dependent deformation. For Model One, however, the difference between bonded and unbonded tendons was considered negligible since tendons were placed over a short distance, and the model was not planned for analysis of time-dependent factors. It also provided an opportunity to test reliability of the computer analysis program for unbonded tendons. Model Two and the Brook Avenue bridge will serve to test the program's reliability for bonded tendons. This decision also simplified model construction and material selections.

Longitudinal tendons were stressed while the slab was on formwork near the floor, thereby creating sufficient strength to resist cracking when the slab was lifted by the overhead crane. While the longitudinal tendons were stressed, strain gages attached to the reinforcing bars were read to test effectiveness of the data acquisition system and software. Results of this test are shown in Table 5 in Appendix III and graphically in Section 4.2.

2.6 Transverse Tendons

In order to study effects of transverse tendons in the actual bridge, it is desirable to carefully maintain equivalent scaled spacing in the model. Therefore, 0.6-in. (15-mm) monostrands were placed 5.4 in. (137-mm) on center, instead of a more convenient spacing. For transverse tendons, VSL T6 anchors were used as shown in Fig. 10. Using custom-made bearing plates, this type of anchor allowed the close spacing required by similitude.

After the slab was poured, cured, stressed longitudinally, and placed on the column, transverse strands were stressed to determine effects of banded post-tensioning. Shimming procedures, similar to those used for longitudinal tendons, were repeated for the transverse tendons. Each tendon was jacked to 38 kips (169 kN) which corresponds to 177 ksi (1.23 MPa). The summation of 9 tendon forces divided by the cross-sectional area of concrete bounded by the tendon band (Fig. 3) gives an estimate of the stress at 780 psi (5.4 kPa), which is the same as in the design of the prototype bridge. On the other hand, if the total force of nine transverse tendons is divided by the cross-sectional area of the entire slab width, the

concrete stress is 352 psi (2.43 MPa). With the exception of stress concentrations near the anchors, the actual transverse stress varies in a continuous manner between these two bounds.

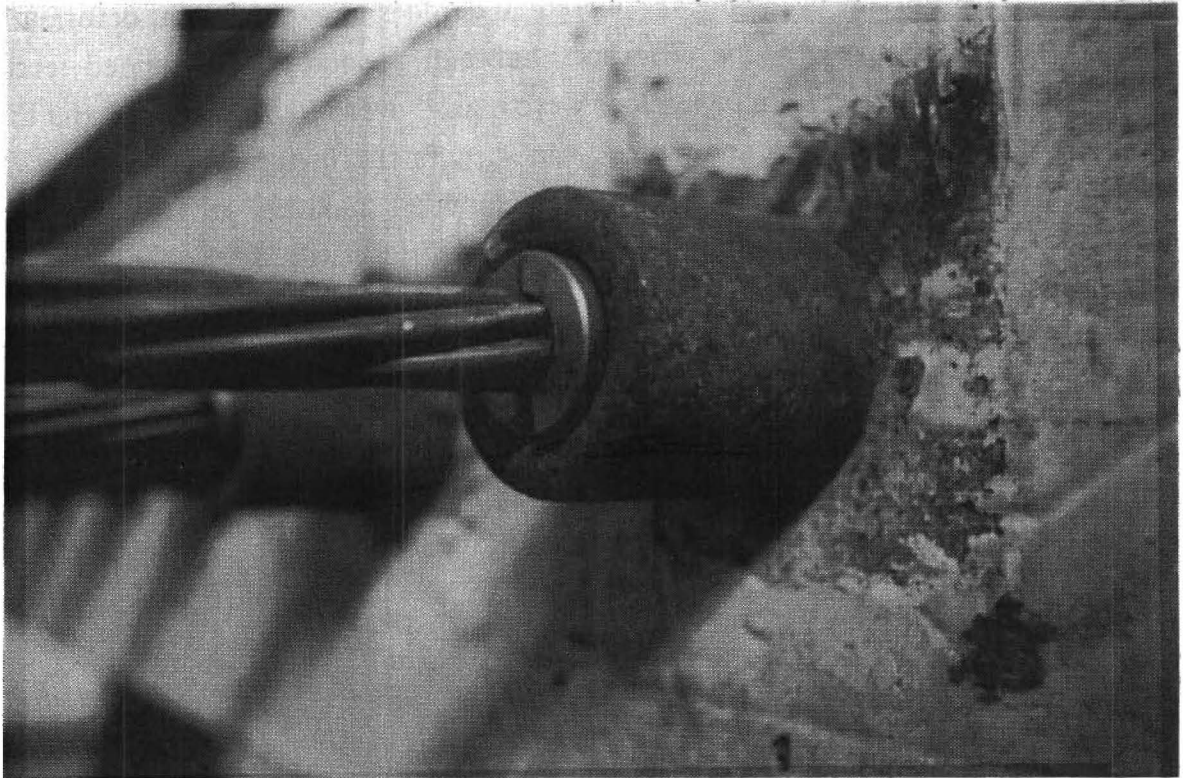


FIG. 10. Transverse Tendon Anchor

Transverse tendons were stressed during the elastic loading procedure in the same manner as the longitudinal tendons. Data readings of transducers were recorded at various stages of the operation. Analogous to calculations described for longitudinal tendons, total elongation of each transverse tendon is calculated according to:

$$\frac{38(9)(12)}{(0.215)(28,000)} = 0.682 \text{ in. (17.3 mm) (20)}$$

An approximate target elongation was taken as 11/16 in. (17.5 mm).

2.7 Concrete

Ready-mix concrete was delivered to the laboratory by a local concrete supplier. Concrete compressive capacity, f_c , was specified to be 5,000 psi (34.5 MPa),

which was the same as that specified for the prototype Taft Boulevard overpass. Maximum coarse aggregate size is 3/4 in. (19.1-mm). SDHPT design (Cox 1985) specifies a class H concrete (*Standard* 1982) for the prototype, but does not specify the aggregate size. According to SDHPT (*Standard* 1982), 1-1/2 in. (38.1 mm) is the largest maximum aggregate size to be used for class H concrete. On the other hand, the 3/4-in. (19.1-mm) coarse aggregate, which is considerably smaller than the 9-in. (229-mm) thickness of the slab, is permissible for the same class concrete. Although this practice does not follow scaling factors as specified in Table 2, the 3/4-in. (19.1-mm) aggregate was chosen as a compromise to maintain the concrete properties.

The concrete contained a plasticizing admixture which followed actual practice and facilitated construction of the laboratory model. The 6-in. (152-mm) slump obtained from concrete with the plasticizer expedited spreading the material in the slab form, as well as placed the concrete in a pedestal and column form.

2.8 Pedestal

The slab portion of Model One rests atop a pedestal specifically designed for this study. Original design of the pedestal was based on research conducted at the University of California, Berkeley (Davis 1978). The column of the pedestal for Model One was designed with a 10.8-in. (274-mm) diameter in order to maintain the 3/10ths scale factor. However, due to availability of formwork cylinders, 10 in. (254 mm) was chosen as the design diameter. To compensate for the smaller diameter, the amount of reinforcement was increased slightly. Ten No. 4 (12.7 mm), grade 60 steel bars were used for compression reinforcement along with a 3-in. (76.2-mm) pitch, No. 3 (9.53 mm), grade 60 steel spiral.

Footing of the pedestal was 4 ft x 4 ft (1.22 m x 1.22 m) which allowed half of a standard 4 ft x 8 ft (1.22 m x 2.44 m) plywood sheet to be used as the bottom part of its formwork. The footing was also made large enough to allow for bolting to the laboratory floor using four steel bolts through holes located 3 ft (9.15 m) on center in both directions (Fig. 5). Since the pedestal could be of any convenient height, 5 ft (1.53 m) was chosen as the top of the concrete column. This was similar to Davis' bridge (1978), and gave sufficient clearance for work conducted below the slab. The 2-ft (610-mm) high footing allowed 3 ft (915 mm) for the column height.

According to AASHTO (*Standard* 1989), section 8.16.5.2.5, and ACI (*Building* 1989), section 10.11.4.2, the following formula determines buckling characteristics of the column:

$$\frac{k l_u}{r} < 22 \dots \dots \dots (21)$$

where $k l_u$ is the effective length of the column, which is dictated by end conditions, and r is the radius of gyration. If the inequality is satisfied, the column is expected to be stable. Since the column of Model One was fixed by a 2-ft (610 mm) thick footing at one end and free at the other, the equivalent length $k l_u$ for this column is twice the actual length, or $k = 2$. For a circular section, the radius of gyration may be taken as 1/4th the diameter, in accordance with AASHTO, section 8.6.5.2.2, and ACI, section 10.11.3. Using these values, Eq. 21 becomes as follows:

$$\frac{2 l_u}{0.208} < 22 \dots \dots \dots (22)$$

Solving for l_u :

$$l_u < 2.3 \text{ ft (701 mm)} \dots \dots \dots (23)$$

which means that if the column height is more than 2.3 ft (701 mm), buckling may become a problem. Since the column had a 3-ft (915-mm) height, further consideration of stability was warranted.

According to the stability analysis of a column as described in AASHTO, section 8.16.5.2.7, and ACI, section 10.11.5.1, the load required to buckle a 3-ft (915-mm) column may be given by the following:

$$P_c = \frac{\pi^2 EI}{(k l_u)^2} \dots \dots \dots (24)$$

where EI is determined by AASHTO, section 8.16.5.2.7, and ACI, section 10.11.5.2, and $k l_u$ is the equivalent length. The equation for EI is:

$$EI = \frac{E_c I_g / 2.5}{1 + \beta_d} \dots \dots \dots (25)$$

where E_c is the elastic modulus of the concrete, I_g is the moment of inertia of the gross column section, and β_d is the ratio of maximum factored axial dead load to maximum total factored axial load. Since dead load of the slab is much smaller than the imposed failure load, β_d is taken to be zero as a first approximation. Therefore:

$$EI = \frac{E_c I_g}{2.5} \dots \dots \dots (26)$$

The moment of inertia for a circular column is calculated according to:

$$I = \frac{\pi r^4}{4} \dots \dots \dots (27)$$

For a column with a 10-in. (254-mm) diameter, I is calculated as 491 in.⁴ (2.04 x 10⁸ mm⁴). According to AASHTO, section 8.7.1, and ACI, section 8.5.1, the modulus of elasticity for normal-weight 5,000 psi concrete may be obtained from:

$$E_c = (145)^{1.5}(33)\sqrt{f'_c}$$

$$= 4,074 \text{ ksi (28.1 GPa)} \dots \dots \dots (28)$$

Using these numbers, Eq. 24 becomes as follows:

$$P_c = \frac{\pi^2 E_c I_g / 2.5}{(kl_u)^2}$$

$$= \frac{\pi^2 (4,074)(491) / 2.5}{[2(36)]^2}$$

$$= 1,523 \text{ kips (6,779 kN)} \dots \dots \dots (29)$$

which is much higher than the load available in the laboratory.

The axial force capacity of the column, according to AASHTO (*Standard*, 1989), section 8.16.4.1.2, and ACI (*Building* 1989), section 10.3.5.1 is:

$$\phi P = 0.85\phi[0.85f'_c(A_g - A_s) + f_y A_s] \dots \dots \dots (30)$$

where A_g is the area of the column, A_s is the area of reinforcing steel, and f_y is the yield strength of reinforcing steel. For the Model One column, A_g was 78.5 in.² (50,700 mm²), and f_y was 60 ksi (413 MPa). With 10 No. 4 (12.7 mm) reinforcing bars, A_s was 2.0 in.² (1,290 mm²). From AASHTO, section 8.16.4.1.2, and ACI, section 9.3.2.2, ϕ for a spiral reinforced column is 0.75. From these numbers, the ultimate load P is:

$$0.75P = 0.85 \times 0.75 \times [0.85 \times 5 \times (78.5 - 2.0) + 60 \times 2.0]$$

$$0.75P = 284 \text{ kips (1,264 kN)}$$

$$P = 378 \text{ kips (1,682 kN)} \dots \dots \dots (31)$$

Therefore, the column would provide adequate axial and stability support for the model.

2.9 Pickup Points and Safety Cables

As described earlier, the prototype slab simply rests on a neoprene pad mounted on top of each column. Likewise in the model, column and slab are connected by a straight No. 4 bar which protrudes from the concrete column into a

short piece of PVC pipe embedded in the bottom of the slab. To avoid accidents caused by unintentional overturning moments, the slab was tied to the pedestal by four safety cables (Fig. 11). Under eccentric loading, tension in one or more of the cables would keep the slab from tipping. When downward vertical load was applied symmetrically, the cables would relax and not carry any load. Under uniaxial tension, a sample of the safety cable failed at 3.3 kips (14.7 kN), which provided enough strength to restrain the slab for test preparation and data acquisition. In order to facilitate tightening of the cables, a turnbuckle was inserted between each cable and the slab connection.

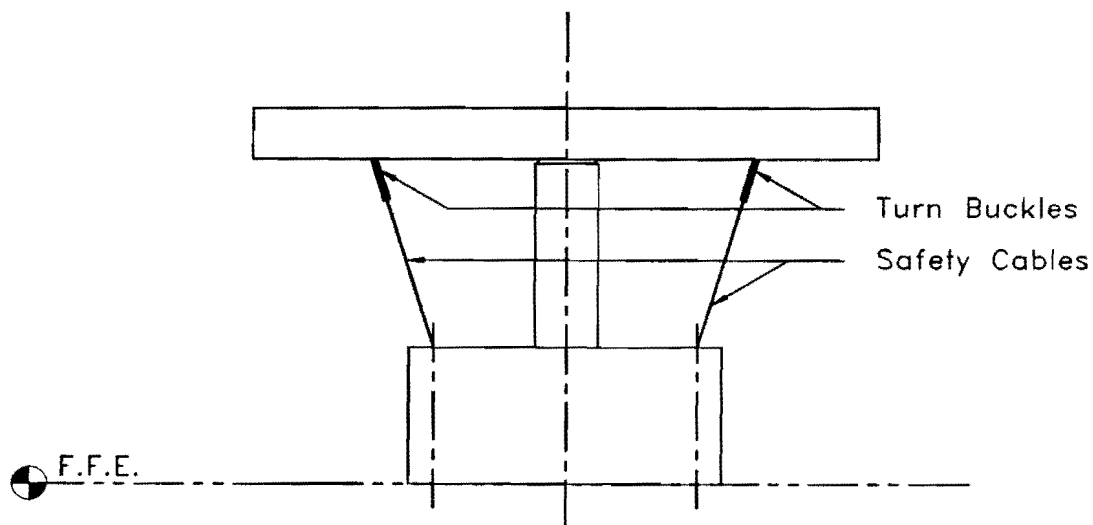


FIG. 11. Safety Cables

When the slab was placed on top of the column and the safety cables were drawn taut, the structure was found to be reasonably stable. However, strain gage readings started to give unreasonably high values. When the turnbuckles were loosened, gage readings returned to normal. Thereafter, turnbuckles were tightened whenever personnel presence was required atop the slab and loosened whenever strain gage readings were taken.

Pickup cables, used to attach crane hooks and lift the slab, were located directly above the anchor connections for the safety cables. Connections themselves were made from 5-ft (1.53-m) long pieces of safety cable looped several times between top and bottom re-bars (Fig. 12). Anchors were located at the corners of a 5.4-ft (1.65-m) concentric square. These locations were determined as optimum for minimization of stresses in the slab from prior research (Tiv 1987).

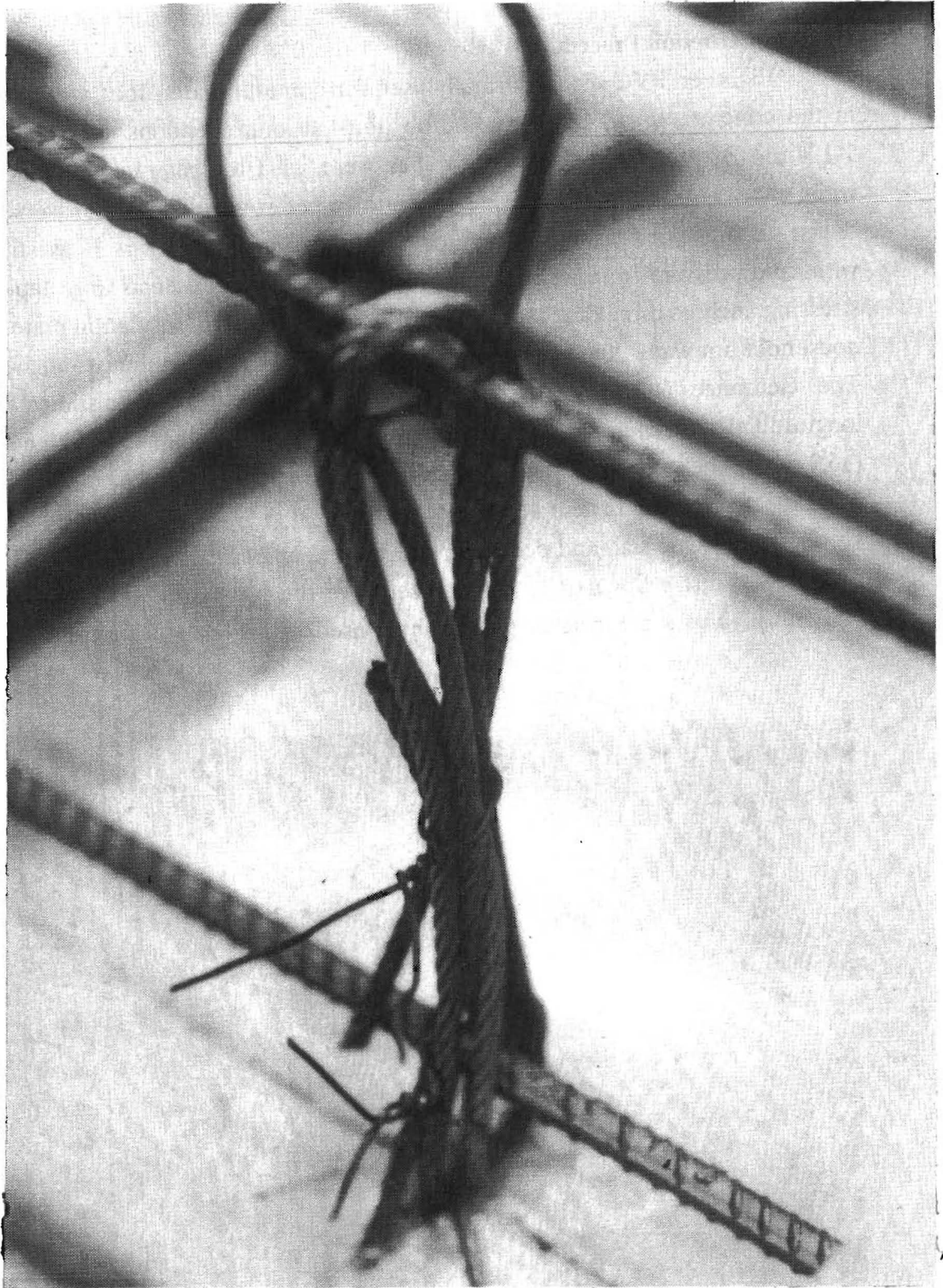


FIG. 12. Pickup Point

2.10 Construction Procedure

Eighteen PVC pipes, normally used for domestic water lines, were embedded in the concrete to act as ducts for the post-tensioning tendons. A series of nine 1-1/4-in. (32-mm) inside diameter pipes were used as longitudinal tendon ducts, while nine 3/4-in. (19-mm) inside diameter pipes were used as transverse tendon ducts. PVC material was chosen for cost and availability, as well as strength to withstand pressure from wet concrete. Longitudinal tendon ducts were taped to the stressing anchors using duct tape (Fig. 13). A short length of insulation material for a household hot water line was used to center each PVC pipe within its anchor cavity. The clearance and PVC pipe thickness forced the vertical distance between longitudinal and transverse tendons to be slightly more than the designed 0.6 in. (15.2 mm). The average distance of the tendons from the top of the column, however, was expected to remain near 4.2 in. (107 mm).

Model One slab and pedestal were poured on September 15, 1988, along with 24 concrete test cylinders. Due to presence of the plasticizer, the slump was 6 in. (152 mm). The same type of plastic sheet used to line the formwork was used to

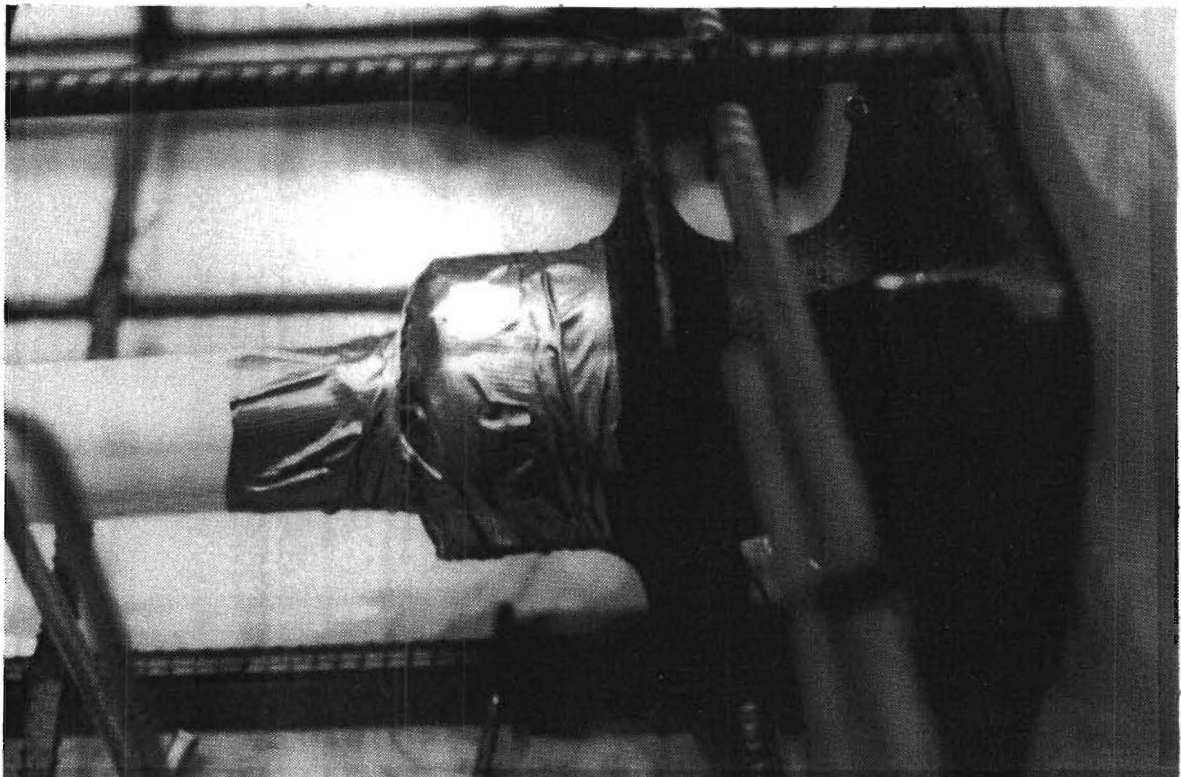


FIG. 13. Longitudinal Tendon Duct

cover the slab immediately after pouring. A temporary mortar dyke was made on the perimeter of the slab to allow water to be poured on top of the concrete. Water was added to the pond for 14 days to ensure adequate curing of the slab. Increase in concrete capacity as measured by cylinder tests is shown in Fig. 14.

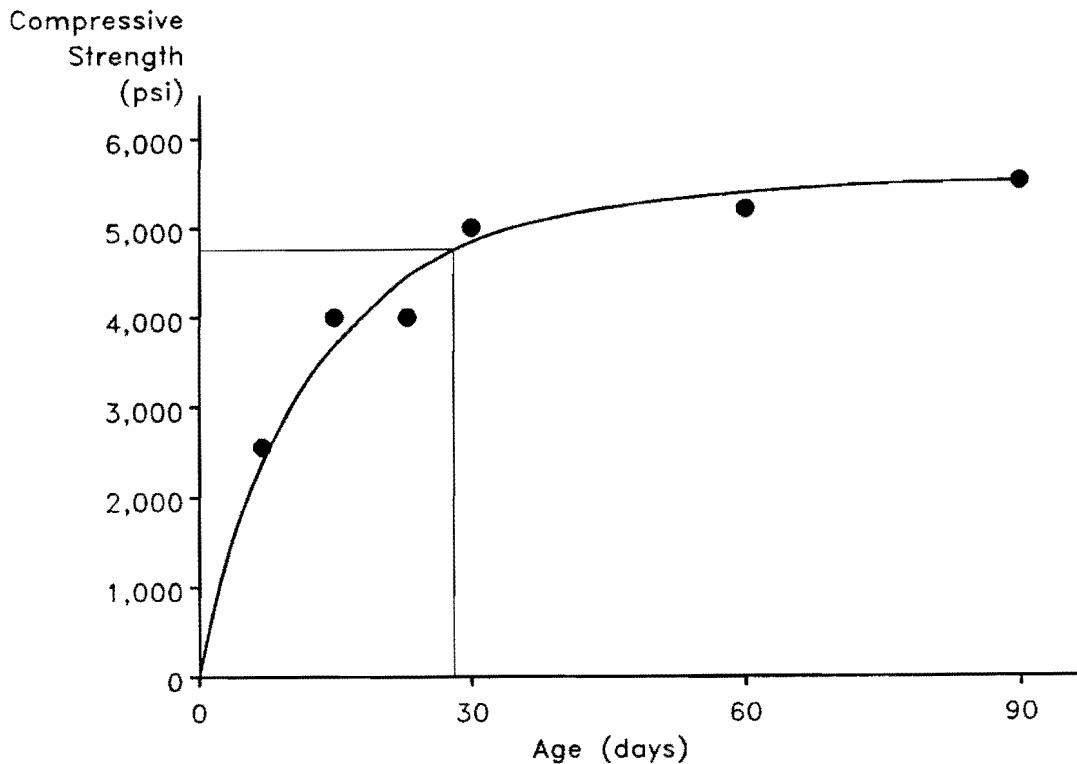


FIG. 14. Result of Concrete Cylinder Tests

Prestressing jacks arrived at the laboratory on October 19, 1988. A practice session for use of jacks was conducted under supervision of a representative from the VSL Corporation so that the jacks could be operated safely. Longitudinal tendons were stressed on November 20, 1988. Strain gage readings were taken at the same time in order to test instrumentation and data acquisition procedures. The first two tendons, the central tendon and one adjacent to it, were each elongated to 17/32-in. (13.4-mm) to obtain a force of 84 kips (374 kN) each. After anchors at the jacking end were allowed to set, shims were inserted to restore the 84-kip (374-kN) force. After anchor set was consistently found to be 1/4 in. (6.4 mm), subsequent tendons were stressed to 25/32-in. (19.8-mm) elongation to obtain a force of 123.9 kips (551 kN) before anchor set losses. This reduces to the desired 84-kip (374-kN) force after anchor set. Maximum temporary stress was 202.5 ksi (1.4 GPa), which was

within the AASHTO- and ACI-prescribed limits as described earlier. The stressing sequence, which started with the central tendon and moved outward, approximated actual construction procedures in the Taft Boulevard bridge. Unlike the actual bridge, however, the tendency for concrete to burst at the anchors was not observed in Model One.

The actual bridge has two additional transverse tendons near the ends of the slab in the longitudinal tendon anchor area to avoid the possibility of concrete bursting. In Model One, visual observation could not locate any cracks in the concrete after post-tensioning.

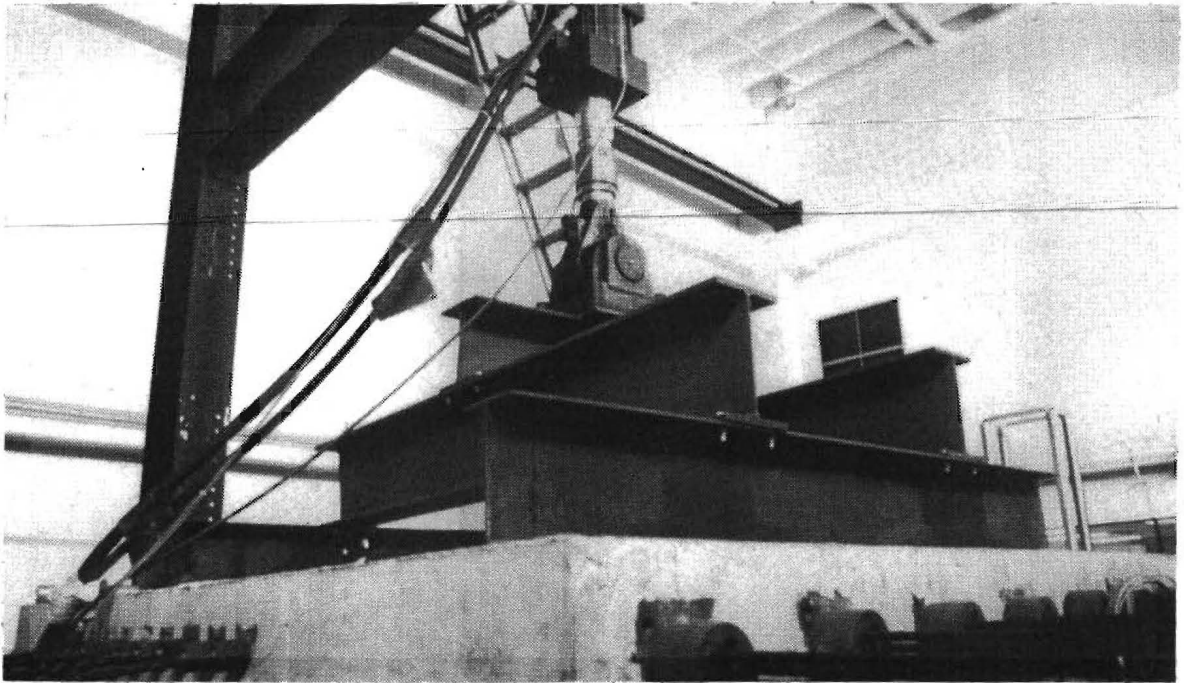
After completing longitudinal prestressing, the slab was hoisted into place on the column on November 23, 1988. On November 29, 1988, a W24 x 117 steel beam was attached to two W14 x 61 steel columns to form an overhead loading frame. A 110-kip (490-kN) actuator was then placed onto the beam by means of a specially fabricated adaptor plate. After testing operation of the actuator, a loading square, made of W10 x 39, W12 x 45, and W10 x 22 beams, was attached to the bottom of the actuator (Fig. 15).

Transverse tendons were placed loosely in the ducts while the slab was on the floor. As described earlier, the 0.6-in (15.2-mm) monostrand tendons were stressed by a VSL jack suspended from the overhead crane (Fig. 16).

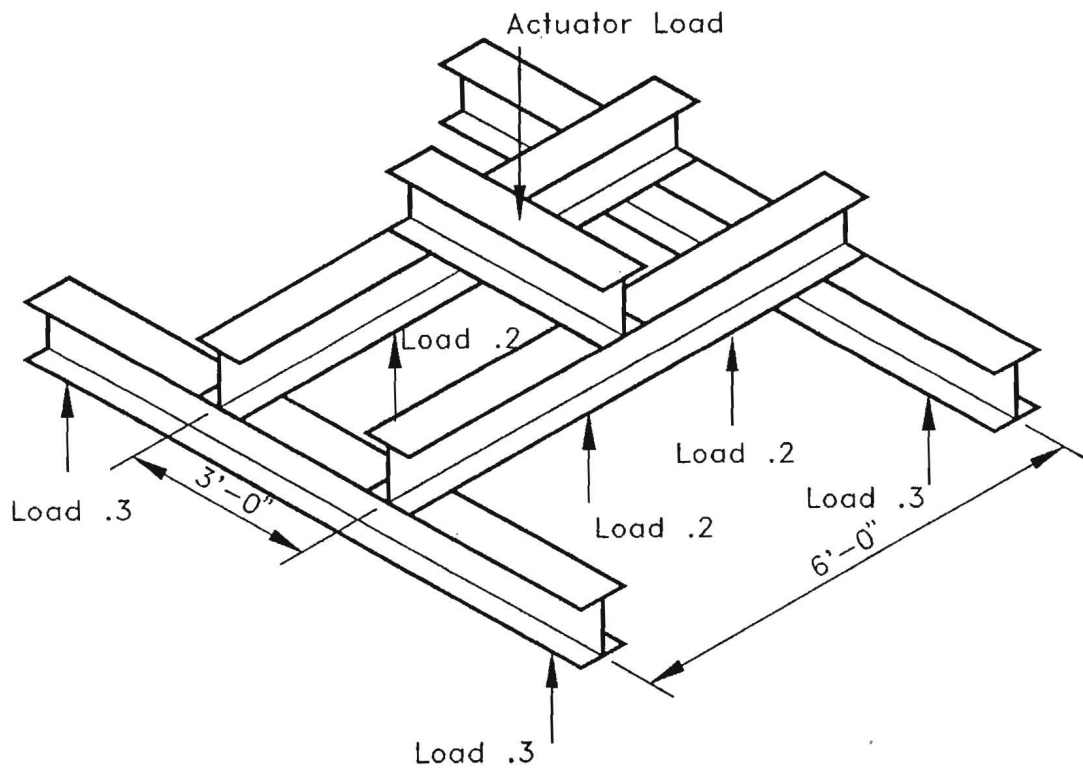
2.11 Instrumentation

Strain in the slab was measured by 6-mm gage length, 120- Ω , type FLA-6 foil strain gages manufactured by Tokyo Sokki Kenkyujo Co., LTD, which were attached to the reinforcement bars (Fig. 17). A total of 88 gages were placed in 24 locations (Fig. 18). At each location, gages were placed in longitudinal and transverse directions on top and bottom re-bars, with exceptions in the neighborhood of the longitudinal anchors, where gages in the transverse direction were omitted. Each pair of top and bottom gages measured differential strain at two elevations, which could be used to compute internal tractions and be readily related to numerical simulation.

Vertical deflections were measured by 2-in. (50.8-mm) stroke, DC-DC, linear variable differential transformers (LVDTs), which have Model No. 0245-0000, and are manufactured by Trans-Tek, Inc. (*Displacement* 1984). The LVDTs have internal signal conditioning units designed so that both input and output use direct current. This feature greatly simplified signal-conditioning requirements. Thirteen LVDTs, each attached to a base as shown in Fig. 19b, were placed beneath the slab in an array as shown in Fig. 20. Two LVDTs were attached directly to the column by duct tape in order to measure compression of an elastomeric bearing pad (Fig. 19a). Readings

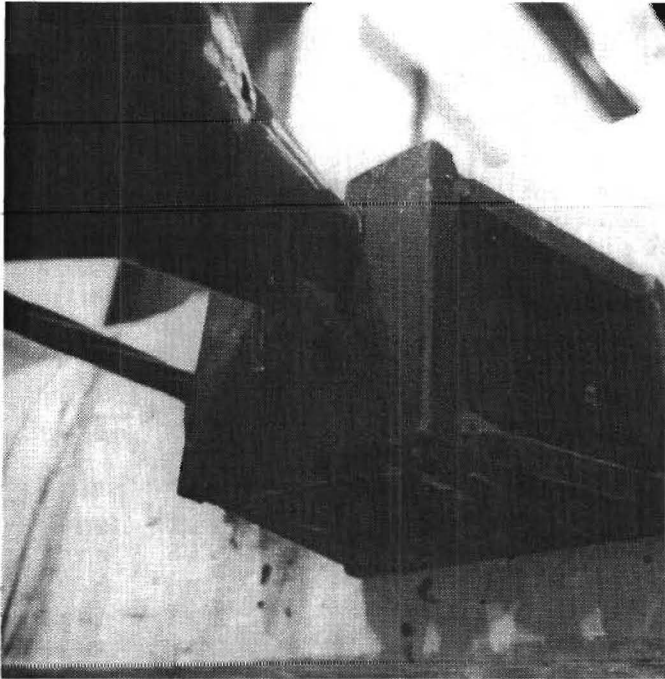


(a)

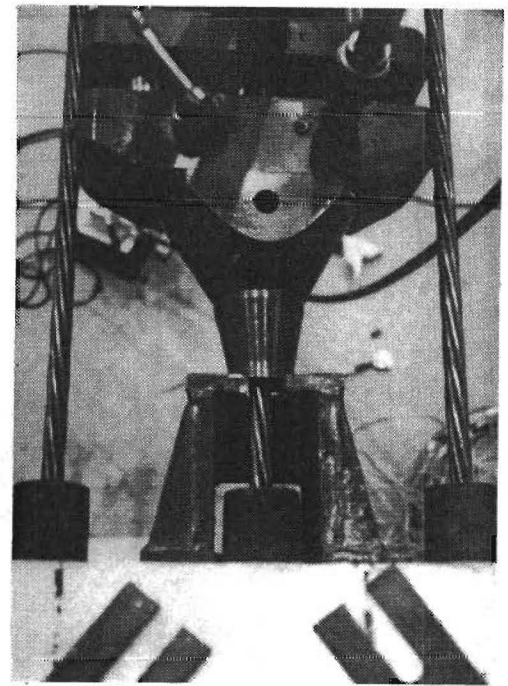


(b)

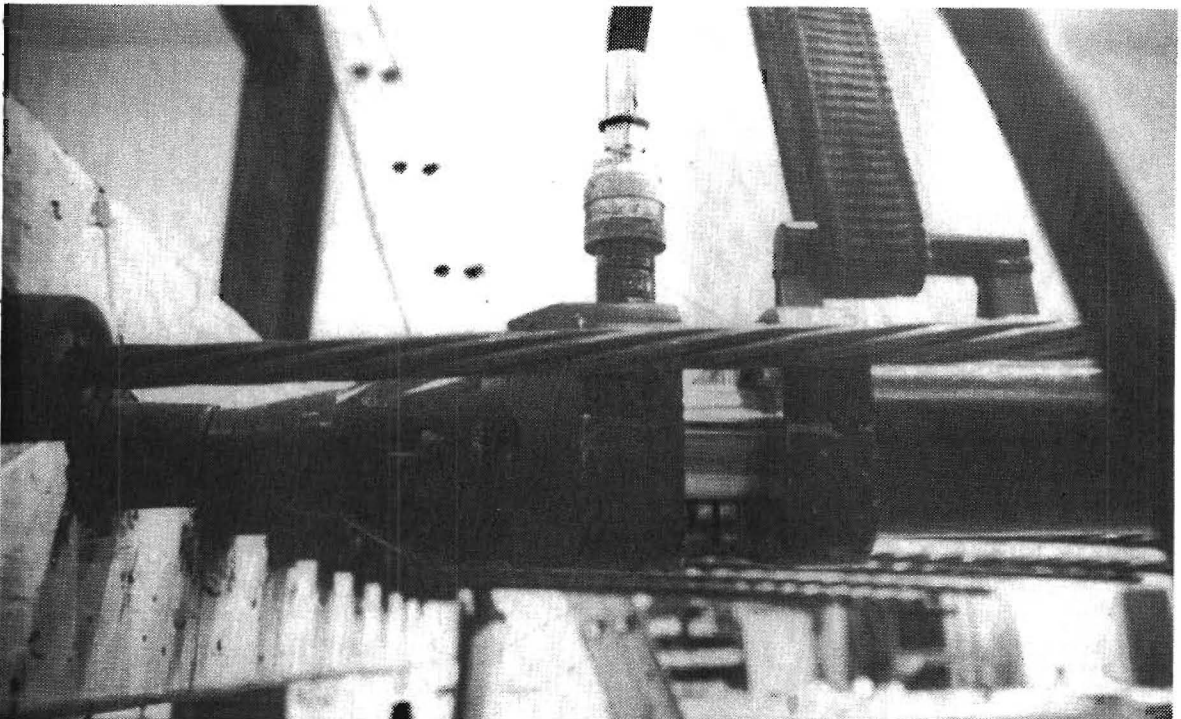
FIG. 15. Loading Square. (a) Installed; (b) Schematic



(a)



(b)



(c)

FIG. 16. Transverse Tendon Jacking. (a) Bottom View with Chair; (b) Top View with Chair and Shims; (c) Side View

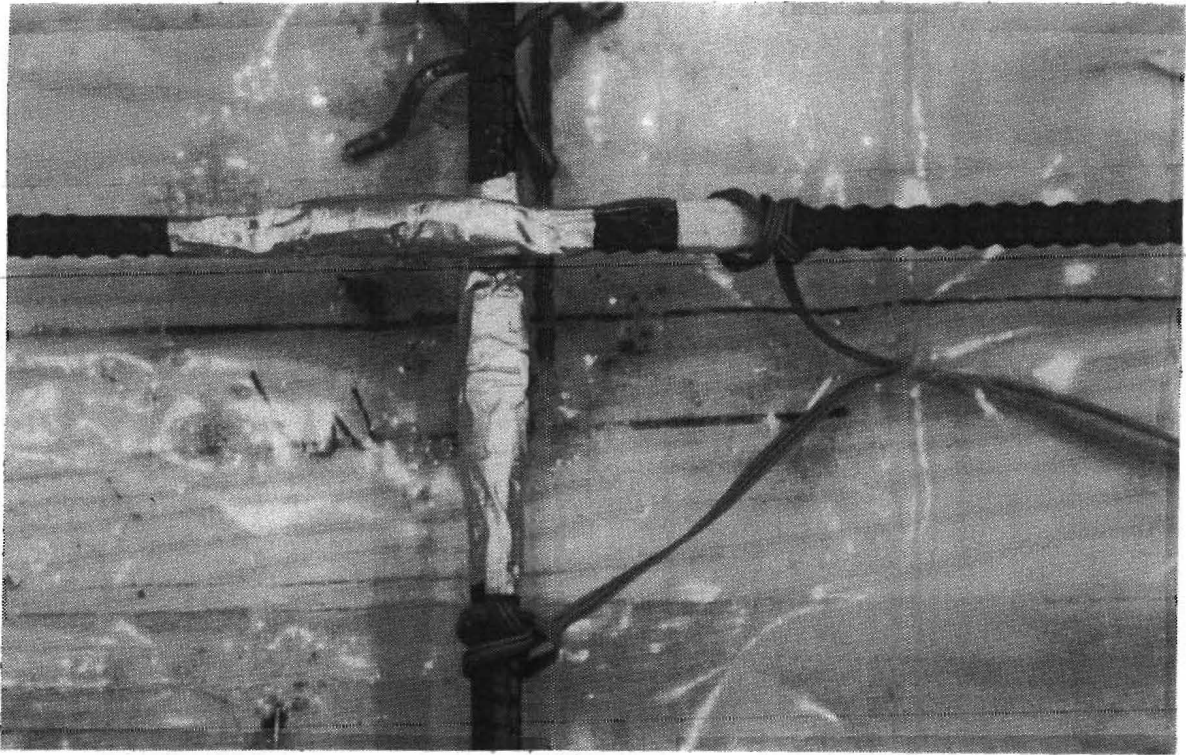
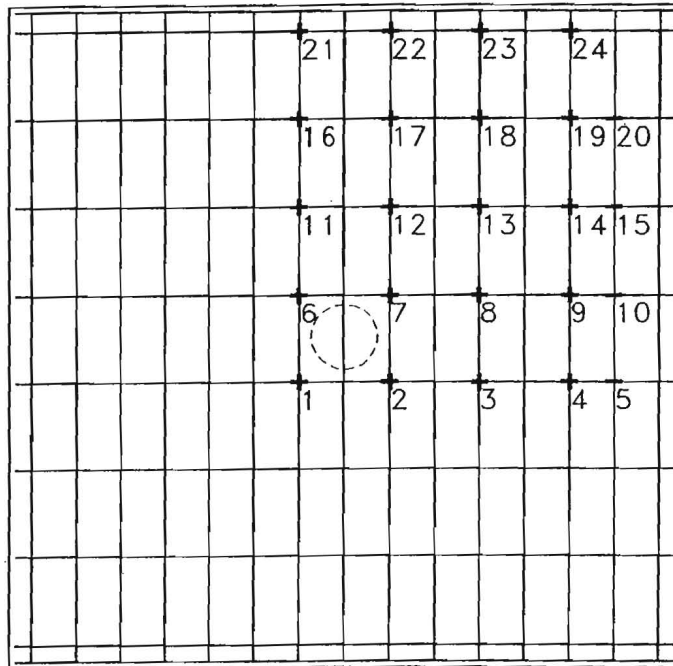


FIG. 17. Installed Strain Gages



Longitudinal Direction →

FIG. 18. Strain Gage Locations

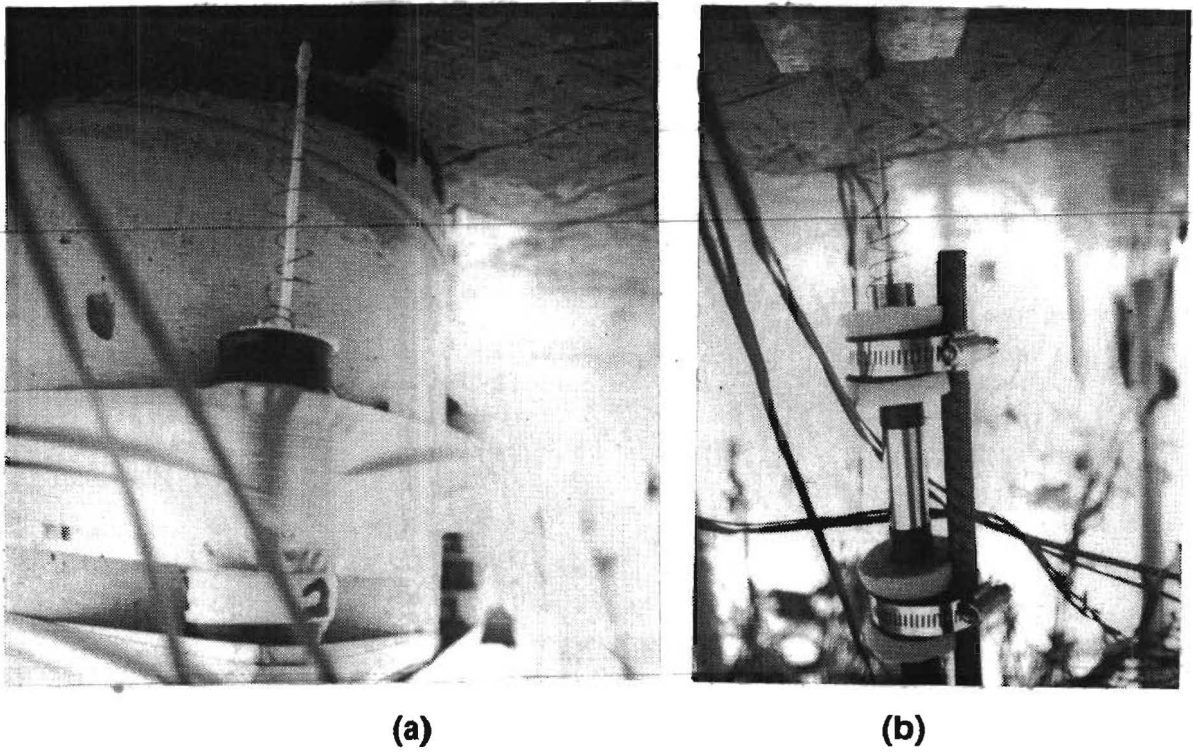


FIG. 19. Installed LVDTs. (a) Attached to Column; (b) On LVDT Stand

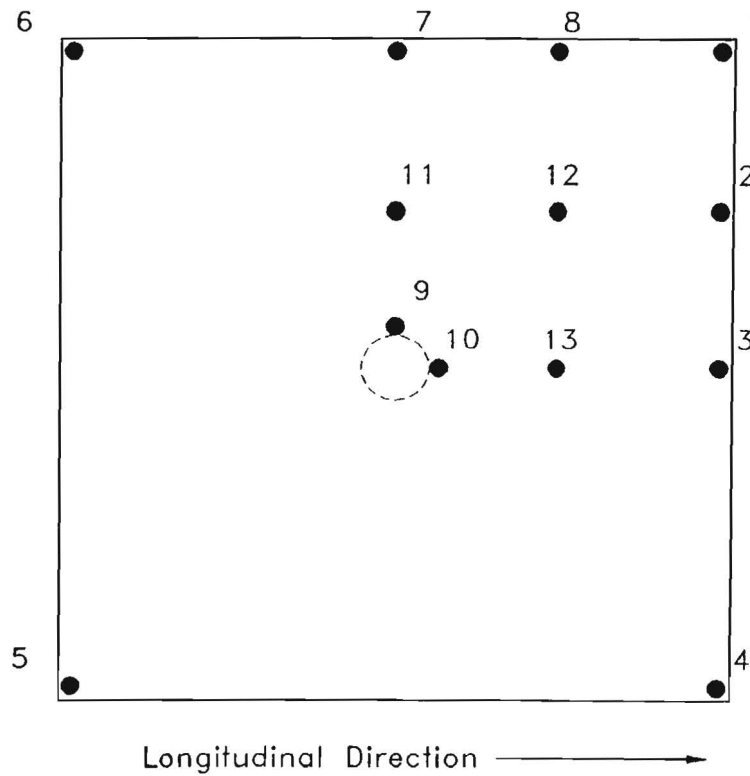


FIG. 20. LVDT Locations

from LVDTs on the column were used as reference values so that the reading of each of the other LVDTs would show a true relative deflection after the amount attributed to elastomer compression was subtracted. The LVDT itself has a negligible reactive force, especially when compared with the large force required to deflect the slab.

The load was applied according to a single digital value displayed on the MTS actuator control panel. In order to determine distribution of the total load, four 50-kip (223-kN) load cells, manufactured by AL Design, Inc., were placed at load points on the slab. This load data enabled more accurate analysis of applied force.

Data was collected through a Hewlett-Packard 3497A data acquisition unit and sent to a microcomputer for analysis and interpretation. The HP unit had three 44427A strain gage cards, each with 10 channels, which offered a total of 30 channels for the unit. In order to read 88 gages, 25-pin RS-232 connectors were switched manually. Data was read into the computer using Lotus Measure (1986) and placed in a Lotus 1-2-3 spreadsheet (1986). A schematic of the data acquisition system is shown in Fig. 21.

2.12 Elastic Loading Procedure

As described earlier, test loads were applied to the model slab by one 110-kip (490-kN) actuator which was attached to a load frame as shown in Fig. 15. The loading square facilitated changes in load pattern application. The load schedule outlined in Fig. 22 enabled strain distribution determination for a variety of tendons and loading patterns. Use of the loading square eliminated movement of the actuator for each load configuration, thereby decreasing laboratory preparation time.

The first digit of each load phase in Fig. 22 designates the number of the tendons stressed, while the second number designates the load configuration for the particular number of stressed tendons. For example, Load 5.2 means that five transverse tendons are stressed and the second load case is specified, namely a 3 ft x 3 ft (914 mm x 914 mm) square pattern.

Loads 0.1 through 0.3 were used as reference cases for the remaining load phases so that changes in strains due to addition of tendons could be studied. After preliminary computations by computer program NOPARC, the magnitude of applied loads 0.2 through 9.3 was assigned to be a total of 20 kips (89 kN), which ensured that strains remain in the elastic range. This computation is discussed in a later section.

According to similitude, this is equivalent to 222 kips (989 kN) on the prototype bridge, which is about 3 times that of a 72-kip (320-kN) HS-20 truck, as specified by AASHTO (*Standard* 1989).

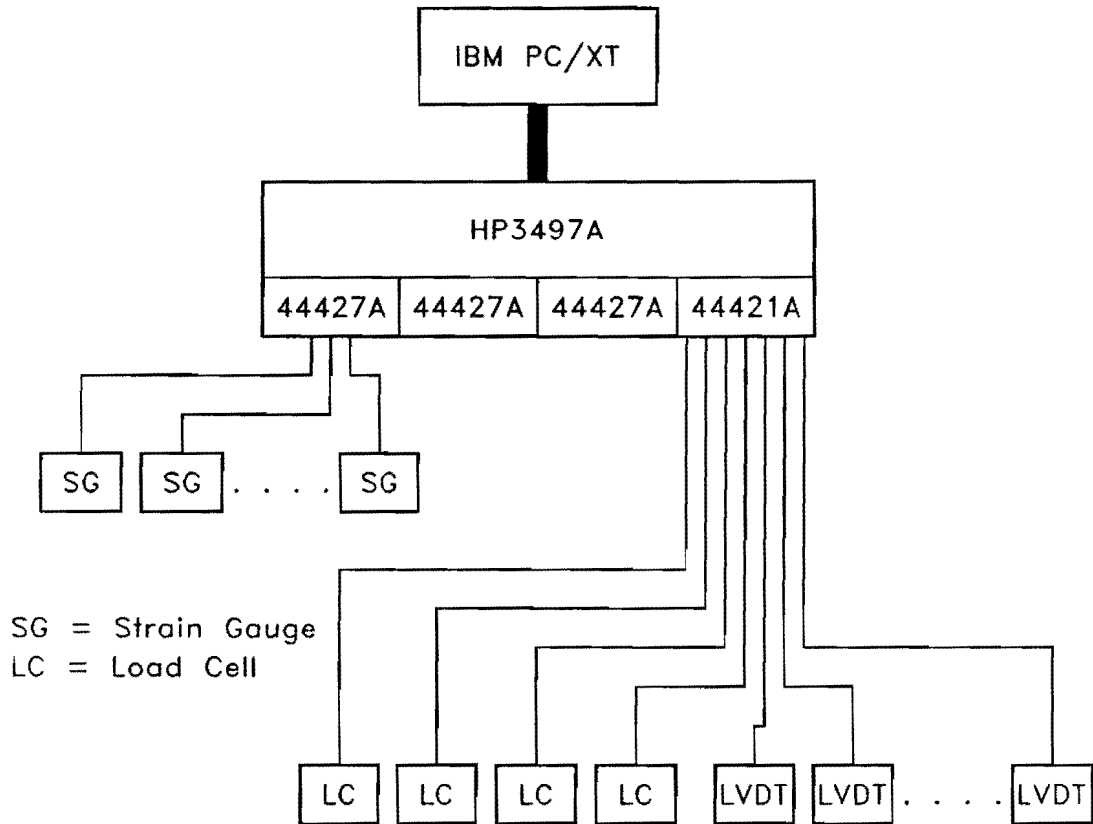


FIG. 21. Data Acquisition Schematic

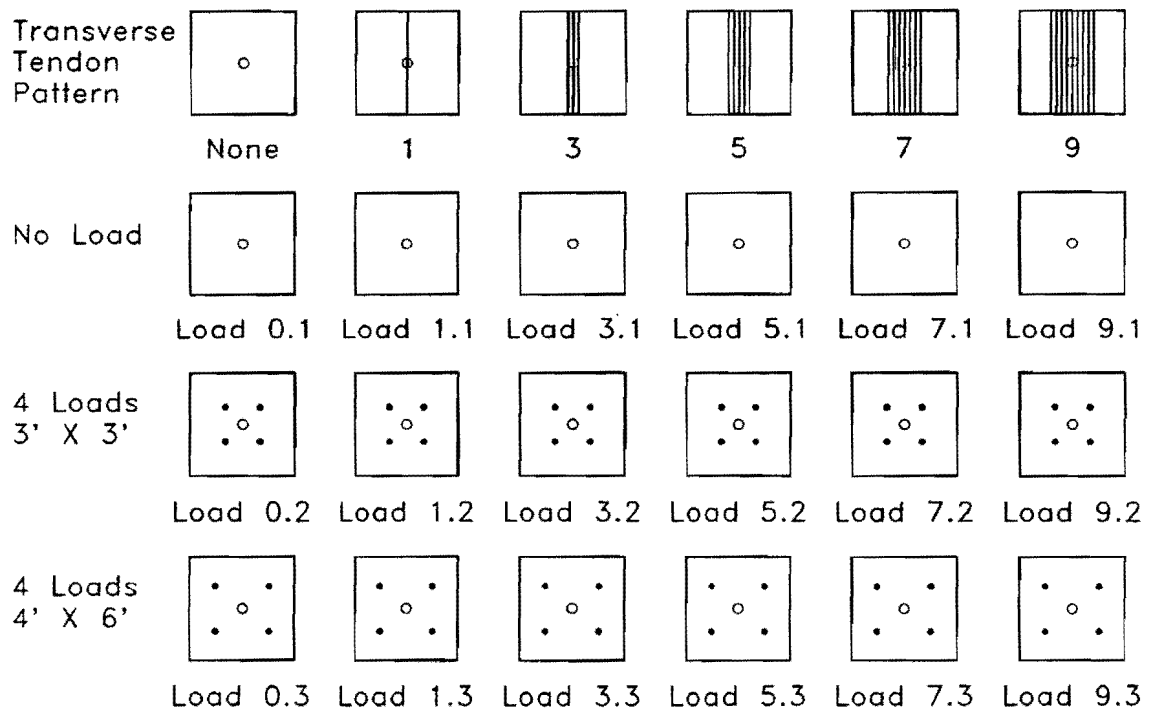


FIG. 22. Elastic Loading Schedule

One load configuration that has no live load applied to the slab is included for each tendon pattern. This case serves as a reference to determine the effect of transverse tendons acting alone and also as a basis for comparison with the effect of applied live loads. These patterns are designated as load series 0.1 through 9.1.

Loads 0.1 through 0.3 serve as reference cases for the remaining load phases so that changes in concrete strains due to addition of tendons may be studied. Based on results of preliminary finite element method (FEM) computations, the actuator load for cases 0.2 through 9.3 is specified to be 20 kips (89 kN), which ensures that strains remain well within the elastic range.

One load configuration that does not have a live load applied normal to the slab is included for each tendon pattern. This case provides a reference to determine the effect of transverse tendons acting alone, and also as a basis for comparison with the effect of applied live loads. These patterns are designated as load series 0.1, 3.1, 5.1, 7.1, and 9.1. Loads in the series 0.2 through 9.2 are applied at the corners of a 3-ft (914-mm) square which is concentric with the column. This series applies loads near the column in order to limit moment in the slab and increase the relative contribution of shear forces. Finally, 4 loads, placed in a rectangular formation of 4 ft (1.22 m) by 6 ft (1.83 m), are applied in load series 0.3 through 9.3. This step induces behavior of the slab under application of larger bending moment.

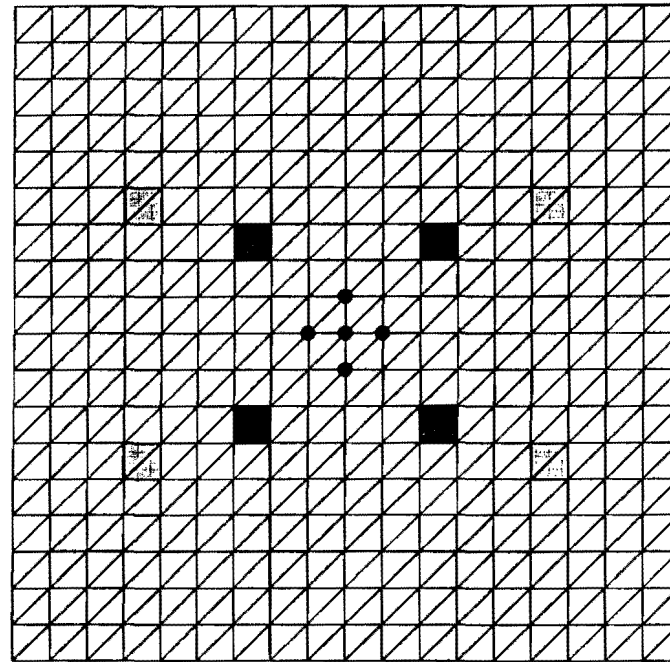
After an initial practice series, load cases 1.1 through 9.3 were applied to the slab through the load frame on January 17-18, 1989. Major difficulties during the actual test lay in equalizing forces at the 4 load points. After trial and error during load phases 0.2 and 0.3, each load point came to within 500 lbs (2.23 kN) of its target magnitude of 5 kips (22.3 kN).

III. NUMERICAL SIMULATION

Experimental and numerically simulated strains are compared for each elastic loading pattern in order to validate the computer program. The FEM code is run in a nonlinear geometric and material mode, with a 361-node, 648-element mesh, as shown in Fig. 23a. Each finite element is divided into 10 concrete layers and 4 steel layers as shown in Fig. 23b. Boundary conditions on 5 nodes are designed to simulate column support of the slab. The program is capable of using only constant-stress triangles and does not consider transverse shear deformation. This shortcoming is not critical for typical bridge structures, where moment capacity is of prime concern. It does, however, preclude use of the code for prediction of ultimate punch-through capacity of the column.

Program output locations do not precisely coincide with the actual gage locations. Strains are averaged from the three integration points of the finite element that contains the gage location. Deviations of location for strain gages in the actual slab from their intended locations, as shown in Fig. 18, are also a consideration; gages in the laboratory slab are not located precisely at the intersection of reinforcing bars but are adjacent to the intersection (Fig. 17). Despite these differences, discrepancies between gage locations in the slab and their numerical counterparts are minimal. The computer program was custom-formatted for Model One so that strain output is printed only for the elements that contain gage locations. Some of the output data are processed using the PATRAN Plus graphics software (*Patran* 1988), so that distribution of results, such as strain, can be evaluated visually.

NOPARC runs on a Digital Equipment Corporation VAX 8800/8650 machine under a VMS operating system and on an IBM Model 80 personal computer at Texas A&M University. The personal computer runs under the OS/2 operating system, version 1 (*Operating* 1988), so that memory capacity is not limited to 640 kilobytes as it is with the DOS operating system. NOPARC is compiled using the Microsoft FORTRAN 4.1 Compiler (*Microsoft* 1987) for use with OS/2. For a typical problem in this study, the mainframe VAX computer takes approximately 8 minutes of central processing unit time, and 2-3 hours of elapsed time. Elapsed time on the 32-bit microcomputer is approximately 2 hours, which is comparable to that of the mainframe computer. Naturally, complexity of a particular problem affects computer time. A small problem may be solved in a few minutes, whereas an extremely complex problem may take more than a day of CPU time.

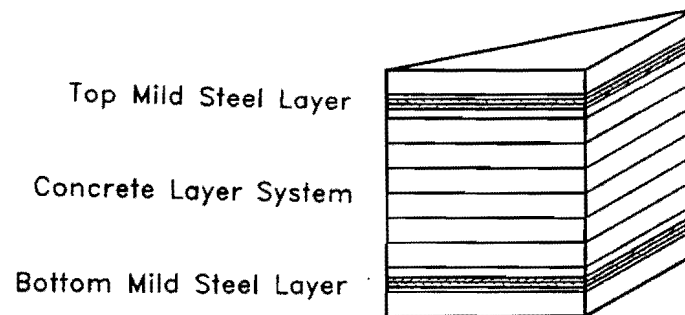


Longitudinal Direction →

- Boundary Elements
- ▲ Loaded Element for 3'X3' Load
- ▴ Loaded Element for 4'X6' Load

Note: 1' = 304.8 mm

(a)



(b)

FIG. 23. Finite Element Model. (a) Mesh for Model One; (b) Element Layers

Various trial loads are applied to the finite element mesh, which simulates a slab supported by a column, before magnitudes of loads are chosen to be applied to the laboratory model. As an example, consider Load 0.3. In this case 20 kips (89 kN) of force is applied in small increments at each of the four loading points of the computer model. In order to maintain service load conditions of the reinforced concrete, load is distributed to four 5-kip (22.3 kN) loading points. According to AASHTO, section 8.15.2.1.1, and ACI code Appendix A, concrete may be used for service loads until stress reaches 40 and 45 percent, respectively, of compressive strength, f'_c . Because the actual 28-day strength was not known during the preliminary design, the design value of 5,000 psi (34.5 GPa) is used for f'_c . The actual compressive capacity is smaller than the design capacity by 4 percent (Table 2). Using the design elastic modulus of 4,074,000 psi (28.1 GPa) as found in Eq. 28, temporarily neglecting two-way action, and applying a guideline from ACI code section A.3.1 (*Building* 1989), the maximum permissible strain is approximated as:

$$\begin{aligned} \epsilon_{\max} &= \frac{0.45f'_c}{E_c} \\ &= \frac{0.45 \times 5,000}{4,074,000} \\ &= 552 \times 10^{-6} \dots \dots \dots (32) \end{aligned}$$

Computer analyses predict that the total applied load of 20 kips (89 kN) results in maximum strain not exceeding 400 microstrains as shown in sample data files (Appendix V). This level of strain is below allowable AASHTO and ACI service load limits.

In order to simulate the application of concentrated loads through load cells and their bearing plates, an equivalent surface load was applied over the two triangular elements that form a 6-in. (152-mm) square at each load point location. This simulates the actual loading more accurately than nodal point loads, because loads on the slab in the laboratory are applied by means of 6-in. (152-mm) square steel plates.

IV. RESULTS OF LINEAR ELASTIC LOAD TESTING

Data collected from laboratory testing is compared to numerical predictions. After laboratory results are determined to support computer predictions with reasonable accuracy, further analysis and discussion are based on computer models. Computer results allow more involved presentation of effects in the slab, as shown in many of the figures in this section. Strain values predicted by the computer program are tabulated and compared to the actual strain gage data collected (Tables 5-23, Appendix III). Locations without a gage are indicated by a blank entry, and damaged gage locations are shown by a dash in the tables. To avoid confusion between abbreviations for "Top" and "Transverse," "X" and "Y," respectively, are used to indicate longitudinal and transverse directions, and "B" and "T," respectively, indicate bottom and top reinforcing bar layers.

4.1 Deflection of Laboratory Model

Readings were obtained from LVDTs for deflection measurement. During testing of a similar single-column slab, Gerber and Burns (1971) took deflection measurements throughout the loading cycle, but downplayed the significance of the deflection data because of a stability problem. Since the slab portion of Model One simply rested on a column pedestal, tilting, which Gerber and Burns refer to as a stability problem, occurred at a very low load and resulted in inaccurate readings. The slab also showed a tendency to rotate about the vertical axis under applied load, which further impaired the LVDT readings.

FEM predicts downward displacement of 0.0307 in. (0.780 mm) at the slab corners relative to the center support due to longitudinal tendon eccentricity and dead load; displacement only increases slightly with the addition of transverse tendons. Regardless of the number of transverse tendons, 3 ft x 3 ft (914 mm x 914 mm) and 4 ft x 6 ft (1.22 m x 1.83 m), 20-kip (89-kN) loads normal to the slab induce numerically predicted deflections in the 0.005-in. (0.0127-mm) to 0.013-in. (0.330-mm) range. As a consequence, analysis of displacement data was not emphasized.

4.2 Strains of Transverse Tendons and Elastic Loading

Strains obtained from transducers show discrepancies over time; Hewlett-Packard (*Operating* 1981) predicts as much as a 56-microstrain deviation from strain gage aging alone for a quarter-bridge configuration placed for 6 months. In order to

minimize effects of strain gage drift due to unexpected time-dependent factors, gage readings for elastic loadings are referenced to gage readings measured on January 17, 1989. They are then added to the strain values taken just after placing the slab for the first time on the column on November 23, 1988. Since this process neglects the time-dependent effects on the laboratory model as well as drift in strain gages, the computer program is run without time-dependent factors. Results of these simulations are tabulated in Tables 5-23 in Appendix III and graphically represented in Figs. 24-30. Tables 5-23 summarize strain and internal moment at each strain gage location obtained from laboratory and numerical results for each load case outlined in Fig. 22. Figs. 24-30 graphically summarize and compare the strains at each gage location obtained from laboratory and numerical results for each load case of Fig. 22. Numerical predictions are represented by lines in Figs. 24-30, and laboratory results are shown by data symbols. Table 5 and Fig. 24 present results of longitudinal prestressing before the slab was placed on the column.

Tables 6-23 and Figs. 25-30 show results of transverse tendons being stressed and a 20-kip (89-kN) vertical load being applied in accordance with the load schedule in Fig. 22. Tables 6-8 and Fig. 25 present three load cases with no transverse tendon. Likewise, Tables 9-11, 12-14, 15-17, 18-20, and 21-23, in conjunction with Figures 25, 26, 27, 28, 29, and 30, present three load cases with one, three, five, seven, and nine stressed transverse tendons, respectively.

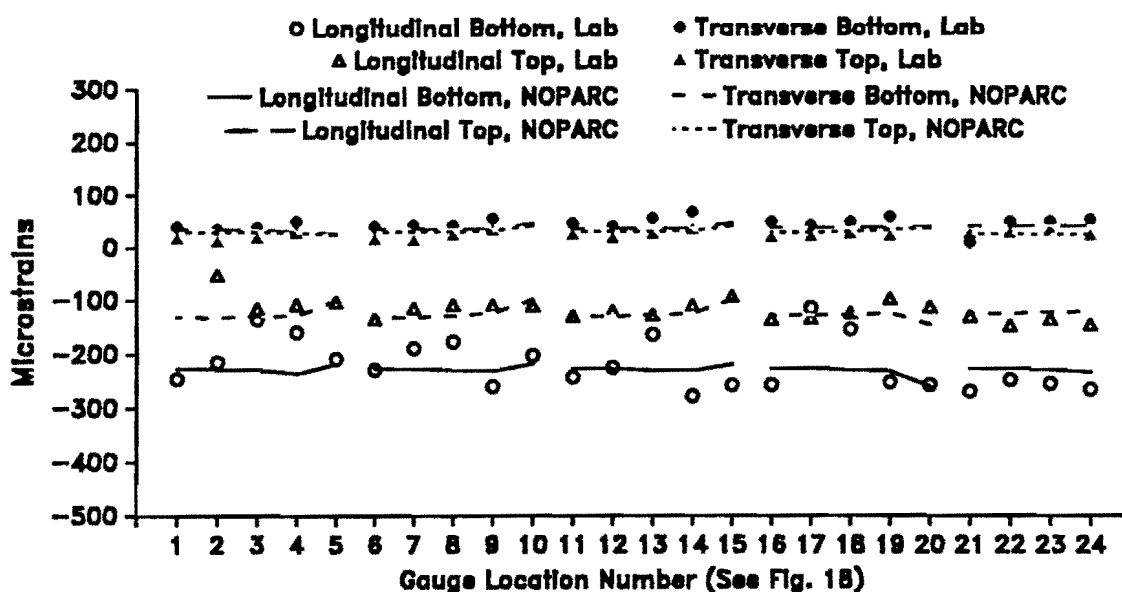


FIG. 24. Strains with Longitudinal Tendons before Placement on Column

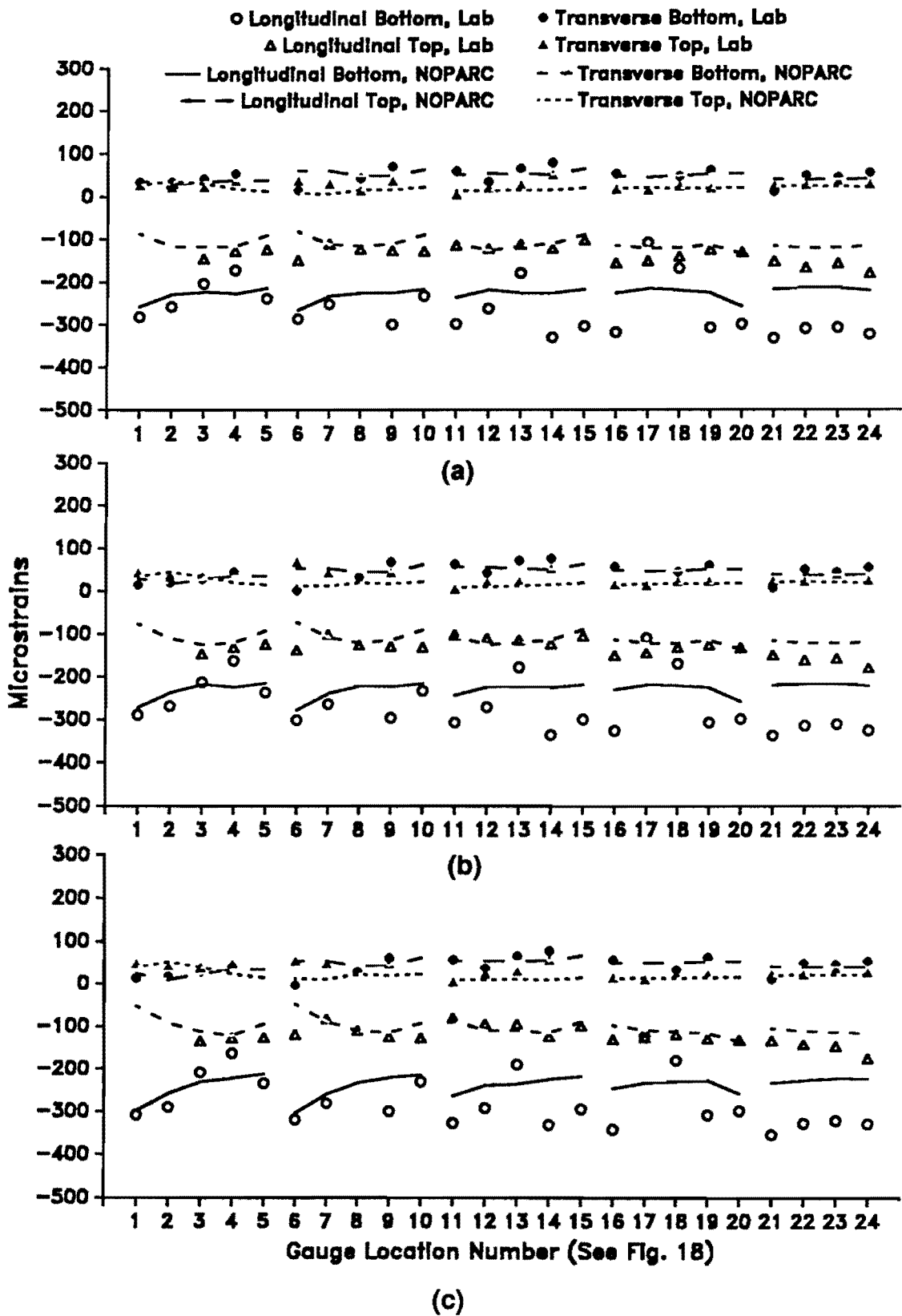


FIG. 25. Strains with No Transverse Tendon. (a) Load 0.1; (b) Load 0.2; (c) Load 0.3

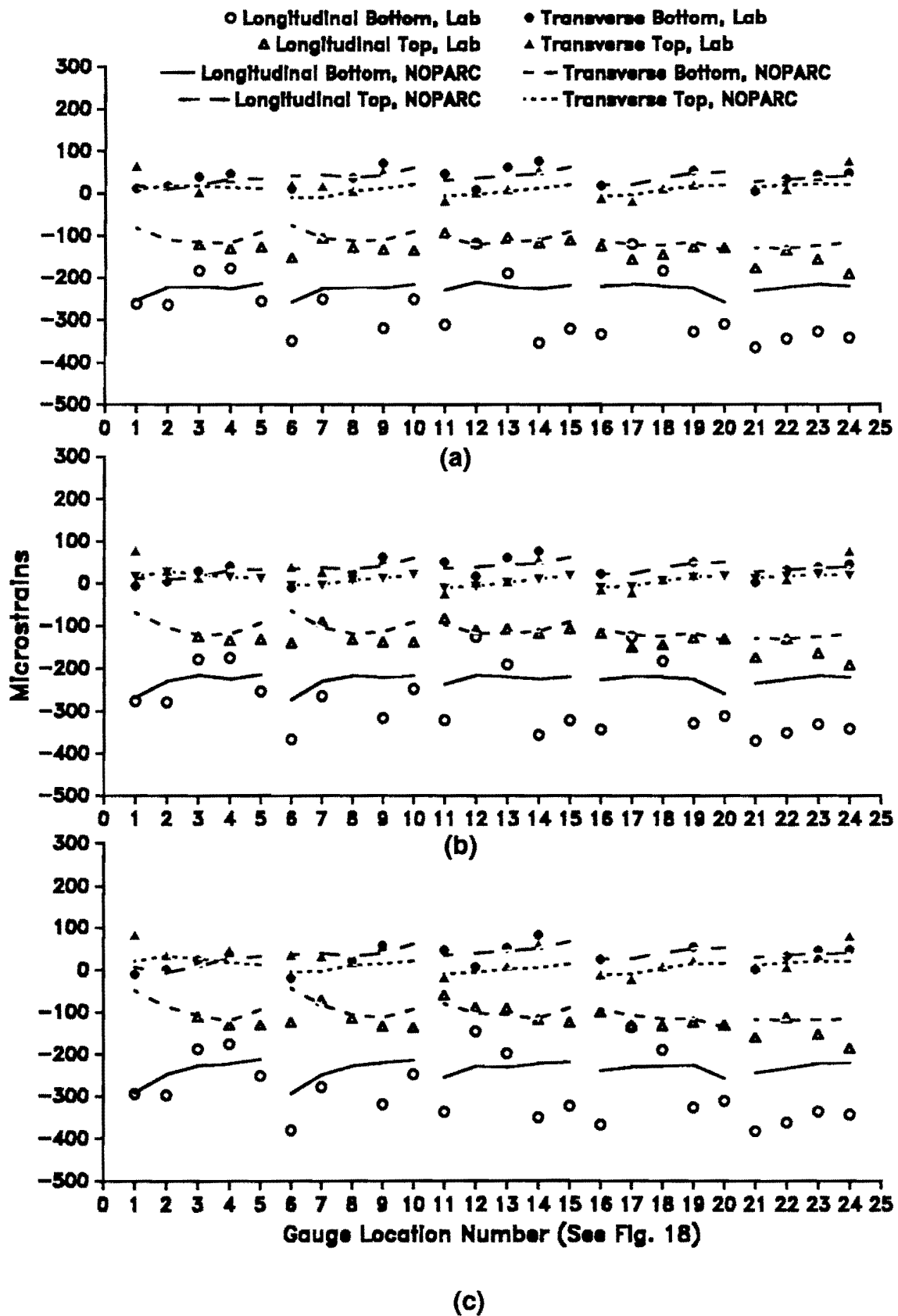


FIG. 26. Strains with One Transverse Tendon. (a) Load 1.1; (b) Load 1.2; (c) Load 1.3

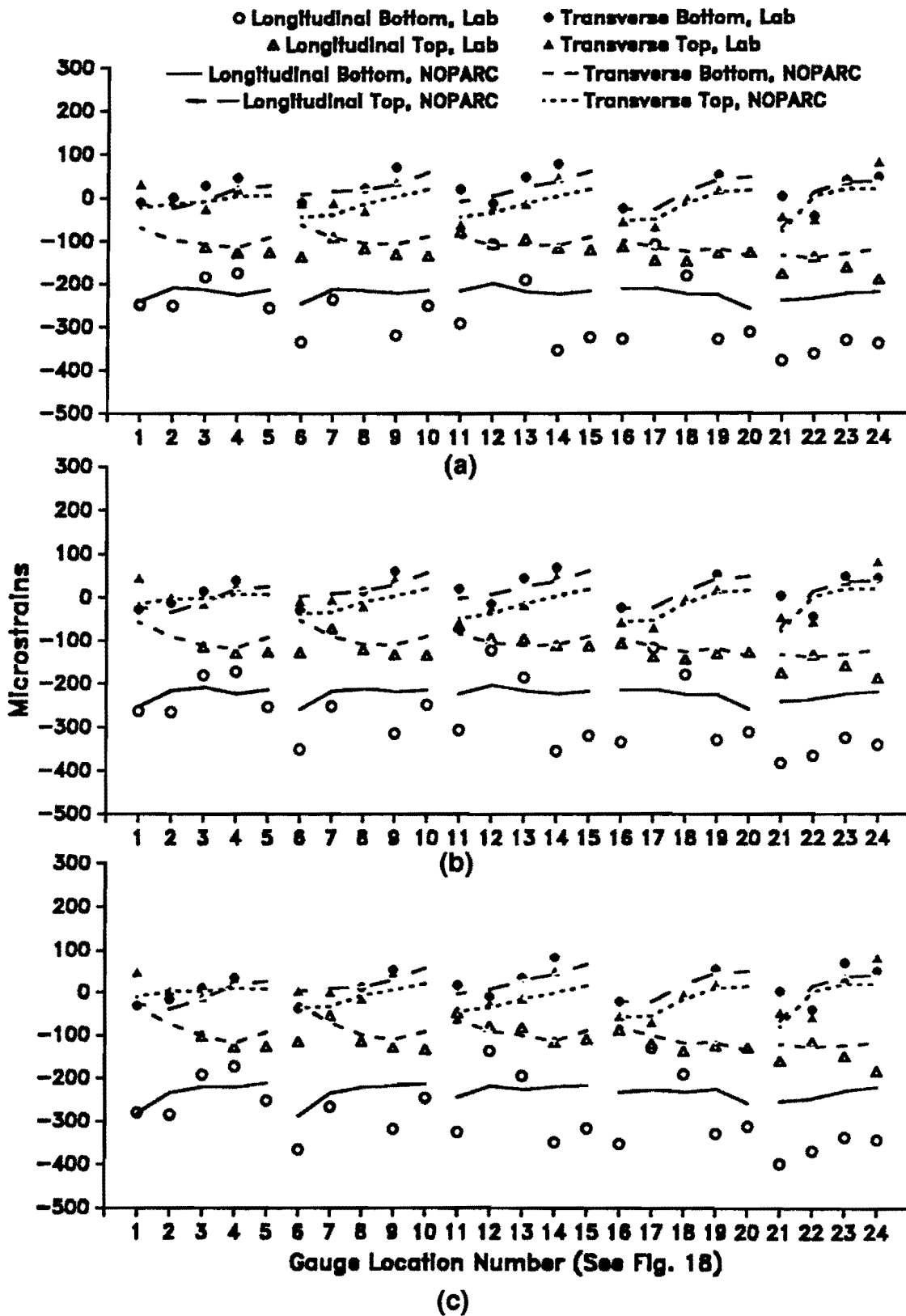


FIG. 27. Strains with Three Transverse Tendons. (a) Load 3.1; (b) Load 3.2; (c) Load 3.3

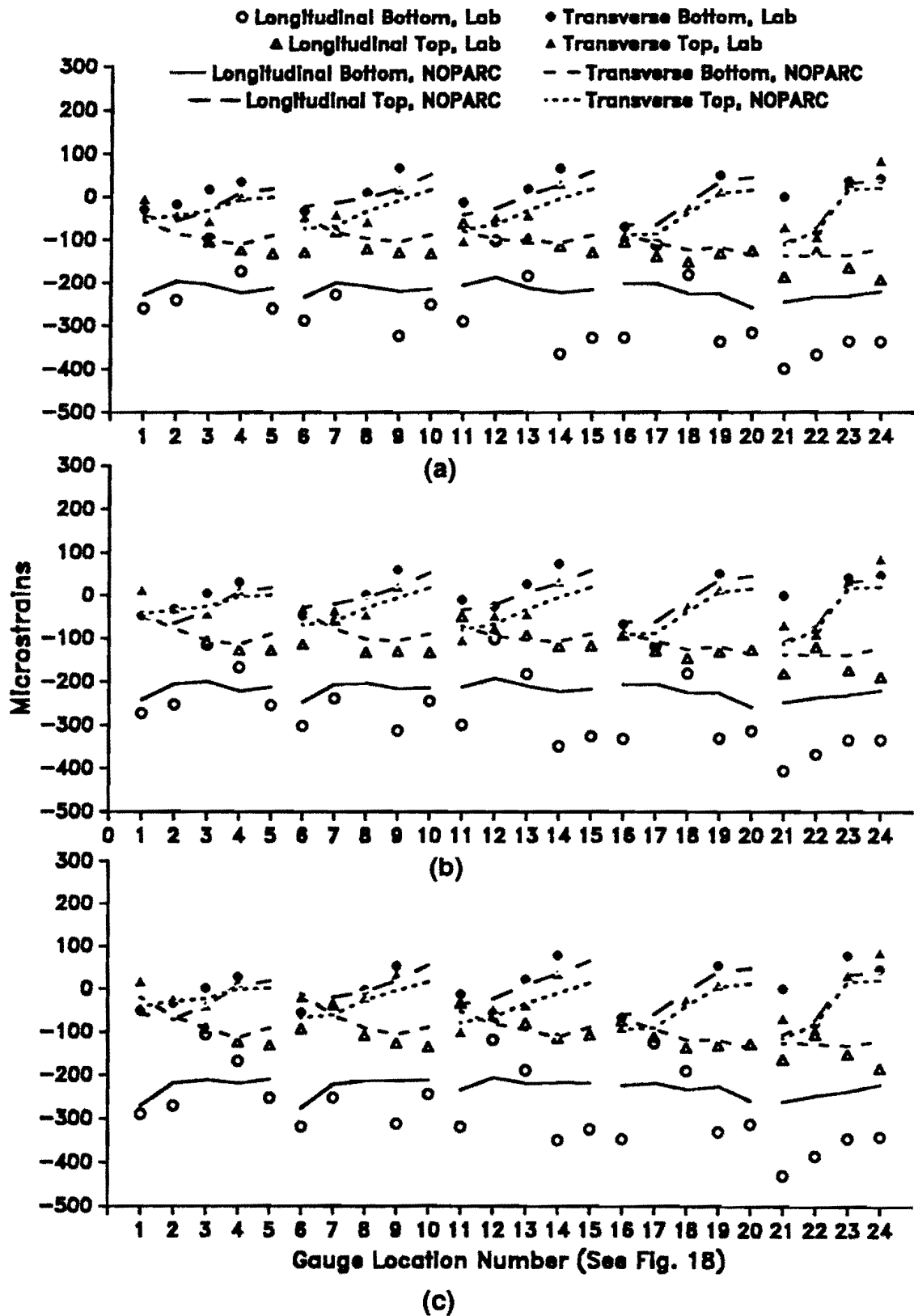


FIG. 28. Strains with Five Transverse Tendons. (a) Load 5.1; (b) Load 5.2; (c) Load 5.3

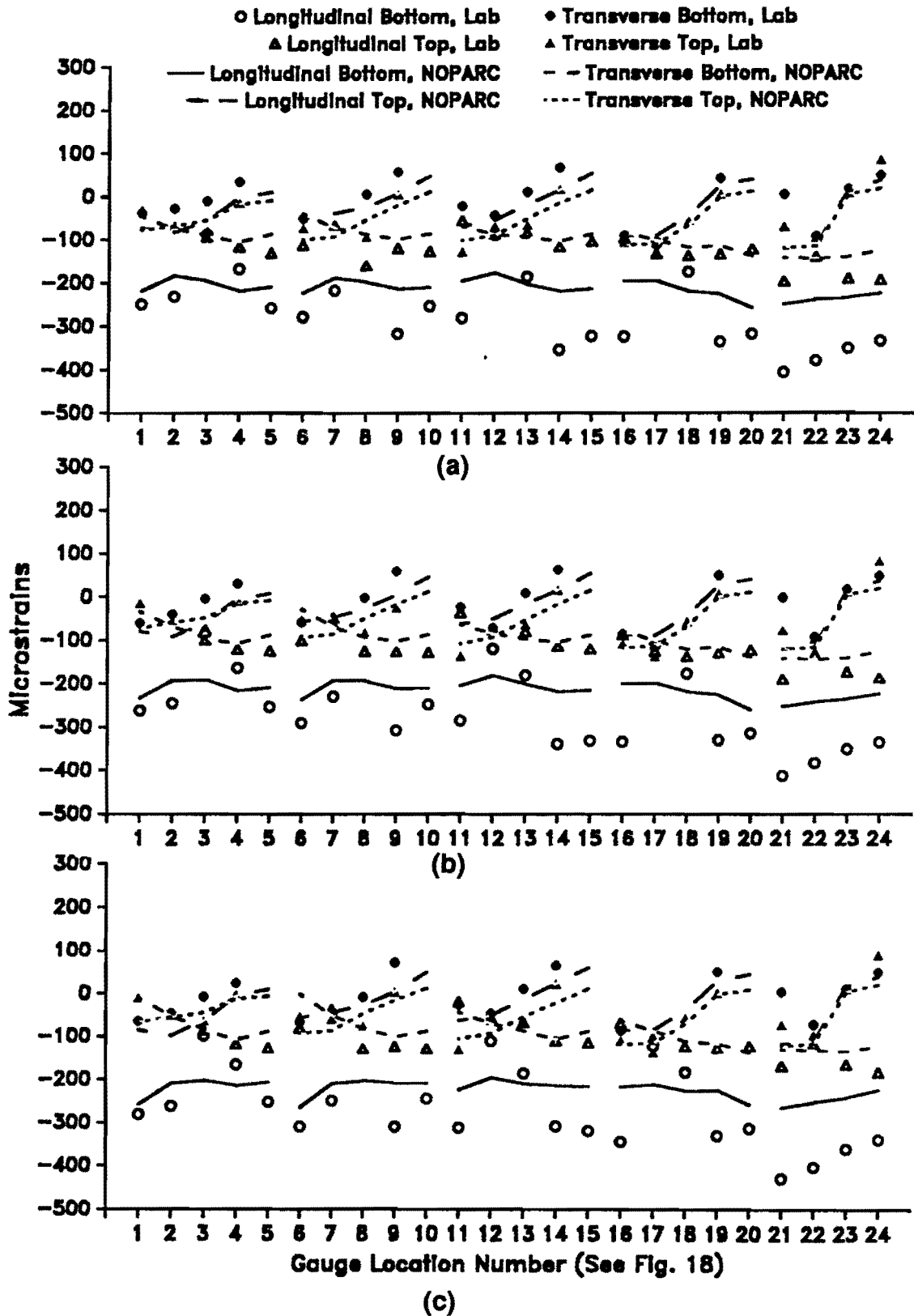


FIG. 29. Strains with Seven Transverse Tendons. (a) Load 7.1; (b) Load 7.2; (c) Load 7.3

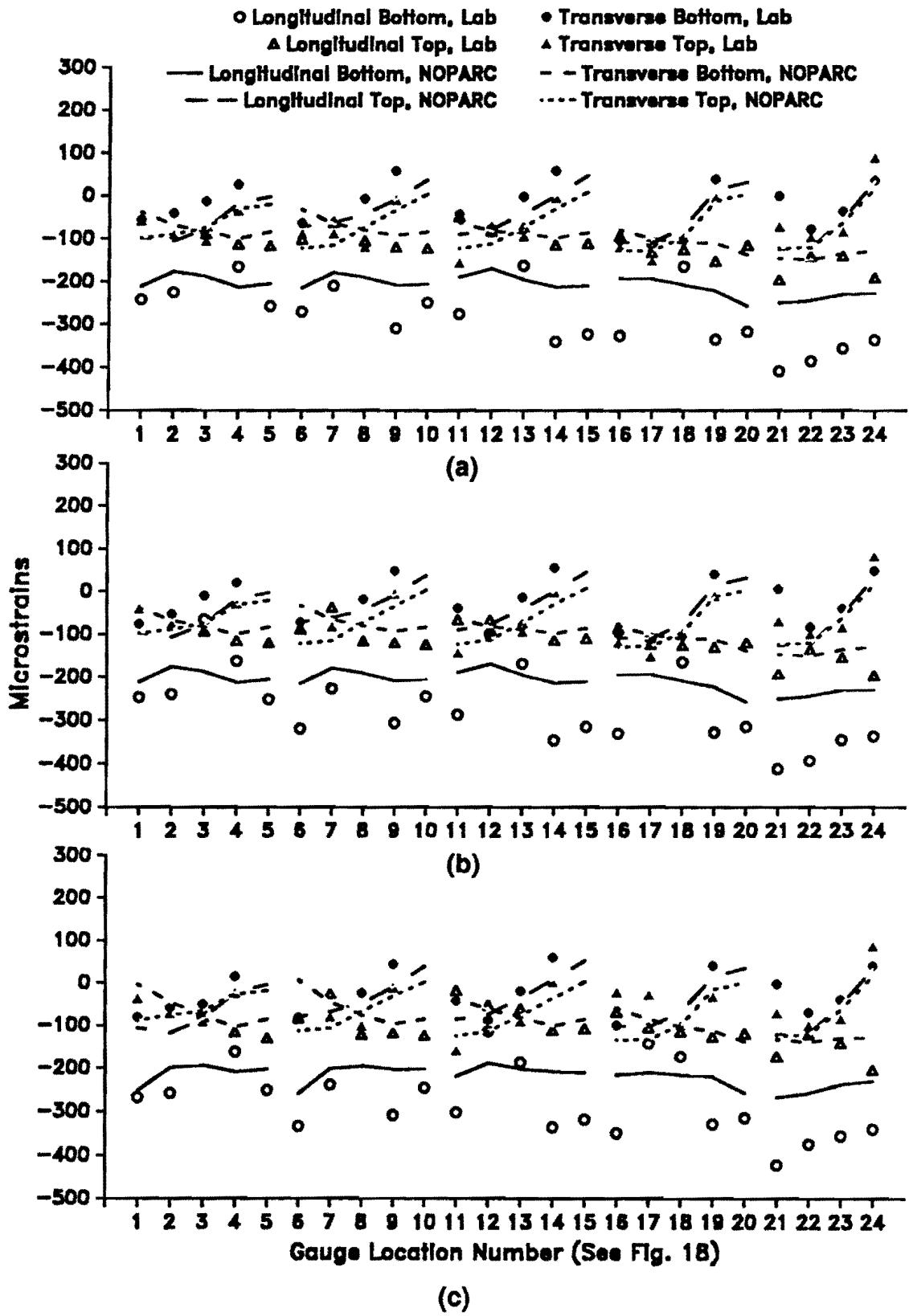


FIG. 30. Strains with Nine Transverse Tendons. (a) Load 9.1; (b) Load 9.2; (c) Load 9.3

As the number of stressed transverse tendons increases, the slab experiences a tendency toward tensile force in the longitudinal direction due to Poisson's effect, as seen in Load 0.1 compared to Load 9.1 (Figs. 25, 30).

4.3 Internal Moment

Internal slab moments, M_x and M_y , per unit length along the slab middle surface are calculated from an assumed linear stress block shown in Fig. 31. Since strain in the concrete is adequately small and within the working stress range of AASHTO (Standard 1989), section 8.15.2.1.1, and ACI Appendix A, (*Building* 1989) the concrete remains in the linear, elastic range. Therefore, a straight-line stress-strain assumption is valid. Furthermore, increase in slab stiffness due to prestressing tendons themselves is ignored since the tendons are unbonded.

Burns and Hemakom (1977) calculate internal moment of a slab using a linear stress-strain relationship of the form:

$$M = - \frac{\epsilon E_c I}{c} \dots \dots \dots (33)$$

where ϵ is strain in concrete as measured by strain gages on reinforcement bars, E_c is the elastic modulus of concrete, I is the moment of inertia of the slab per unit width of middle surface, and c is the distance from the neutral axis to the fiber where strain is measured. Because of slight asymmetry, the neutral axis in the 9-1/4-in. (235 mm) slab of the Model One lies 4.622 in. (117.4 mm) above the bottom fiber. Values of c become:

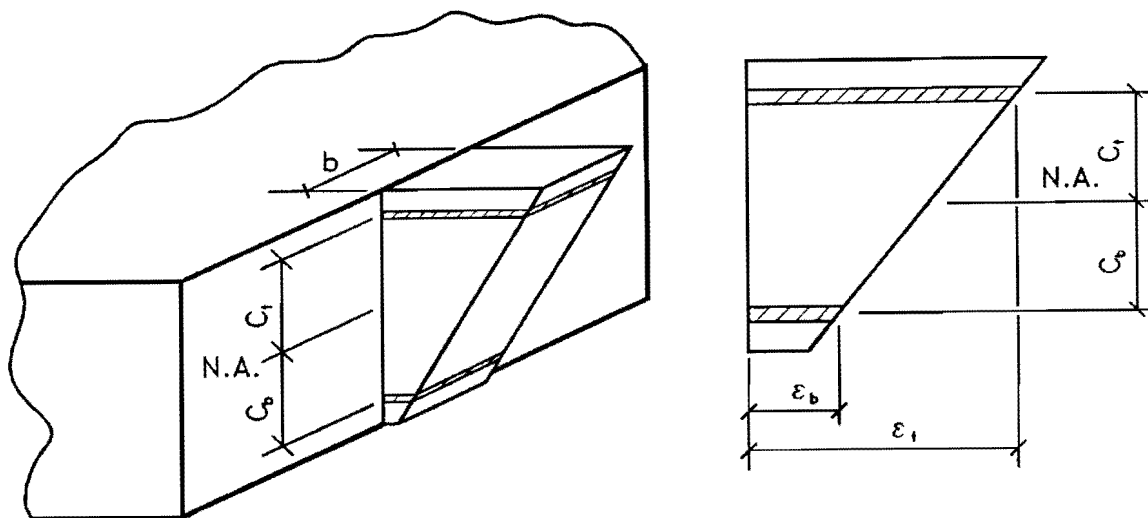


FIG. 31. Stress Block for Moment Computation

$$\begin{aligned}
c_{bx} &= -3.0652 \text{ in. } (-77.856 \text{ mm}) \\
c_{by} &= -3.4402 \text{ in. } (-87.381 \text{ mm}) \\
c_{tx} &= 3.3098 \text{ in. } (84.069 \text{ mm}) \\
c_{ty} &= 3.6848 \text{ in. } (93.594 \text{ mm}) \dots \dots \dots (34)
\end{aligned}$$

where subscripts "b" and "t" indicate bottom and top layers, respectively, and "x" and "y" indicate longitudinal and transverse directions, respectively. A transformation of steel into equivalent concrete sections leads to a total moment of inertia in the following form:

$$I = I_c + I_{sb} + I_{st} \dots \dots \dots (35)$$

or, for the longitudinal and transverse directions:

$$\begin{aligned}
I_x &= \frac{bh^3}{12} + \left(\frac{A_s}{S_x}\right) \left(c_{bx}\right)^2 \left(\frac{E_s}{E_c}\right) + \left(\frac{A_s}{S_x}\right) \left(c_{tx}\right)^2 \left(\frac{E_s}{E_c}\right) \\
I_y &= \frac{bh^3}{12} + \left(\frac{A_s}{S_y}\right) \left(c_{by}\right)^2 \left(\frac{E_s}{E_c}\right) + \left(\frac{A_s}{S_y}\right) \left(c_{ty}\right)^2 \left(\frac{E_s}{E_c}\right) \dots \dots \dots (36)
\end{aligned}$$

where h is the thickness of the slab, which is 9-1/4 in. (235 mm); b is the unit width of the slab; A_s is the area of reinforcement bars; s is the reinforcement bar spacing; E_s is the elastic modulus of steel; and E_c is the elastic modulus of concrete. These values may be divided by (1 - ν²) to account for two-way plate action.

Substituting Eq. 36 into Eq. 33, moment in the slab induced by strain in the concrete is:

$$\begin{aligned}
M_x &= - \left(\frac{\epsilon_{bx}}{c_{bx}} + \frac{\epsilon_{tx}}{c_{tx}} \right) E_c I_x \\
M_y &= - \left(\frac{\epsilon_{by}}{c_{by}} + \frac{\epsilon_{ty}}{c_{ty}} \right) E_c I_y \dots \dots \dots (37)
\end{aligned}$$

Using these equations and the experimental data, moments are tabulated in Tables 5-22 in Appendix III at each strain gage location.

Longitudinal tendon eccentricity of 0.6 in. (15.2 mm) in the slab causes noticeable bending moment in the longitudinal direction, as shown by the difference in top and bottom strains in Figs. 24-30. Even under loads causing negative moment,

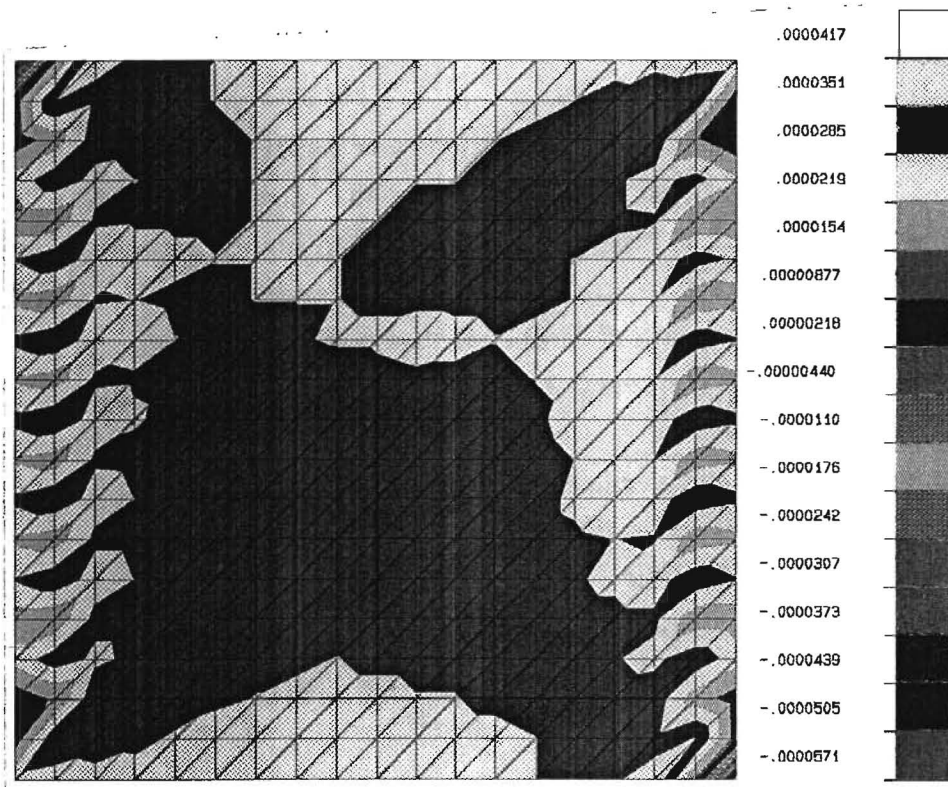
the top longitudinal fibers do not undergo tension at any time due to the high compressive force of the prestressing tendons.

4.4 Discussion of Computer Predictions and Laboratory Data

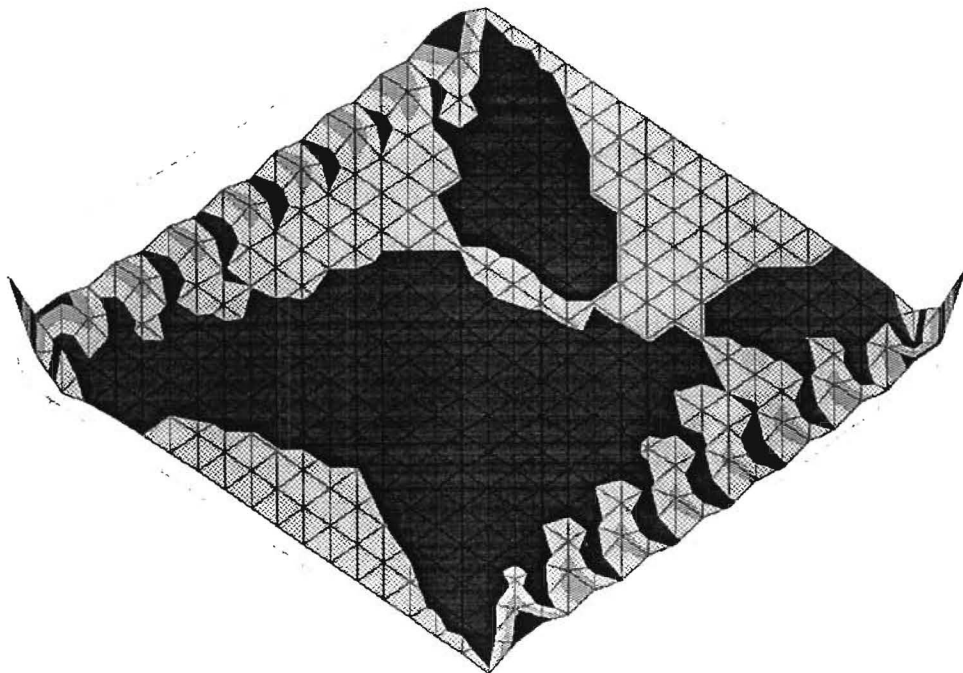
In general, these Figs. 24-30 show that downward vertical loading results in higher bottom fiber compression and lower top fiber compression in the longitudinal direction which, in turn, means that internal moment becomes more negative. A similar increase in strain difference between top and bottom steel strains is recorded by the gages in the transverse direction. However, the magnitude of strain change in the transverse direction due to loading is smaller than in the longitudinal direction. The effect of applied vertical loads becomes insignificant close to the edges of the slab. At locations near the longitudinal tendon anchors, strains remain virtually constant throughout the testing. Eccentricity of longitudinal tendons causes noticeable bending moment in the longitudinal direction as shown by the difference in top and bottom strains. However, even under loads causing negative moment, longitudinal strains at the top steel level do not undergo tension at any time, due to the high compressive force of the longitudinal prestressing tendons. Among the four sets of strain gages, top and bottom groups in two directions, most gages show values or trends reasonably close to the counterpart FEM prediction, except for a few gages which are damaged and the bottom longitudinal gages located near the transverse tendon anchors.

Under all tendon and loading configurations, longitudinal strain remains in the 250-to-300-microstrain range in compression. Since these strains are far from maximum allowable strain, the slab may support much higher load without any damage. By the same token, a less conservative design may be adequate in order to support the same load. Therefore, a thinner slab with wider tendon spacing, smaller tendons in either direction, or any combination of these, may prove to provide an adequate design.

Numerical predictions of transverse axial strain in the slab are processed by PATRAN Plus (1988) for rapid visual evaluation. Fringe plots of computer results for zero, one, three, five, seven, and nine transverse tendons (see Figs. 32-37), show large mid-plane strain gradients near tendon anchors. These gradients are slightly skewed in the direction of the triangular element mesh. In regions of large gradients, a small difference between FEM-reporting locations and strain gage locations may cause a sizable discrepancy in strain. Also since tendon anchors have finite dimensions as opposed to mathematical loading points in the computer model,

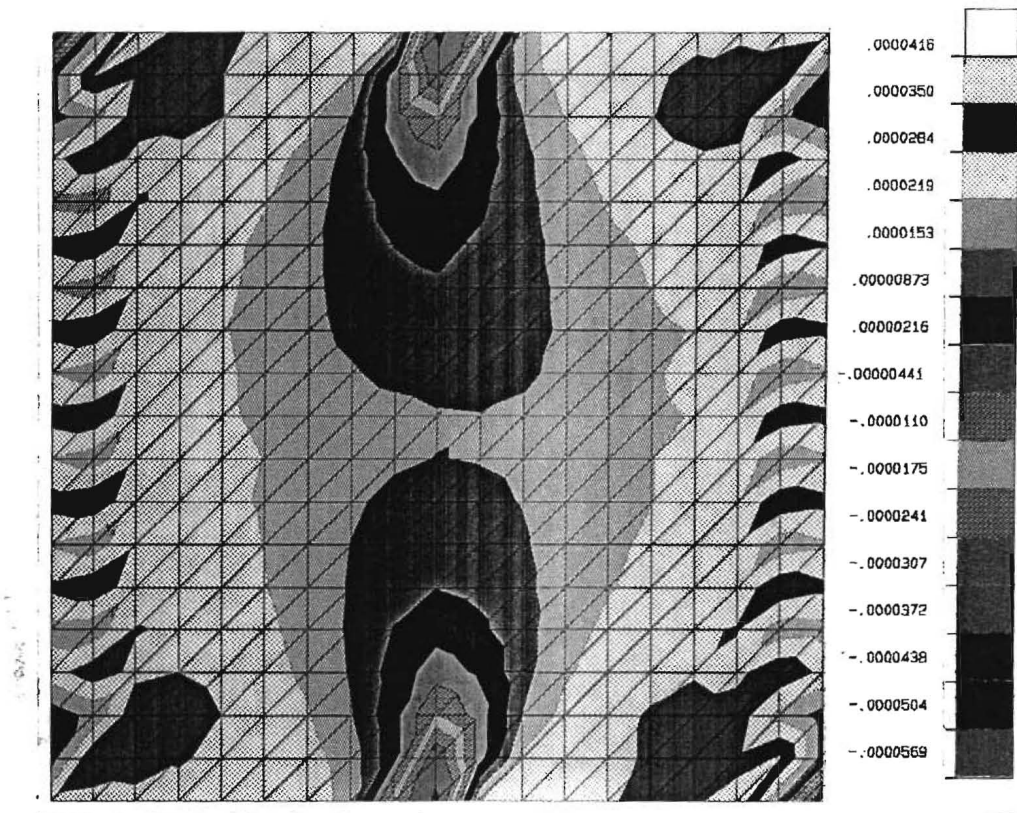


(a)

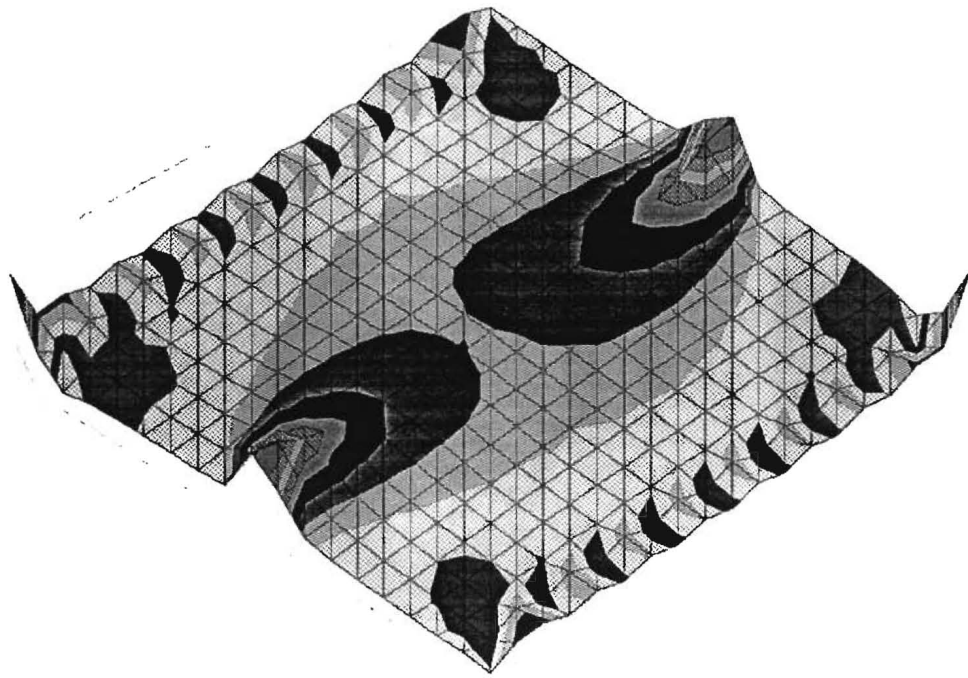


(b)

FIG. 32. Mid-Plane Transverse Strain with No Transverse Tendon. (a) Top View; (b) Isometric View

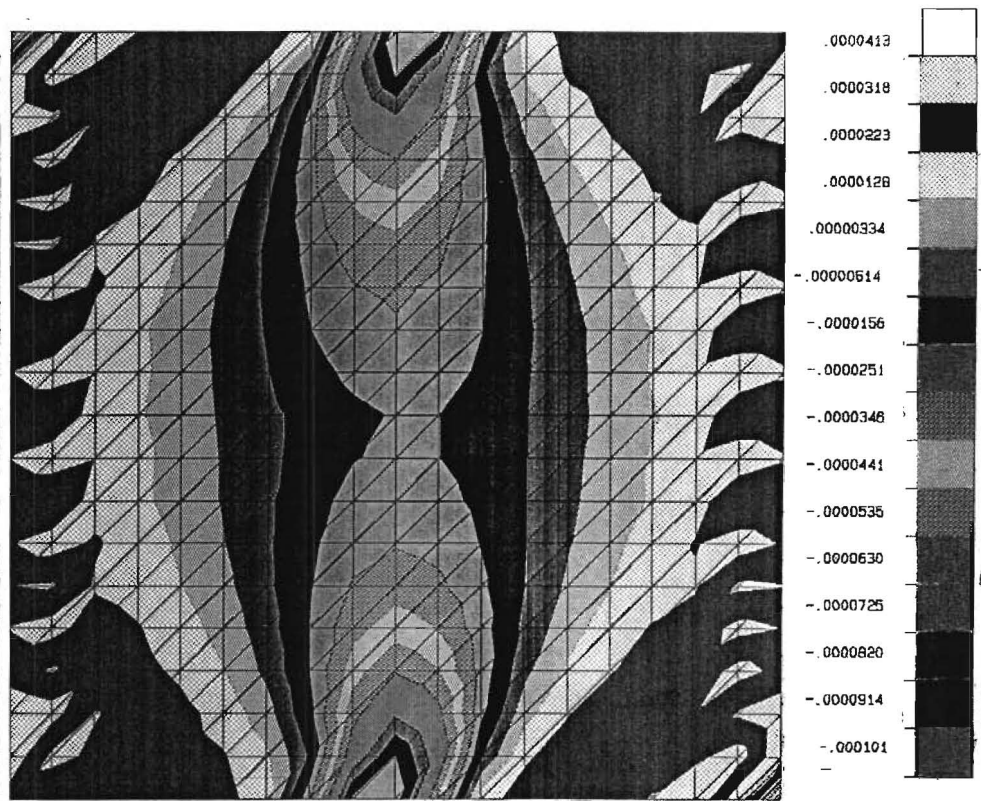


(a)

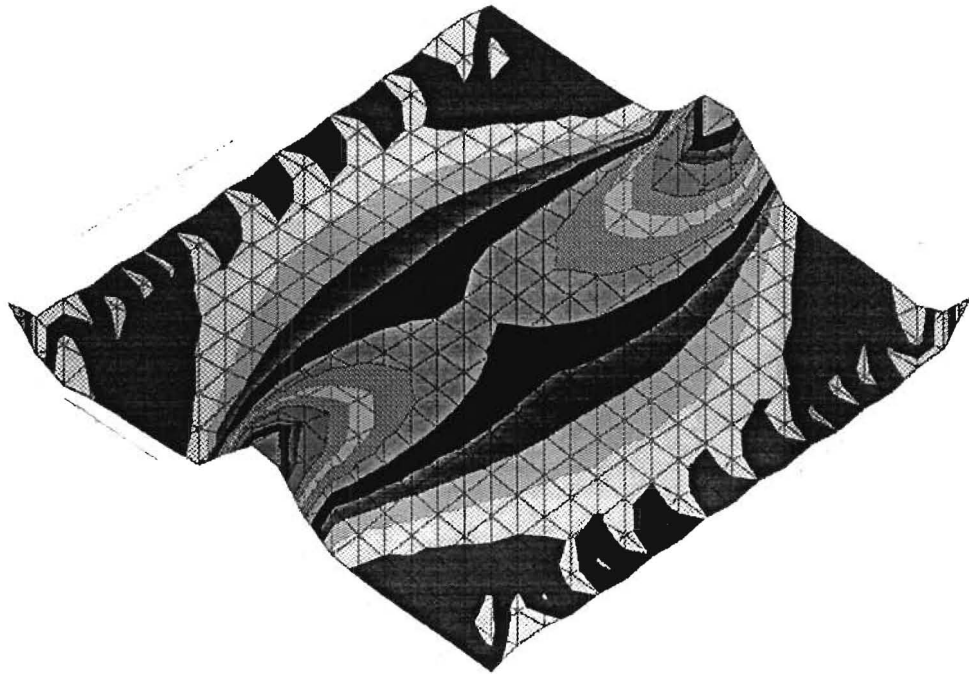


(b)

FIG. 33. Mid-Plane Transverse Strain with One Transverse Tendon. (a) Top View; (b) Isometric View

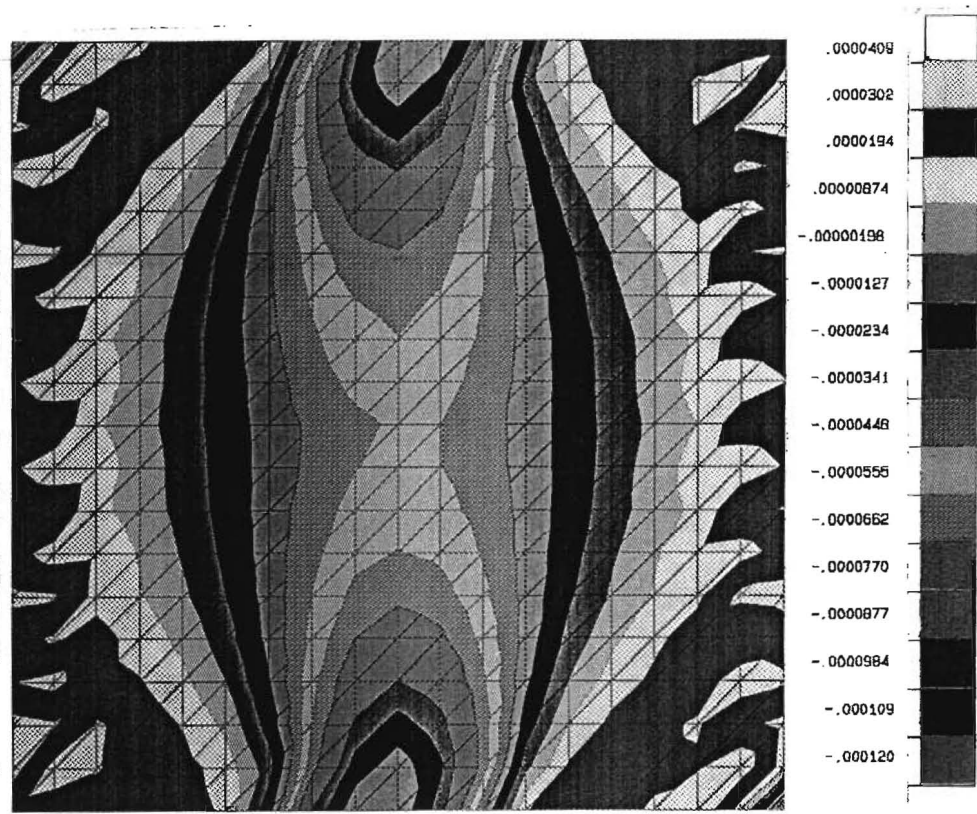


(a)



(b)

FIG. 34. Mid-Plane Transverse Strain with Three Transverse Tendons. (a) Top View; (b) Isometric View

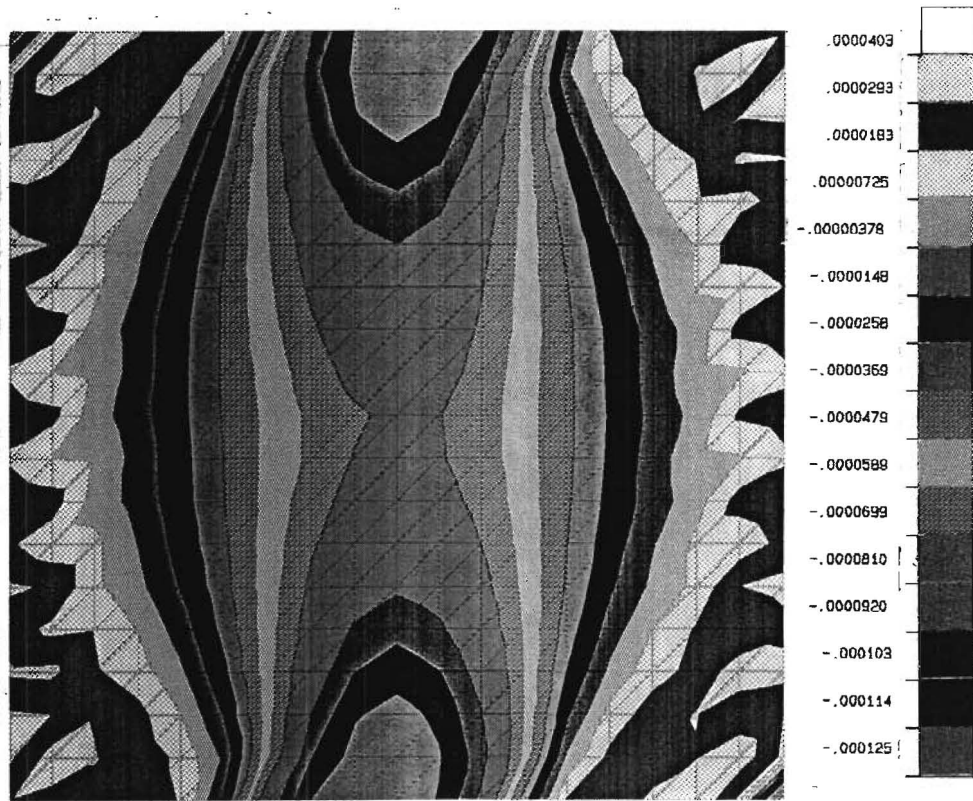


(a)

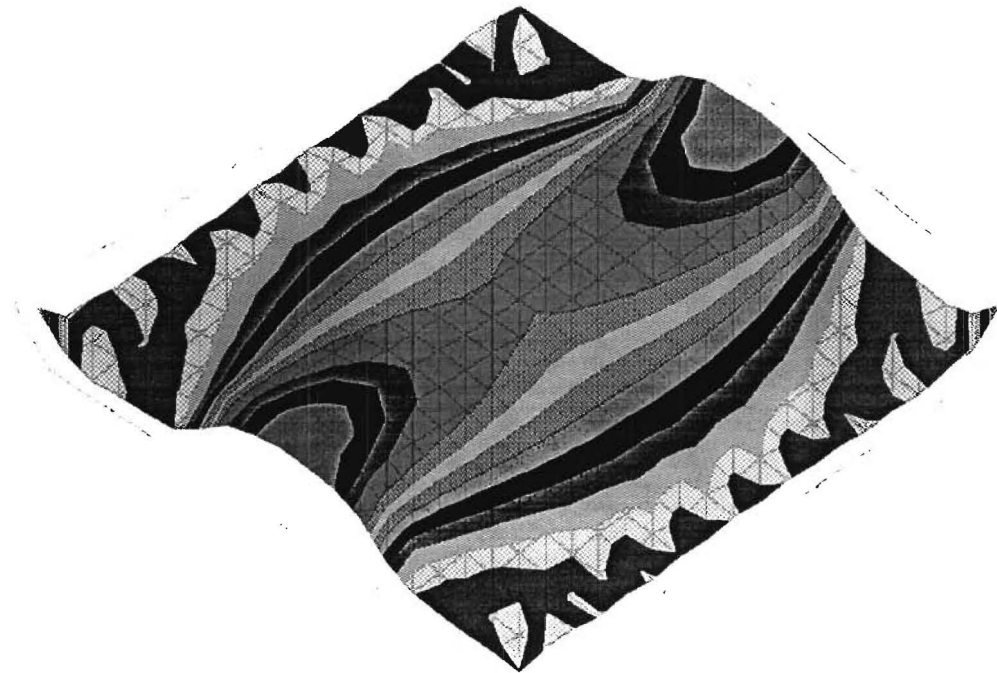


(b)

FIG. 35. Mid-Plane Transverse Strain with Five Transverse Tendons. (a) Top View; (b) Isometric View

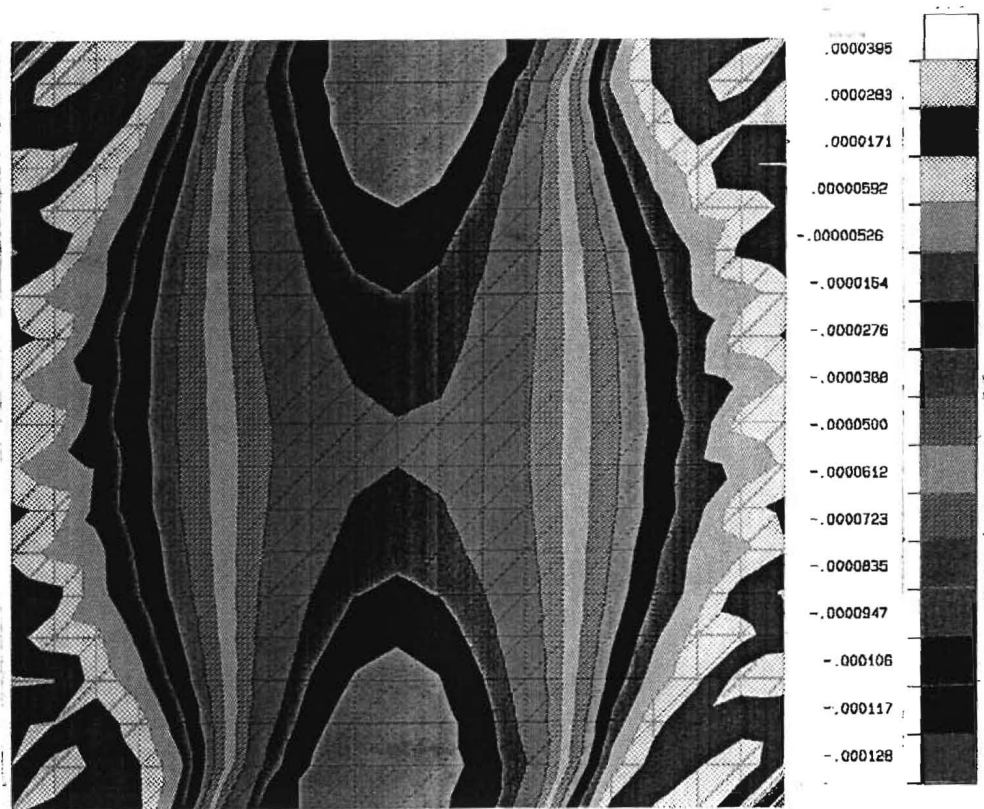


(a)

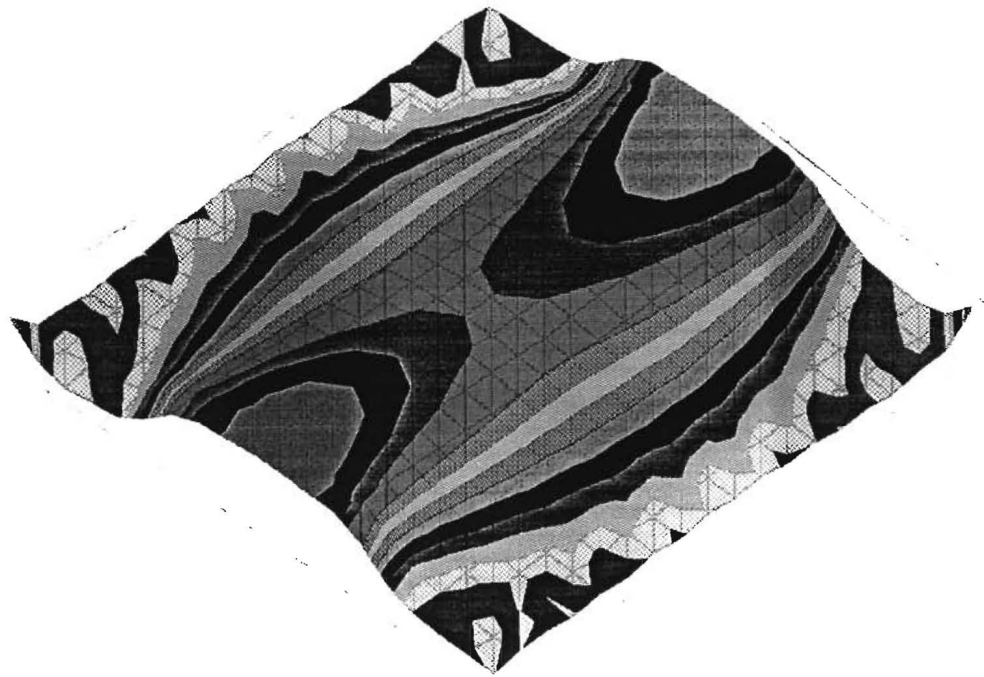


(b)

FIG. 36. Mid-Plane Transverse Strain with Seven Transverse Tendons. (a) Top View; (b) Isometric View



(a)



(b)

FIG. 37. Mid-Plane Transverse Strain with Nine Transverse Tendons. (a) Top View; (b) Isometric View

accuracy of numerical prediction in close proximity to anchors is doubtful. Finally, it is important to note that as the number of transverse tendons increases, transverse strain above the column changes from tension to compression, as seen from a comparison of strains from Loads 1.1 and 9.1 (Figs. 33 and 37).

In accordance with the stress distribution pattern predicted by the SDHPT method (Fig. 3), in-plane stress in the transverse direction at the center of the slab (Point "A," Fig. 38) is obtained from the following equation:

$$\sigma_n = \frac{nF_{ps}}{[S(n - 1) + W_s/2](h)} \dots \dots \dots (38)$$

where σ_n is given in pounds per square inch, F_{ps} is the prestressing force per tendon, n is the number of tendons, s is the tendon spacing, w_s is the width of the bridge, and h is the thickness of the slab. This simple expression takes uniaxial concrete stress into account but neglects reinforcing steel and tendon duct void contributions. In the case of Model One, F_{ps} is 38 kips (169 kN), s is 5.4 in. (137 mm), w_s is 9 ft (2.74 m), and d is 9-1/4 in. (235 mm). Therefore, Eq. 38 becomes as follows:

$$\begin{aligned} \sigma_n &= \frac{38,000n}{[5.4(n - 1) + 9(12)/2](9.25)} \\ &= \frac{38,000n}{50.0n + 449.6} \dots \dots \dots (39) \end{aligned}$$

Total in-plane transverse strain, ϵ_y , is obtained by dividing the axial stress due to transverse tendons, σ_n , by the elastic modulus E_c and superimposing the strain contribution from longitudinal tendons as follows:

$$\epsilon_y = \frac{1}{E_c}(\sigma_y - \nu\sigma_x)$$

which may be rearranged as:

$$\epsilon_y = \frac{\sigma_y}{E_c} - \frac{\nu\sigma_x}{E_c} \dots \dots \dots (40)$$

In Eq. 40, a value of 4,489,000 psi (30.9 GPa), obtained from the computer results (Appendix V), is used for E_c . Although the SDHPT approach uses one-dimensional theory, the two-dimensional Eq. 40 is used for stress-strain conversion. This is done so that the consequences of SDHPT-predicted stress on the plate strain may be discussed, and compared to numerical and laboratory results.

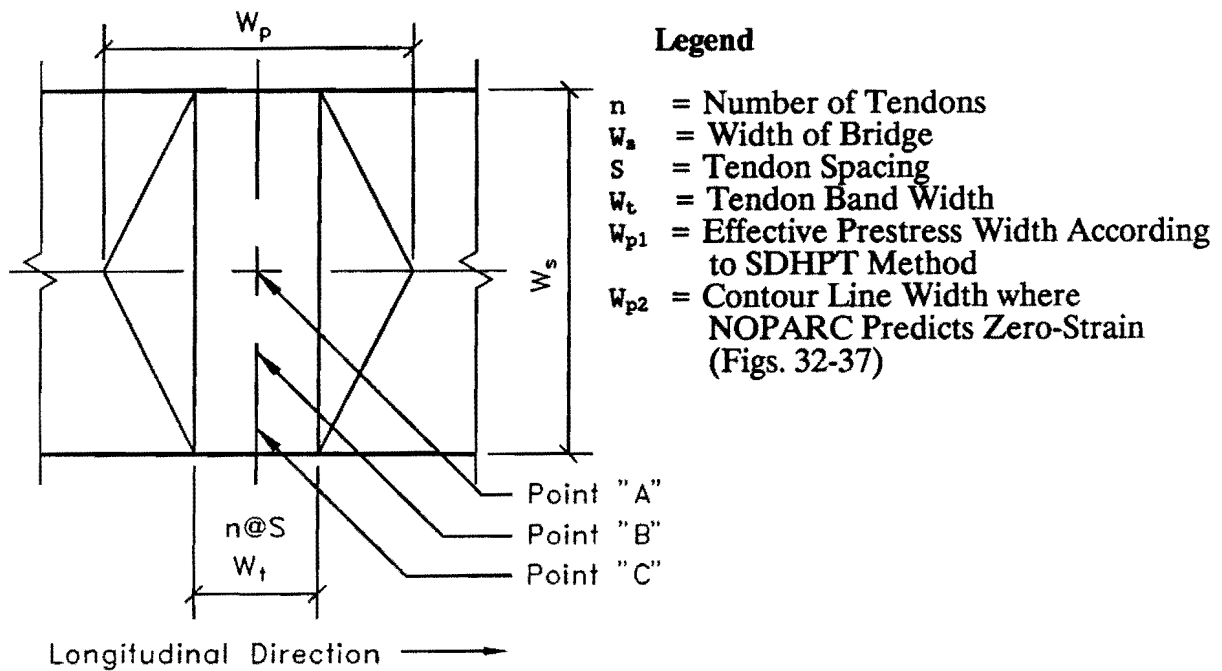


FIG. 38 Assumed Distribution Pattern of Transverse Strain along Center Line of Slab

Calculation of stress and strain levels at this central point obtained by varying the number of transverse tendons leads to the values given in Table 3. NOPARC predictions with and without longitudinal prestress are also included for comparison. A graph of transverse normal strain at the center of the slab versus number of tendons (Fig. 39) shows that the simplified method generally underestimates normal compressive strain at this center point as the number of transverse tendons increases beyond three. When only a small number of transverse tendons are stressed, concrete undergoes tension in the transverse direction at this location due to Poisson's effect (Figs. 33, 34). However, when more than three transverse tendons are stressed, the tensile effect of Poisson's ratio on transverse strains due to longitudinal tendons is more than overcome by the additional transverse stresses (see Figs. 35-37). As a result, for multiple tendon arrangements the predicted in-plane transverse strains are substantially larger than those expected from a simplified approach. The simplified method ignores transverse effects caused by longitudinal tendons and predicts for all cases that the concrete undergoes lower strain than predicted by FEM. Furthermore, if longitudinal tendons are ignored, NOPARC consistently predicts higher compression in the transverse direction due to the lack of a ν term in Eq. 40.

TABLE 3. SDHPT and NOPARC Predictions of Stress and Strain Distribution

n	σ (psi)	$\frac{\mu\epsilon}{S}$	$\frac{\mu\epsilon}{Nt}$	$\frac{\mu\epsilon}{No}$	W_t (in.)	W_{p1} (in.)	W_{p2} (in.)	W_{p2}/W_{p1} (%)
(1)	(2)	(3)	(4)	(5)	(6)	(7)	(8)	(9)
0	0	32	34	0	—	—	—	—
1	- 76	14	17	- 15	0	54.0	—	—
3	- 190	- 11	- 17	- 48	10.8	64.8	48	74
5	- 272	- 30	- 47	- 79	21.6	75.6	67	89
7	- 333	- 43	- 72	-108	32.4	86.4	81	94
9	- 380	- 53	- 96	-131	43.2	97.2	88	91

σ - SDHPT Predicted In-Plane Stress at Center Point
 $\mu\epsilon/S$ - SDHPT Predicted In-Plane Microstrain at Center Point
 $\mu\epsilon/Nt$ - NOPARC Predicted In-Plane Microstrain at Center Point with Longitudinal Tendons
 $\mu\epsilon/No$ - NOPARC Predicted In-Plane Microstrain at Center Point without Longitudinal Tendons
 — - Not Applicable or NOPARC Predicts Tensile Strain
 W_p - see Fig. 38.
 1 psi = 6.89 kN, 1 in. = 25.4 mm

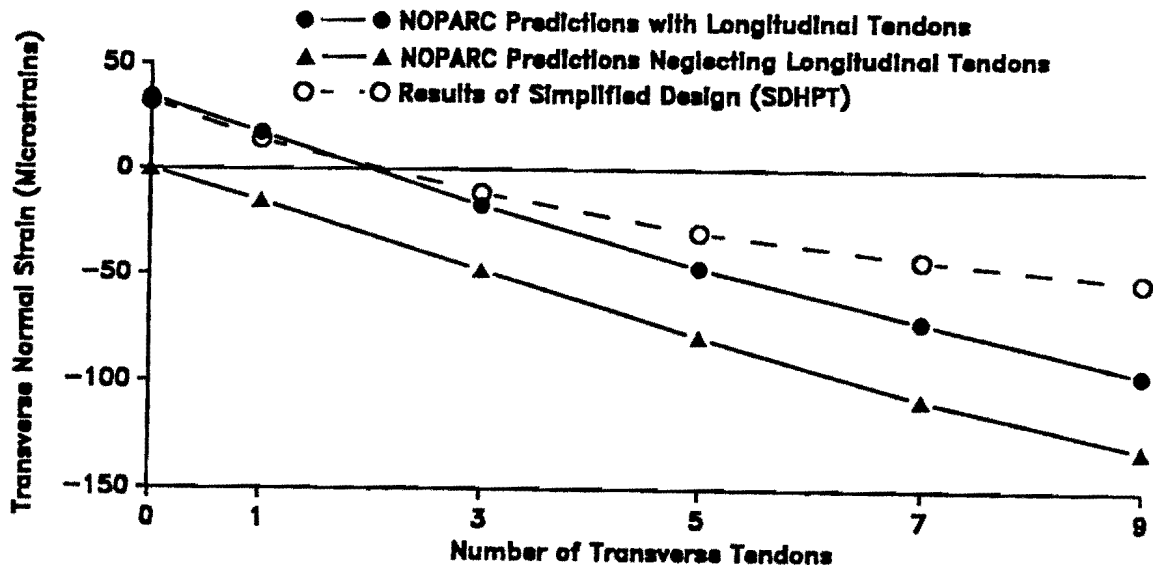


FIG. 39. Transverse Normal Strain Predictions at Center of Slab with Varying Number of Tendons

In all cases the law of diminishing returns is born out since addition of transverse tendons results in a diminishing increase in transverse compressive strain at the center of the slab. This is to be expected since additional tendons are placed increasingly further away from the column. Under all tendon and loading configurations, numerically predicted longitudinal strains at the mid-plane of the slab remain compressive with maximum magnitudes in the 250-300 microstrain range. Since these strains are far from the maximum allowable range limits, the current amount of prestress may support a slab with a much higher live load without any damage.

When seven or more transverse tendons are stressed, NOPARC predicts that the extent of compressive strains reaches the area of longitudinal anchors. In this small, square slab, further spread of the compressive strain region due to additional tendons being stressed is prevented by high stress concentrations from longitudinal tendons (Figs. 32-37). Thus, from a physical limitation of the small model, the maximum angle of dissipation (Fig. 3) is obtained when seven transverse tendons are stressed; in Model One the angle with nine tendons is smaller than that with seven tendons because the tendon band increases in width whereas the compressive strain width remains approximately the same (Figs. 36, 37).

As shown by laboratory results and FEM predictions, strain levels in the transverse direction vary in a continuous manner in the longitudinal and transverse directions, rather than according to the abrupt, discontinuous pattern predicted in the transverse direction by the simplified method. For the case of a gravity normal load the difference between numerically-predicted transverse strain at the slab midplane and strain calculated from the simplified method is shown graphically in Fig. 40. For this illustration, a pattern of seven transverse tendons is chosen for two reasons. First, the Taft Boulevard prototype bridge has seven transverse tendons at each column line. Second, the widest angle of transverse stress distribution in the model is obtained when seven transverse tendons are stressed (Fig. 36).

As an extension of this comparison, experimental, simplified, and numerical strains are plotted at three cross sections in Fig. 41. Here, strains obtained from experimental results, the straight-line approximation, an FEM analysis, and a prediction based on a classical elasticity approach (Timoshenko and Goodier 1951) are compared along three strain gages lines (Fig. 18) for Load 7.1. The simplified method consistently predicts less transverse strain at the center of the tendon band and more strain toward the outside of the hexagonal region than the FEM or

elasticity methods. While good correlation between FEM and elasticity approaches is evident, experimental results are less conclusive.

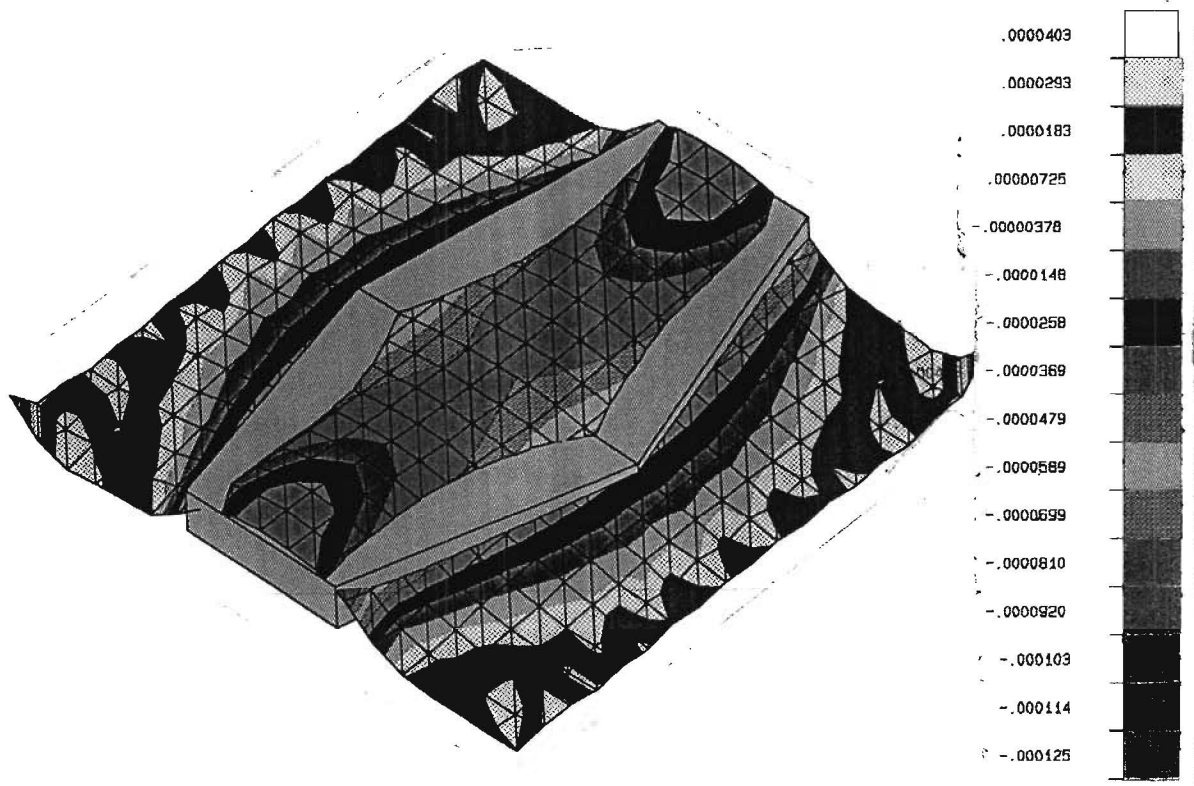


FIG. 40. Comparison of SDHPT and NOPARC Transverse Strain Predictions

Although the graphs seem to have "equivalent areas under the curve," care must be taken in its interpretation as described in what follows. Since the X-axis represents width of the slab and the Y-axis indicates compressive strain, the area remains constant for a given tendon configuration in a given slab due to the following:

$$\text{Area} = \int_{-w_p/2}^{w_p/2} \epsilon dx \dots \dots \dots (41)$$

where w_p is the width of the portion of the graph above the X-axis in Fig. 41. As a simple example, equilibrium of forces at any transverse cross section requires:

$$\begin{aligned} nF_{ps} &= \sigma A \\ &= \epsilon E w_p h \dots \dots \dots (42) \end{aligned}$$

Rearranging the terms in Eq. 42 leads to:

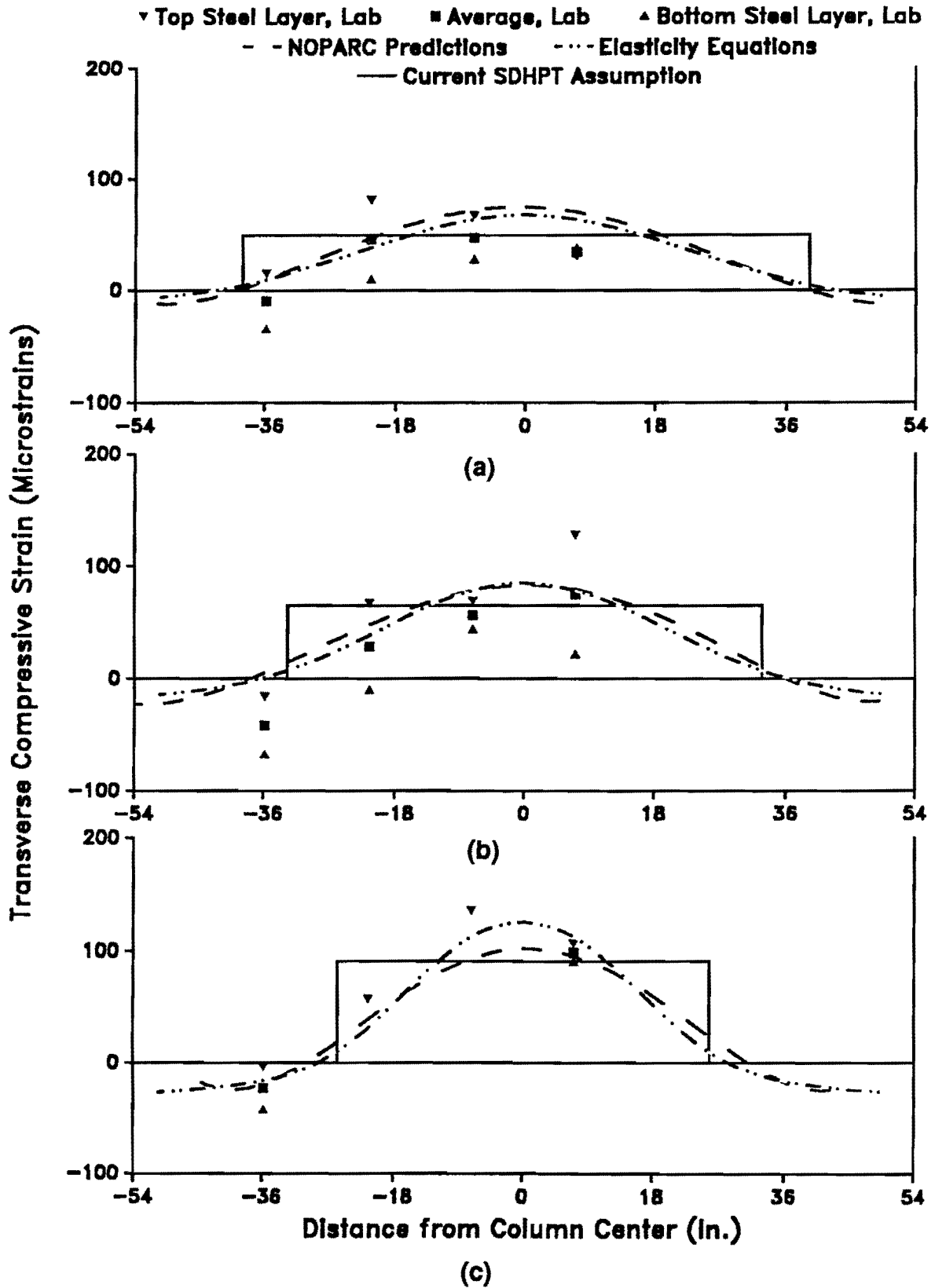


FIG. 41. Transverse Strains. (a) Gages 6-10; (b) Gages 11-15; (c) Gages 16-20

$$\frac{nF_{ps}}{Eh} = \epsilon W_p \dots \dots \dots (43)$$

Therefore, since E , h , n , and F_{ps} are all constant for a given slab and tendon arrangement, the area must be constant. That is, strain distribution varies, but its summation across a section must remain constant due to equilibrium requirements.

Because the transverse post-tensioning is designed to replace a bent cap, the prestressed section must have sufficient moment and shear capacity in and of itself. Design of a transverse section is based on the strain level along the column line. Fig. 42 shows the percent difference between the straight-line method prediction and FEM prediction, which is the standard of comparison, at three points along this line as the number of stressed tendons varies. A positive percentage difference indicates that the simplified approach is underpredicting the FEM value. Differences in predictions of mid-plane strains are plotted for points "A," "B," and "C" whose locations are shown in Fig. 38. This comparison illustrates that the percent difference between these methods for transverse strain predictions at a point directly above the column (Fig. 3) is 35 percent for three transverse tendons and greater than 40 percent when 7 or more tendons are stressed.

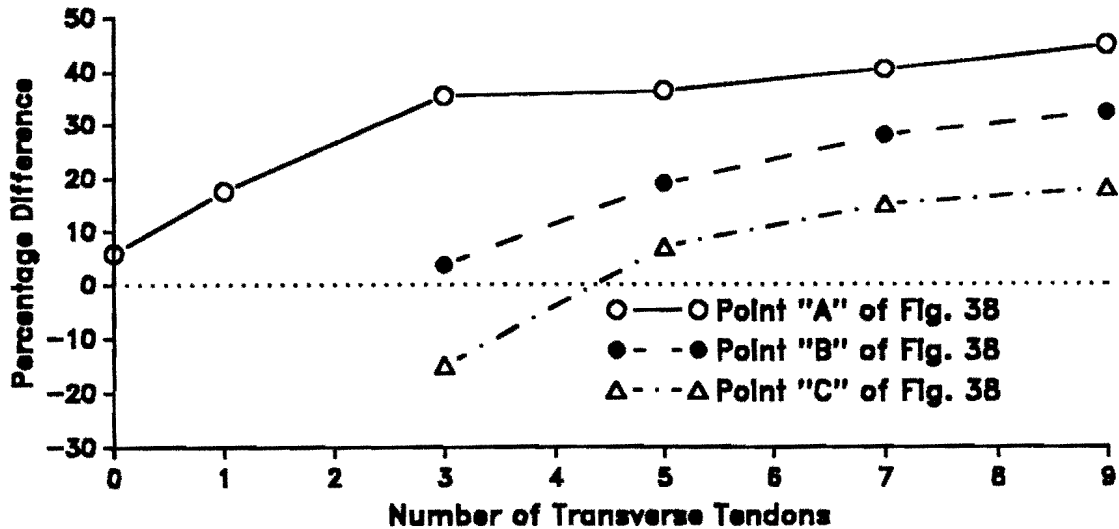


FIG. 42. Percentage Difference between SDHPT and NOPARC Predictions

4.5 Elasticity Predictions

Strain predictions having possible errors in excess of 40 percent (Fig. 42) may not be acceptable; it is desirable to have a simple method that gives a reasonably accurate prediction of in-plane stress distribution in the transverse direction. Timoshenko and Goodier (1951) describe the transverse stress level of a plate loaded in its own plane (see Fig. 43) by the following elasticity-based equation:

$$\sigma_y = -\frac{qa}{l} - \frac{4q}{\pi} \sum_{m=1}^{\infty} \frac{\sin \frac{m\pi a}{l}}{m} \times \frac{(\frac{m\pi c}{l} \cosh \frac{m\pi c}{l} + \sinh \frac{m\pi c}{l}) \cosh \frac{m\pi y}{l} - \frac{m\pi y}{l} \sinh \frac{m\pi y}{l} \sinh \frac{m\pi c}{l}}{\sinh \frac{2m\pi c}{l} + 2\frac{m\pi c}{l}} \times \cos \frac{m\pi x}{l} \dots \dots \dots (44)$$

where σ_y is the transverse compressive stress, q is the total tendon force divided by the cross-sectional area of the tendon band, a is one-half the width of the tendon band, l is one-half the length of the slab, and c is one-half the width of the slab. The stress thus obtained may be compared to the maximum allowable in-plane stress during the actual design. For the comparison shown in Fig. 41, however, the compressive stress is converted to compressive strain by dividing the stress by elastic modulus of concrete, E_c . Then the transverse tensile strain contribution from the longitudinal tendons is superimposed in accordance with Eq. 40. Therefore, the total transverse normal strain becomes:

$$\epsilon_y = \frac{1}{E_c} \left[-\frac{qa}{l} - \frac{4q}{\pi} \sum_{m=1}^{\infty} \frac{\sin \frac{m\pi a}{l}}{m} \times \frac{(\frac{m\pi c}{l} \cosh \frac{m\pi c}{l} + \sinh \frac{m\pi c}{l}) \cosh \frac{m\pi y}{l} - \frac{m\pi y}{l} \sinh \frac{m\pi y}{l} \sinh \frac{m\pi c}{l}}{\sinh \frac{2m\pi c}{l} + 2\frac{m\pi c}{l}} \times \cos \frac{m\pi x}{l} \right] + \frac{\nu \sigma_x}{E_c} \dots \dots \dots (45)$$

where σ_y is taken to be positive in compression.

Although Timoshenko and Goodier state that Eq. 44 is valid only if l is much larger than c , its accuracy for a first approximation is sufficiently good for the case of

$l = c$, especially along the column line. For usual length-to-width ratios of short-span bridges, Eqs. 44 and 45 will provide improved approximation values.

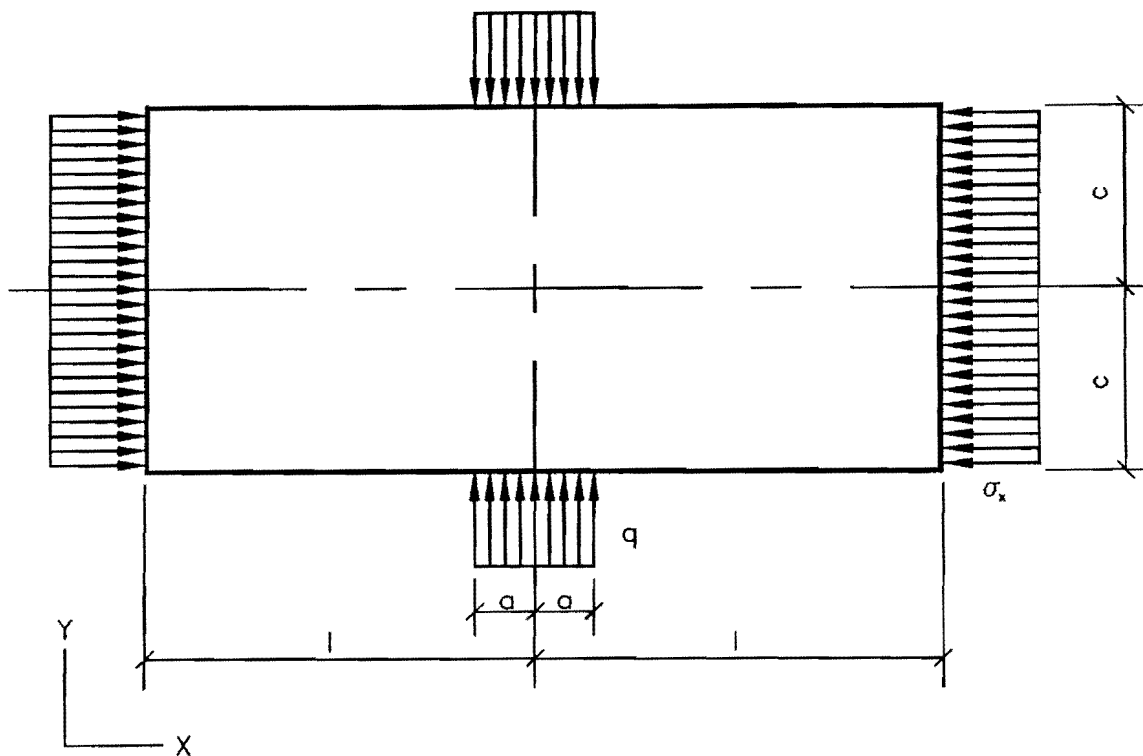


FIG. 43. Loading Pattern for Elasticity Equation

A short computer program listed in Appendix II predicts the transverse stress and strain according to Eqs. 44 and 45 at a small fraction of NOPARC's running time. The elasticity program provides results which are in close agreement with NOPARC (Fig. 41). It is nearly as simple to use as the straight-line approximation currently used by SDHPT, and yet it yields results that closely approximate in-plane finite element strains. A designer may obtain the first approximation of the in-plane effects of transverse tendons based on the elasticity equation program, and thereby generate first trial designs for the number of tendons, tendon forces, and tendon spacing. At some later stage in the design process, this preliminary design may be analyzed by a plate analysis program. By starting the analysis with an accurate approximation of stress and strain, time and effort spent in designing the tendons will be reduced.

V. ULTIMATE LOAD TESTING

Following elastic load testing, the slab was loaded to induce two-way shear failure (Fig. 4). This loading was chosen to augment scarce experimental data for punch-through shear capacity of relatively thick, bidirectionally-prestressed, flat plates resting on circular columns. The failure mode test on the model was attempted on February 28, 1989, using two 110-kip (490-kN) actuators and a pair of load frames (Fig. 44). Failure loads were applied on eight load cells around a 5-ft (1.52-m) diameter circle. This loading pattern was designed to induce punch-through shear failure, similar to the results obtained by Burns and Hemakom (1985) and Gerber and Burns (1971). The slab was loaded and strain gage readings were taken at 20-kip (89-kN) intervals of load. Visual inspection at each load level revealed no surface cracking. Several attempts were necessary to apply a balanced load by placing shims on the load cells so that the slab would not tilt. At approximately 92 kips (409 kN) total load, two actuators buckled about their ball joints, causing the slab to tilt suddenly, slide off the column and fall to the floor. The slab was visually checked for cracks, but none were evident. Minor spalling of concrete was observed near the edges of the slab, and a small piece of concrete spalled off one side of the top of the column.

Minor damage to the slab and column was repaired by using epoxy grout in the ratio of one part Texas Highway Department Epoxy Binder type B-102 to three parts sand. Cube tests conducted on the epoxy grout showed a compressive strength of 7.78 ksi (53.6 MPa) at 7 days. The entire area at the top of the column beneath the neoprene pad was capped by an additional 1/2 in. (12.7 mm) epoxy grout in order to obtain a level surface. Strain gage lead wires that had torn were spliced according to gage location labels attached to the lead wires during construction procedures. Although some tags were torn from gage lead wires, they were attached to correct connections by observing intact tags in the neighborhood. Almost all gages were reattached to RS-232 connectors and external repair was successful. However, two gage wires at one location could not be repaired because of missing tags, and two more gage wires were cut flush with the slab and could not be spliced. Although these four gage connections were repaired outside the slab, some additional connections could not be repaired because of wires severed inside the slab. Casualty of gages after the first failure mode test was higher than the number of wires damaged outside the slab. In all, 15 gages were damaged beyond repair or not functioning. The 73 intact gages, however, were adequate to resume testing. The

majority of gages damaged beyond repair were located on the bottom reinforcement mat. Gages on the top reinforcement mat generally suffered no damage.

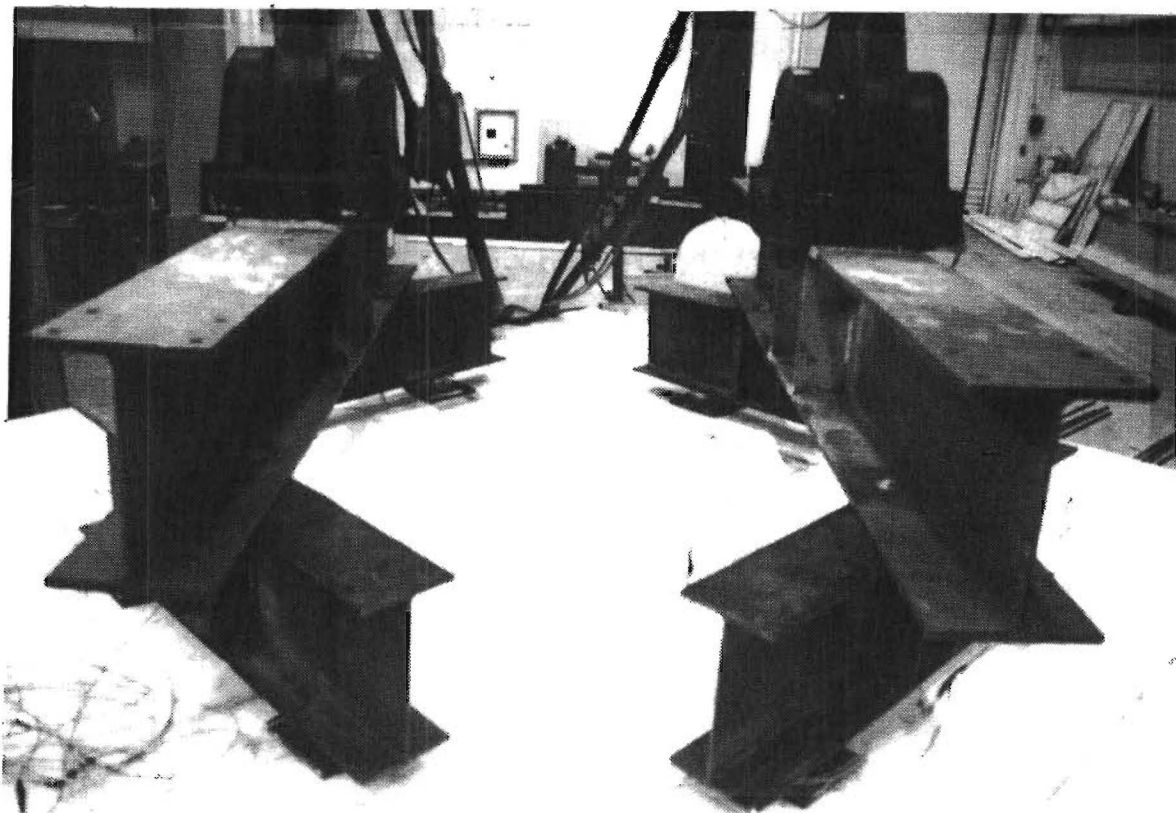


FIG. 44. Load Frame with Two Actuators

5.1 Model Location and Overhead Load Frame

Solution to the stability problem was achieved by placing the four actuators in a square formation (Fig. 45). Overturning moment in the longitudinal direction was balanced by two 110-kip (490-kN) actuators, while overturning moment in the transverse direction was balanced by two 55-kip (245-kN) actuators. The entire model was moved 1.5 ft (457 mm) from the original location for the elastic testing, to a location directly beneath the center line of the overhead cross beam. This allowed two additional columns to be placed next to the transverse anchors to support an additional cross beam perpendicular to the existing cross beam above the center line of the slab (Fig. 46). A W18 x 65 beam was attached to the columns on May 1, 1989, along with two 55-kip (245-kN) actuators.

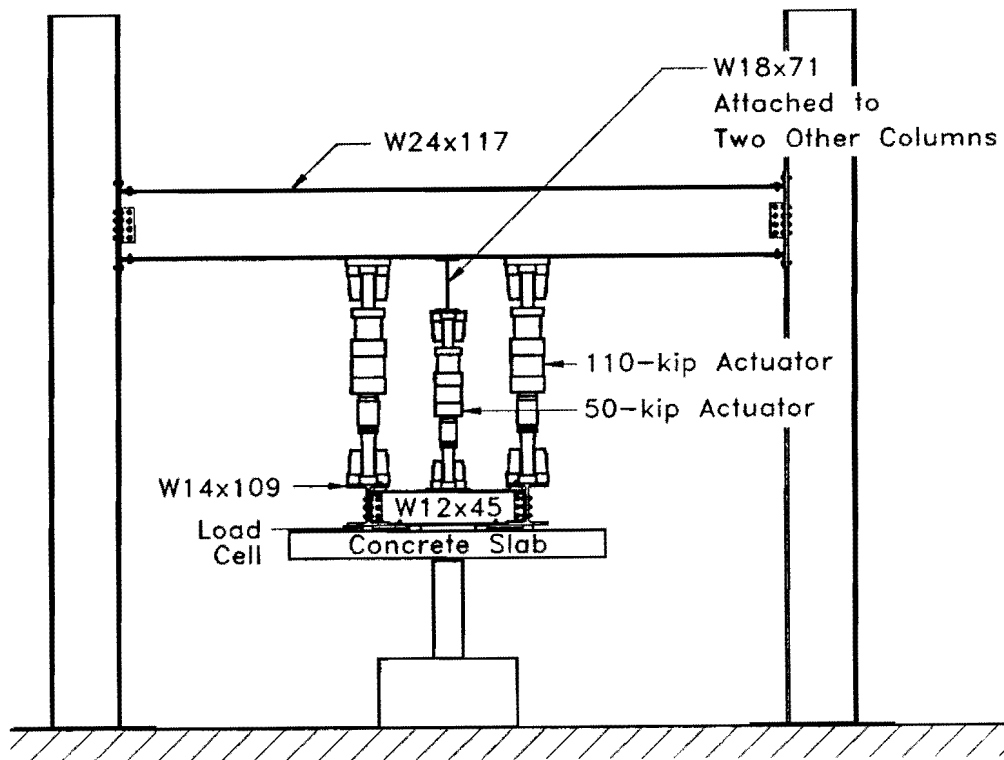


FIG. 45. Load Frame with Four Actuators

5.2 Ultimate Loading

For the second and final attempt at ultimate loading, an eight-point load was applied to the slab using load cells and a load frame made of two W14 x 109 and two W12 x 45 beams, as shown in Fig. 47. The beams were rigidly connected so that the frame would act as a unit which would be loaded and stabilized by four actuators. Eight load points were chosen so that they lay on the circumference of a 58.7-in. (1.49-m) diameter circle, similar to the loading points used during the first attempt to fail the slab by shear.

On May 5 and May 8, 1989, working of the actuators was tested for balance. The data acquisition program used during the elastic-load study was modified to accommodate an increase in the number of load cells from four to eight. On May 10, 1989, the slab was loaded to 50 kips (223 kN) in a 5 ft x 6 ft (1.52 m x 1.83 m) rectangular formation using four load cells, which induced sizable internal moment in the slab. The differential strain and moment caused by the loading is tabulated in

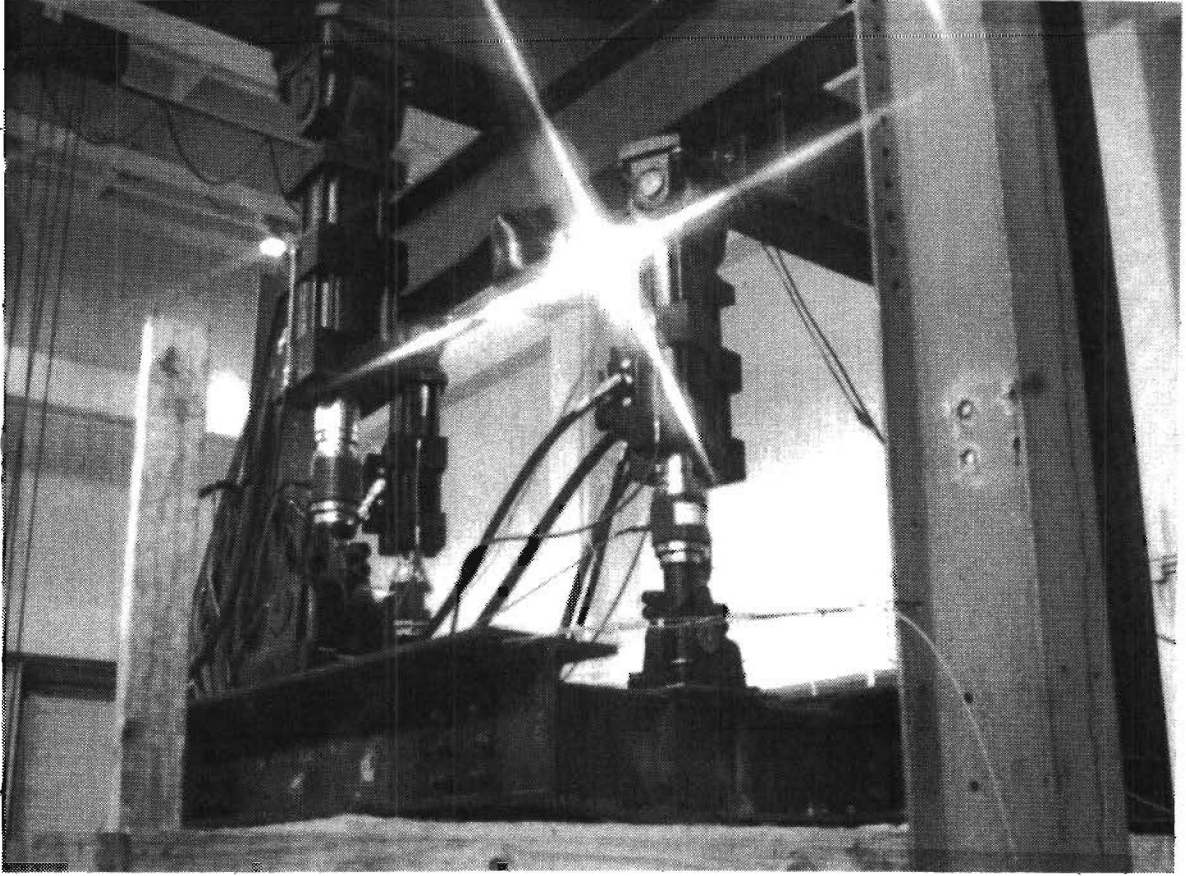


FIG. 46. Model Location below Two Beams

Table 24 in Appendix III. This load checked response of strain gages and the control program for the actuators, by comparing the laboratory data to computer predictions. From results of differential strain readings shown in Fig. 48, performance of transducers was determined to be adequate, with some exceptions close to the edge of the slab.

On June 5-9, 1989, ultimate load testing was conducted. On June 5, a total load of 105 kips (467 kN) was applied with four actuators in load control. Instrumentation readings were taken at intervals of 20 kips (89 kN). Due to instability of the slab, it was determined to be difficult to obtain satisfactory loading beyond this point while the actuators were under load control. As a consequence the actuators were reset to stroke control and recalibrated on June 6. On June 7, loads were reapplied and the slab failed suddenly by punching shear at 198 kips (881 kN) of applied actuator load. Combined with the 9.4-kip (41.7-kN) dead load, slab shear capacity was determined to be 207 kips (923 kN). Sudden failure occurred, with a failure surface approximating an inverted cone which indicates a punching

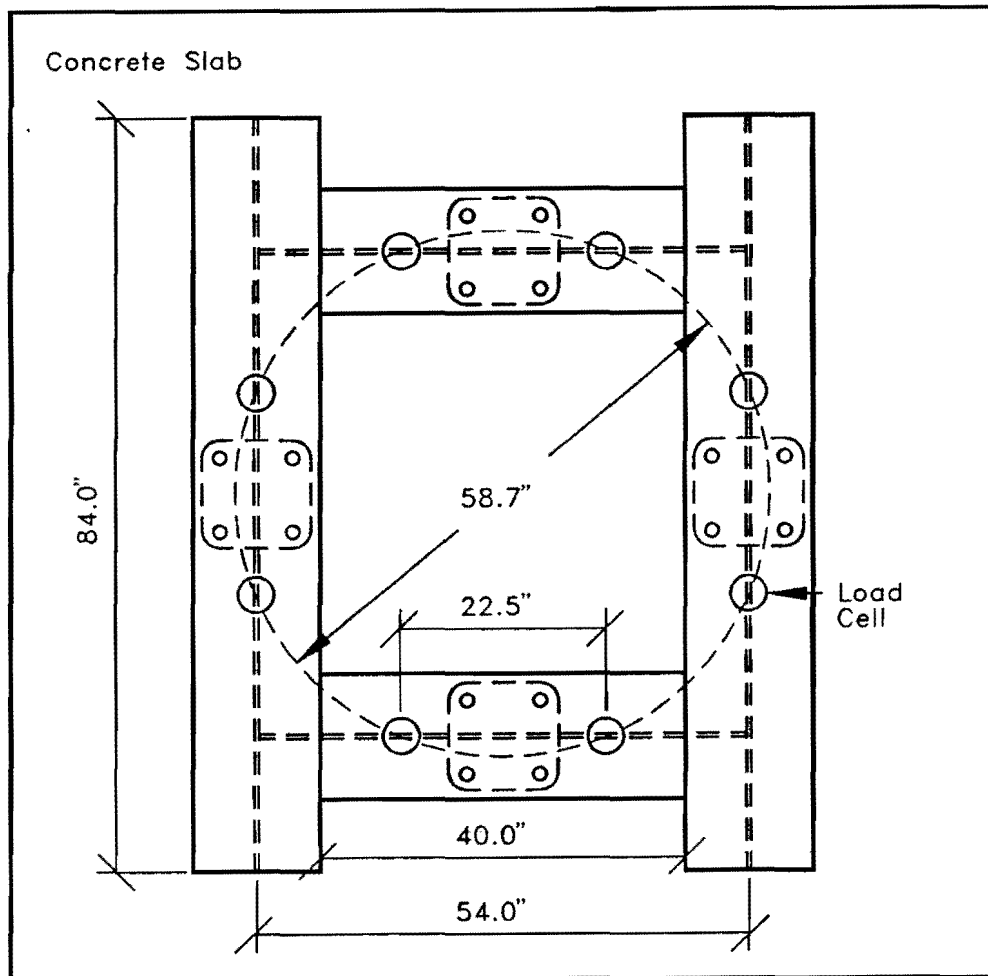


FIG. 47. Loading Frame and Load Cells Approximating Circular Line Load

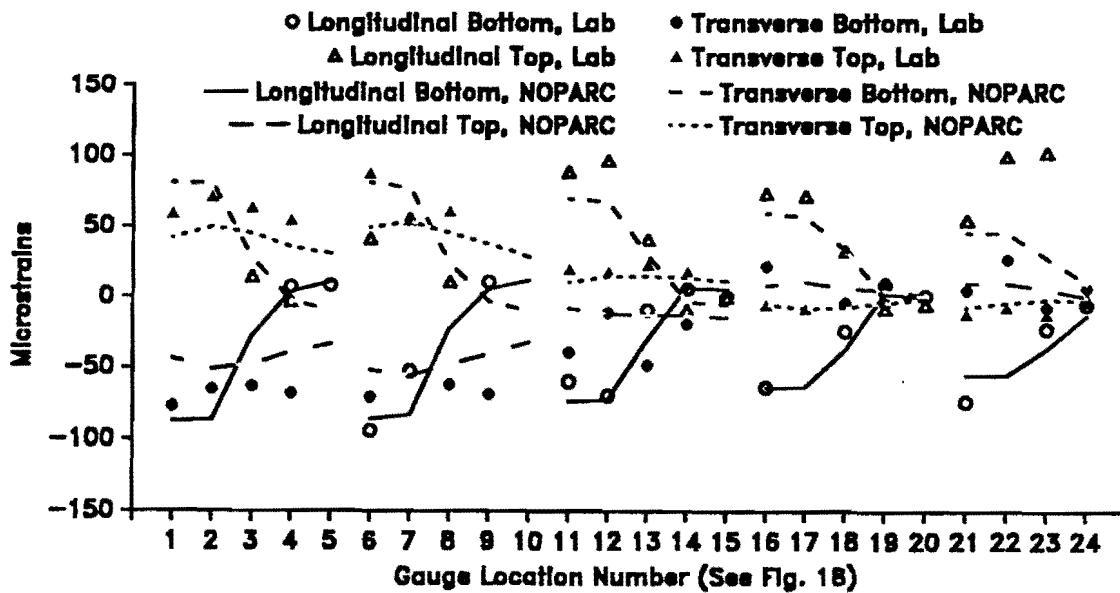


FIG. 48. Differential Strains under 50-kip Load

shear failure. No large cracks were observed until the failure of the slab; at failure, small cracks were found on the top surface of the slab near the loading points. Vertical displacement of the slab rendered the 3/4-in. (19.1-mm) neoprene pad barely visible when viewed from beneath the slab (Fig. 49). No cracks were found on the bottom surface of the slab. Videotape recordings were made of the failure test.

Following punch-through failure, the actuator load was completely removed and subsequently reapplied on June 8-9, until the slab fell onto the column footing on June 9. At 102 kips (454 kN) of applied load, or 111 kips (496 kN) of total load, tendons directly above the column began to break, and the load fell dramatically. Because of a large deflection of up to approximately 18 in. (457 mm), the actuators ran out of stroke several times, necessitating use of timber shims. During the reserve load testing, cracks progressively formed within the region of the failure cone (Fig. 50). After large loose concrete pieces were removed, the failure surface showed the profile indicated in Fig. 51. In plan view the pattern approximated a truncated ellipsoid with major diameters ranging from approximately 5 ft (1.53 m) in the transverse direction to 5.5 ft (1.68 m) in the longitudinal direction. Straight lines approximating the failure surface formed an angle of approximately 20° with the surface of the slab.

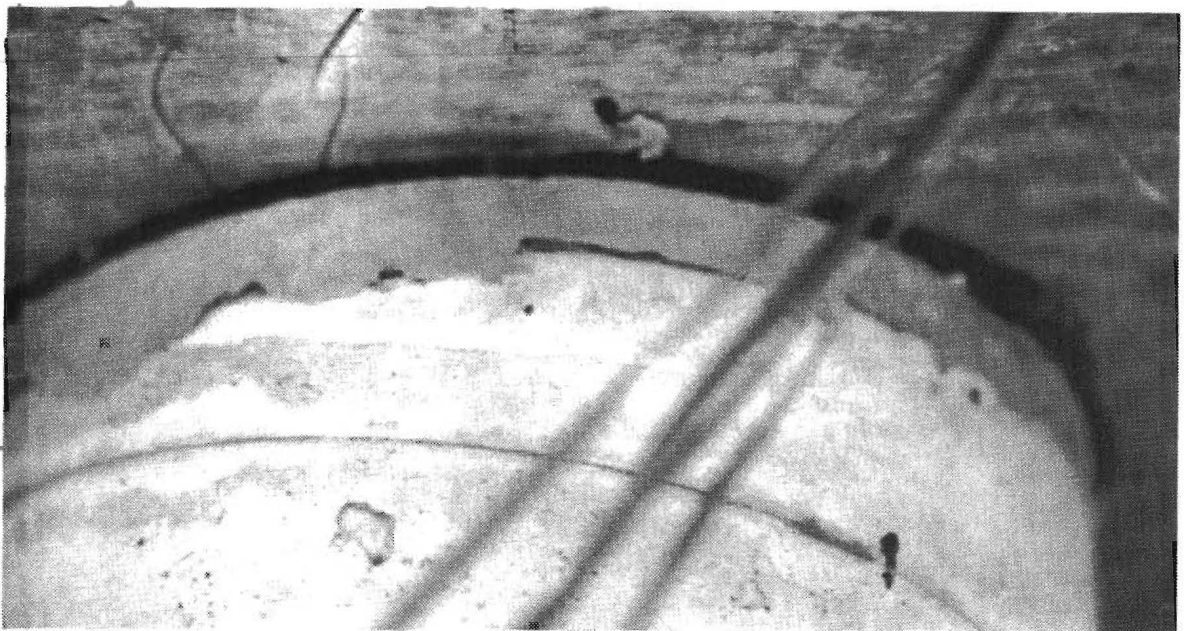
In Fig. 52, readings from two strain gage locations are used as representatives of slab strain during ultimate loading. Figs. 52a and 52b follow the load history of four gages at location No. 1 and 13, respectively (see Fig. 18). In both graphs, Load Case 1 indicates the beginning of ultimate testing with actuators under load control. Load Case 6 marks the maximum reading of 100 kips (445 kN) before load control was abandoned at 102 kips (454 kN). Load Case 7 is the beginning of ultimate testing with actuators under stroke control. Load Case 16 marks the last applied load level of 180 kips (801 kN) at which readings are taken preceding the primary failure at 198 kips (881 kN). Strain gage readings near the column (Fig. 52a) indicate that strain gage wires in the bottom layer remained intact, whereas top layer gages were damaged at failure. Relative lack of change in gage readings away from the column (Fig. 52b) indicates the internal moment was largely confined to lie within the simulated circular load pattern throughout the range of loading.

5.3 Discussion of Ultimate Load

Corner displacement readings taken during ultimate testing (Fig. 53) show sizeable tilting of the slab while the actuators were under load control. Although the average displacement remains relatively constant, two corners displaced excessively.

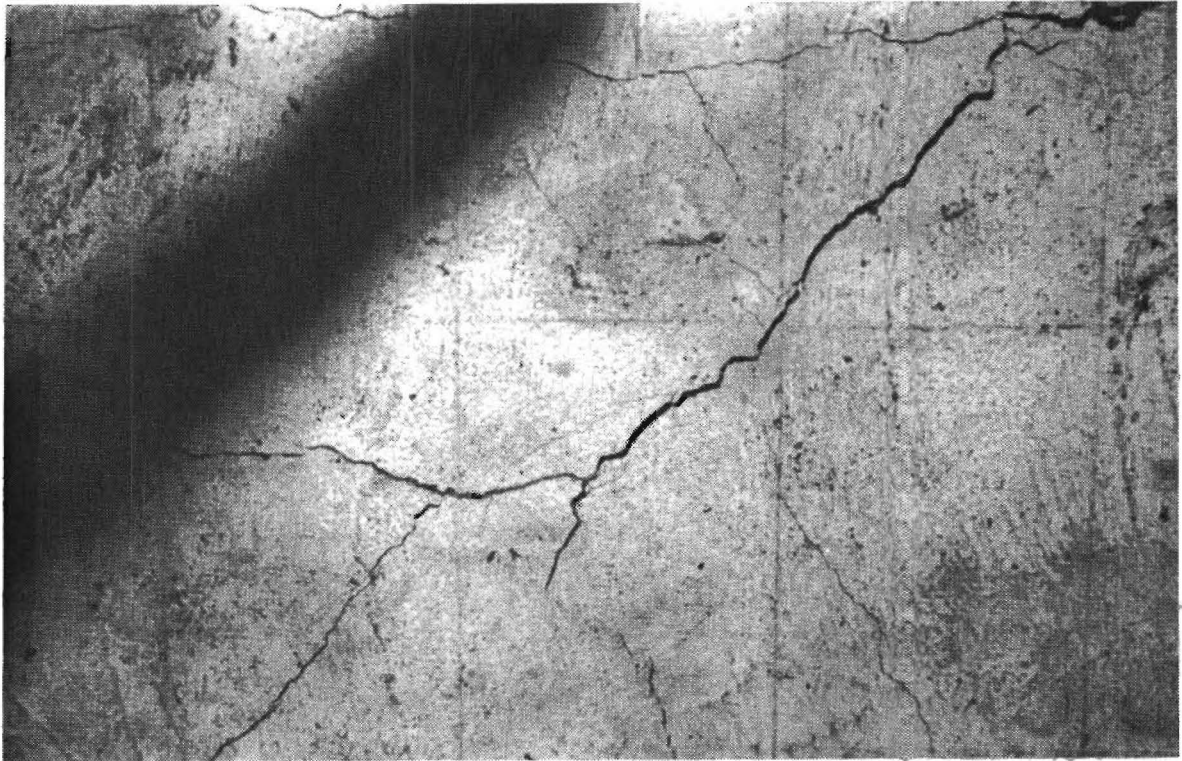


(a)

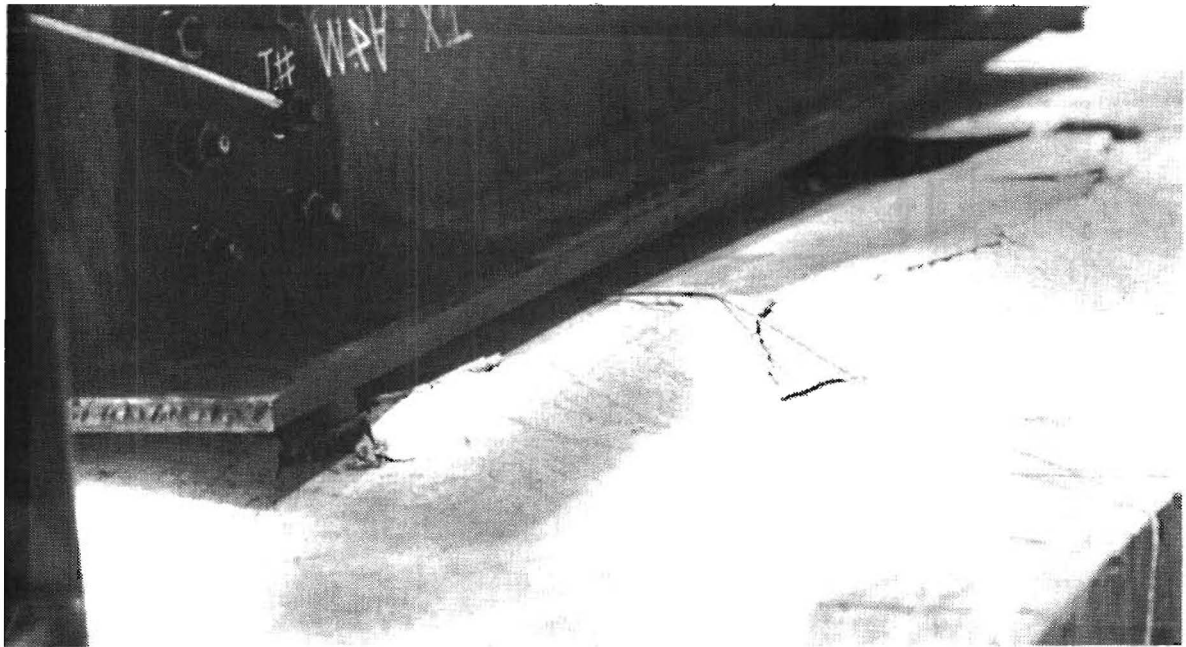


(b)

FIG. 49. Neoprene Pad at Column Capital. (a) Before Ultimate Test; (b) After Ultimate Test

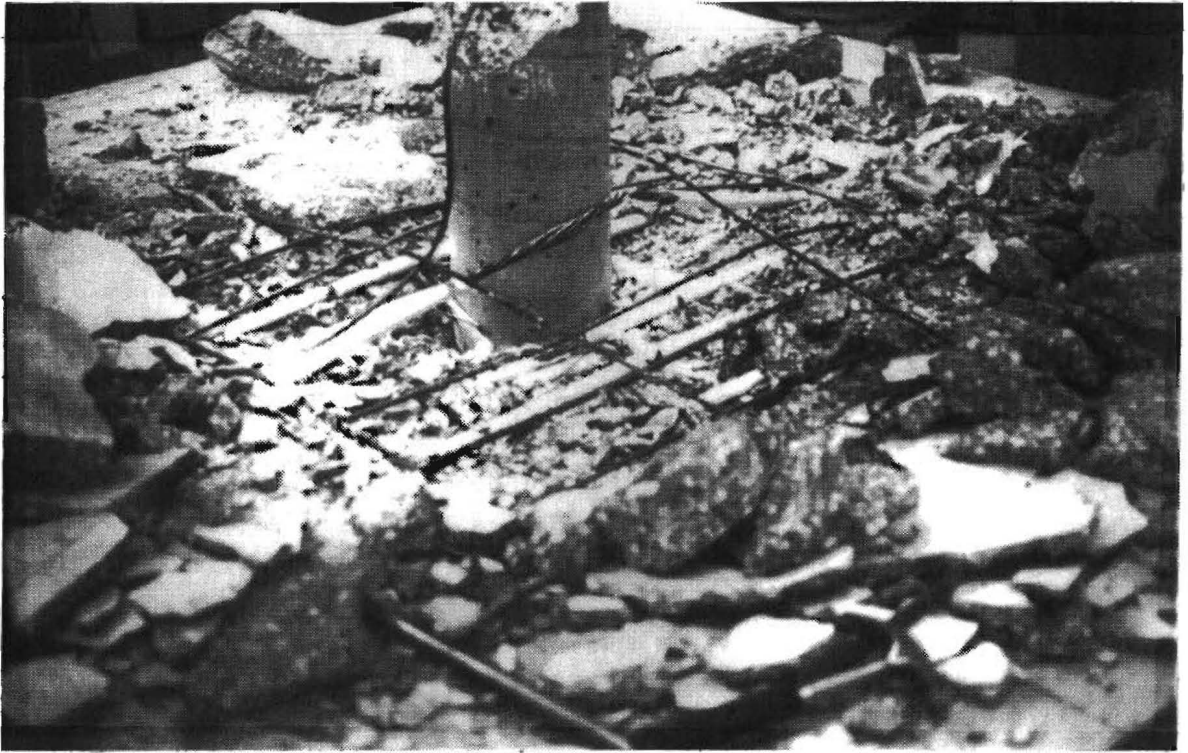


(a)

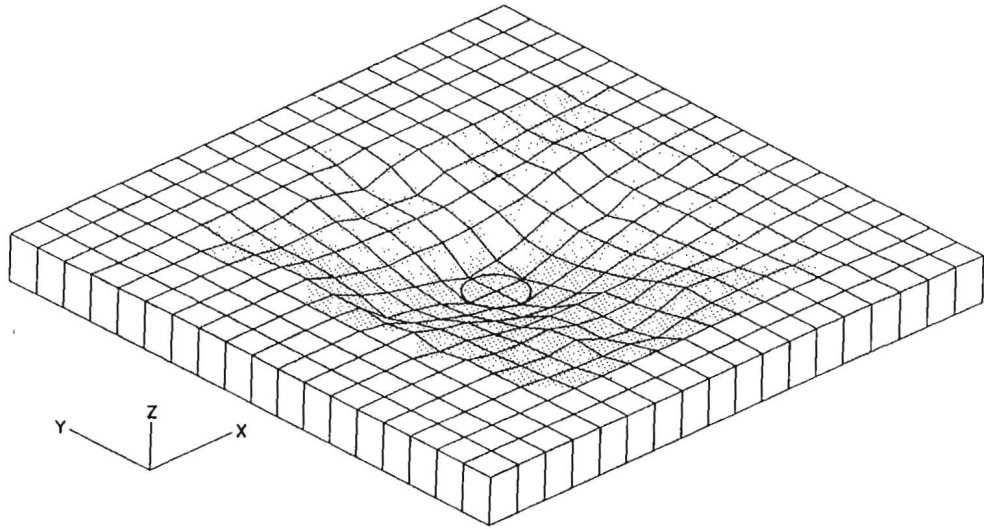


(b)

FIG. 50. Crack Propagation. (a) Top View During Early Part of Reserve Load Testing; (b) Initial Evidence of Conical Failure Surface

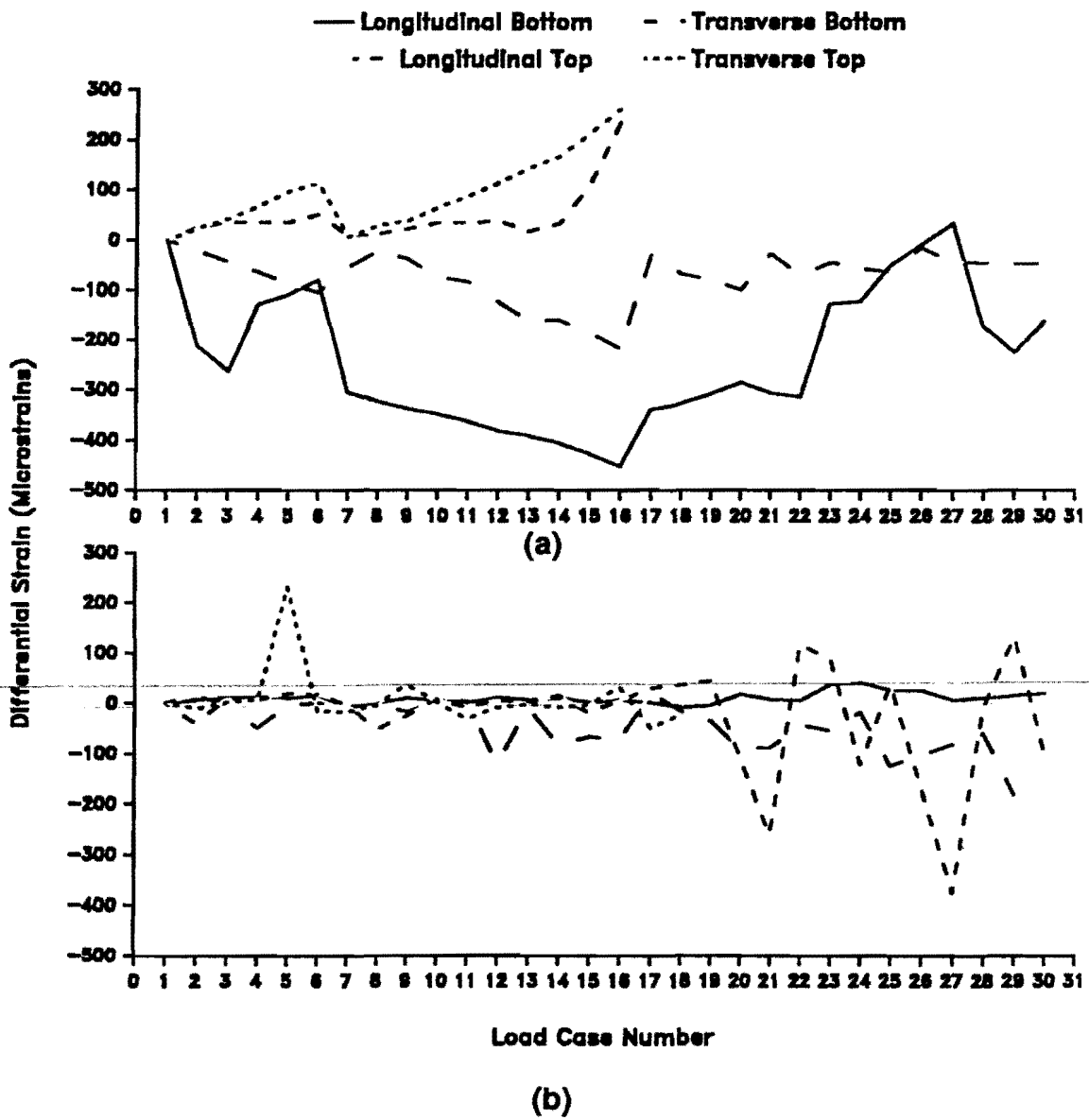


(a)



(b)

FIG. 51. Failure Pattern of the Slab. (a) After the Test; (b) Isometric View

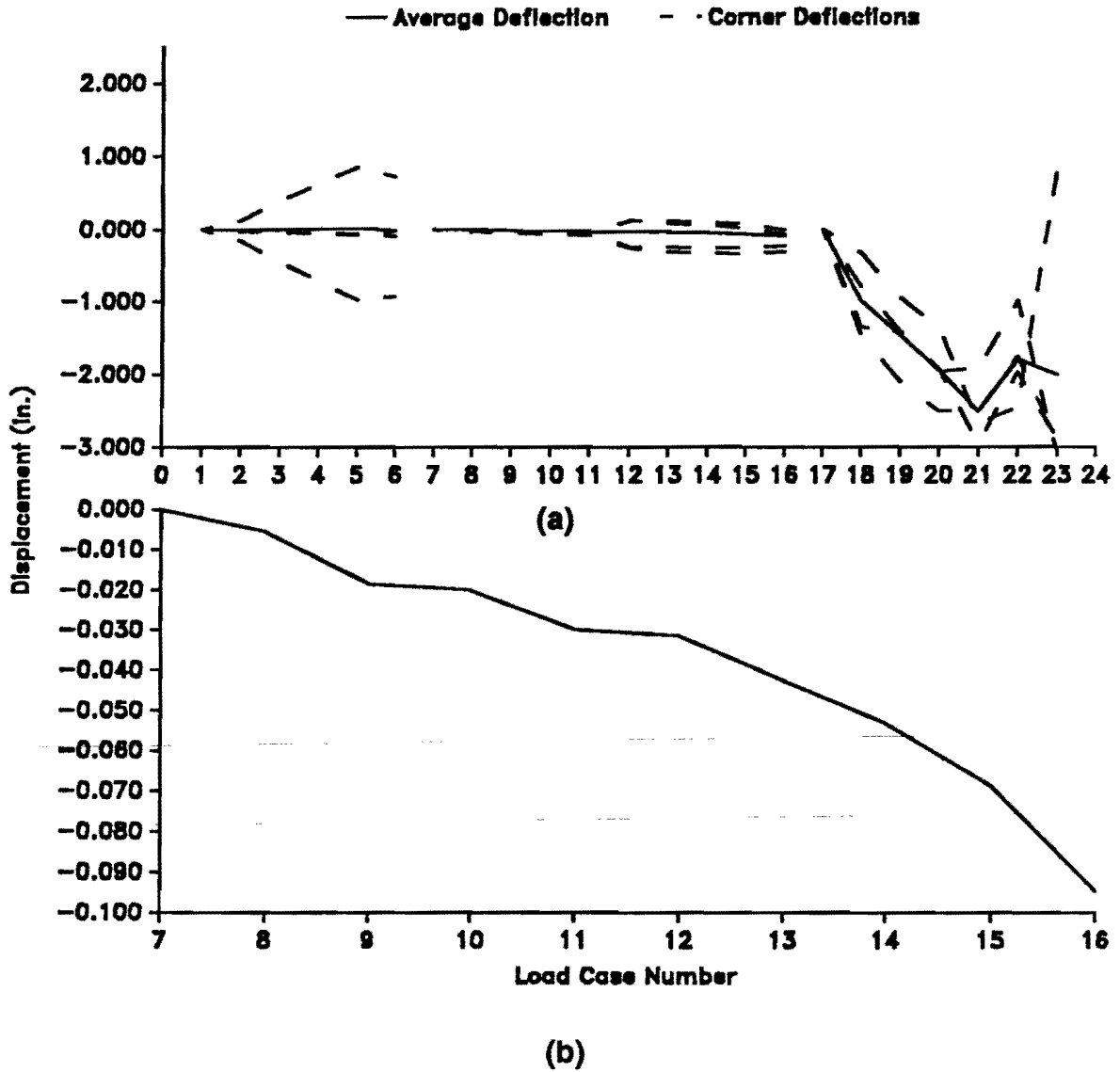


Notes

Load Case No. 6 - Maximum reading of 100 kips reached preceding the maximum of 102 kips under load control.

Load Case No. 16 - Maximum reading of 180 kips reached preceding the maximum of 198 kips under stroke control.

FIG. 52. Differential Strains during Ultimate Testing. (a) Immediately Next to the Column; (b) Midspan of Slab



Notes

Load Case 6 - Maximum reading of 100 kips reached preceding the maximum of 102 kips under load control.

Load Case 16 - Maximum reading of 180 kips reached preceding the maximum of 198 kips under stroke control.

FIG. 53. Corner Displacement during Ultimate Testing. (a) During the Course of Test; (b) During Displacement-Controlled Primary Failure Test with Truncated and Magnified Y-Axis

This tilt was also observed visually during the testing. Such movement was minimized during the displacement-controlled loading. Relative displacements of the actuators were adjusted during the testing procedure to compensate for the slight tilt observed. This adjustment is indicated at load case 12 in Fig. 53. No further large displacement was detected. After the initial slab failure, qualitative discussion of displacement is less helpful, as an increasing number of cracks diminish the integrity of the slab.

A comparison of actual failure load to design load predictions made with Eqs. 5, 8, and 10 is summarized in Table 4. Actual failure at 207 kips (923 kN) is 65 and 18 percent greater than predicted by the AASHTO and ACI methods, which anticipate failure at 125 and 176 kips (557 and 782 kN), respectively. When Eq. 10 is modified by the factor of 1.5 experienced by Gerber and Burns, their prediction of 192 kips (854 kN) is even closer to the actual value.

The 111-kip (496-kN) reserve capacity load is slightly higher than 50 % of the 207-kip (923-kN) initial failure capacity, which is consistent with results obtained by Gerber and Burns (1971). Because of the structure's large deflection of approximately 18 in. (457 mm) at the time of secondary failure, adequate warning of collapse is expected.

TABLE 4. Comparison of Predicted Failure Loads

Method (1)	Load (kip) (2)
AASHTO Method	125
ACI Method	176
Lin, et al.	128
Gerber, Burns	
Average	192
Maximum	233
Model One	207

1 kip = 4.45 kN
1 ksi = 6.89 MPa

VI. CONCLUSIONS

From this study, the following conclusions can be made regarding a bidirectionally prestressed flat slab with banded tendons that are unbonded:

The current method of data acquisition may be used for further testing. It allows for reading of 88 strain gages, 13 LVDTs, and eight load cells. By increasing the number of RS-232 connectors attached to the Hewlett-Packard strain gage card, the number of channels may be increased to accommodate a larger number of transducers for Model Two and the Brook Avenue bridge. Some modifications, however, are recommended. First, mechanical switches should be attached to the RS-232 connectors so that the connections are more secure. Second, better organization of cables is warranted. The latter recommendation is easier to implement for Model Two and the Brook Avenue overpass, which are cast in place, than for Model One, which was hoisted after being cast on the floor. Finally, because the cables are longer for Model Two and the Brook Avenue overpass than for Model One, the effect of background radio frequency noise must be watched closely, as well as the effects of cable resistance and temperature.

All elastic load cases (some of which total more than three times a scaled HS-20 truck) and tendon configurations for the laboratory slab show that the maximum compressive strain in concrete is well within service level limits. Moreover, the load cases show that even under relatively high out-of-plane loading, the concrete remains in compression. Thus, as an alternative design, prestressing may be reduced from the present level without exceeding the allowable tensile stress of the concrete. It follows that further study is warranted to investigate the possibility of overall reduction of material or design with a smaller amount of prestressing. However, since Model One does not closely simulate the actual bridge, Model Two, a scale model of the prototype bridge, is being designed and studied as part of the research for this purpose. Also, since Model Two has bonded tendons as opposed to unbonded tendons in Model One, correlation of numerical simulation and laboratory experimentation for bonded tendons may be studied.

The current design process attempts to provide transverse prestressing for a narrow strip of concrete. Consideration of each column-line region is required because integrity of concrete along the column line is responsible for supporting the structure, similar to the effect obtained from a bent cap. Because the level of transverse normal strain is maximum directly over the center of the column line, as shown in Fig. 4.1, one approach is to base the design of transverse prestressing on

analysis which uses a narrow rectangular strip centered over the columns. Thus a strip of the slab over the column line would be investigated for design adequacy, with strains taken to be those along the column line. For Model One, a total width of 1 ft (305 mm) is small enough for the strain to be considered uniform across the cross section. Although this beam-strip method is available for design, several refined techniques should be considered for the reasons cited below.

While numerical and experimental strains resulting from transverse prestressing forces vary continuously throughout the slab, the simplified analytical approach predicts discontinuous strains and generally leads to overestimation of transverse strains away from the banded center; conversely, it leads to low strain estimates along the center of the band. More specifically, at the center point of the slab, simplified strains differ from their numerically-simulated counterparts by up to approximately 45 percent (Fig. 42).

Although experimental and numerical modelling in this study seeks to quantify the validity of the assumed angle of stress dissipation due to banded transverse tendons, definitive conclusions for this assumption are difficult to draw. Although a crude tabulation of approximate dissipation angles for varying numbers of tendons and forces could be formulated, designers are encouraged to use more refined analysis tools for this type of slab structure. Improved accuracy for in-plane strain prediction is possible either through an FEM or classical elasticity approach. The elasticity formulation is flexible in that it is not limited to estimating transverse strains only within the crucial region above a column. Since a relatively simple computer program is sufficient for a first approximation of transverse normal stress and strain, its use rather than the current straight-line method is recommended. This method, however, is limited to calculation of strain due to in-plane prestressing force; it is not intended to predict strain induced by internal moment. Accurate investigations should involve extensive use of plate analysis software, and FEM is recommended for such applications.

Ultimate loading lead to a brittle shear failure. The ACI equation for punch-through shear capacity, with variables assumed according to conventional engineering practice, may be applied with reasonable confidence and safety to the laboratory model. The reserve capacity of 111 kips (496 kN) is lower than the maximum capacity of 207 kips (923 kN) and yet provides adequate warning against complete failure. Clearly, the reserve capacity is not large enough to prevent progressive collapse if the failure load is sustained. However, under most bridge loading conditions, the structure's large deflection of approximately 18 in. (457 mm) provides adequate warning against complete failure.

VII. REFERENCES

- Analysis and Design of Reinforced Concrete Bridge Structures.* (1988). Amer. Concr. Inst., ACI-ASCE Committee 343, Detroit, Mich.
- Bazant, Z. P., and Cao, Z. (1987). "Size Effect in Punching Shear Failure of Slabs," *ACI Journal*, Amer. Concr. Inst., Detroit, Mich., 84(6), 44-53.
- Building Code Requirements for Reinforced Concrete.* (1989). Amer. Concr. Inst., ACI Committee 318, Detroit, Mich.
- Burns, N. H., and Hemakom, R. (1977). "Test of Scale Model Post-Tensioned Flat Plate," *J. Struct. Engrg.*, ASCE, 103(6), 1237-1255.
- Burns, N. H., and Hemakom, R. (1985). "Test of Post-Tensioned Flat Plate with Banded Tendons," *J. Struct. Engrg.*, ASCE, 111(9), 1899-1915.
- Cox, W. R. (1985). "Bridge Design Example from Taft Boulevard Overpass," State Department of Highways and Public Transportation, Bridge Division, Austin, Tex.
- Davis, R. E. (1978). "Structural Behavior of a Skew Two-Span Reinforced Concrete Box Girder Bridge Model," Report No. FHWA-CA-ST4187-78-01, Dept. of Civ. Engrg., Univ. of California, Berkeley, Calif.
- Displacement Transducer, DC-DC Series 240, Bulletin No. SO12-0030-KHD.* (1984). Trans-Tek, Inc., Ellington, Conn.
- Elstner, R. C., and Hognestad, E. (1956). "Shearing Strength of Reinforced Concrete Slabs," *ACI Journal*, 28(1), 29-58.
- Gerber, L. L., and Burns, N. H. (1971). "Ultimate Strength Tests of Post-Tensioned Flat Plates," *PCI Journal*, 16(6), 40-58.
- Hobbs, D. W., Pomeroy, C. D., and Newman, J. B. (1977). "Design Stresses for Concrete Structures Subject to Multi-Axial Stresses," *The Structural Engineer*, 55(4), 151-164.
- Kupfer, H., Hilsdorf, H. K., and Rusch, H. (1969). "Behavior of Concrete under Biaxial Stresses," *ACI Journal*, 66(52), 656-666.
- Lin, T. Y., Scordelis, A. C., and May, H. R. (1957). "Shearing Strength of Reinforced and Prestressed Concrete Lift Slabs," Institute of Engineering Research, Series 100, Issue 4, University of California, Berkeley.
- Lotus 1-2-3, Manual Release 2.01.* (1986). Lotus Development Corporation, Cambridge, Mass.
- Lotus Measure Reference Manual.* (1986). Lotus Development Corporation, Cambridge, Mass.

- Microsoft, *FORTRAN 4.1 Optimizing Compiler*. (1987). Microsoft Corporation, Redmond, Wash.
- Naaman, A. E. (1982). *Prestressed Concrete Analysis and Design, Fundamentals*, McGraw-Hill Book Company, New York, N. Y., 20-21, 297-303.
- Operating and Service Manual for Hewlett-Packard Model 44427A, Strain Gage/Bridge Assembly (120 Ohm Gage, Option 070), Manual Part No. 44427-90001*. (1981). Hewlett-Packard Company, Loveland, Colo.
- Operating System/2* Standard Edition Version 1.1*. (1988). International Business Machines Corporation, Armonk, N. Y.
- PATRAN Plus User's Guide*. (1988). PDA Engineering, Santa Ana, Calif.
- Post-Tensioning Manual*, fourth edition. (1985). Post-Tensioning Institute Phoenix, Ariz., 149-160, 303-304.
- "Recommendations for Concrete Members Prestressed with Unbonded Tendons." (1983). Amer. Concr. Inst., ACI-ASCE Committee 423, Detroit, Mich., 61-76.
- Scordelis, A. C., Lin, T. Y., and Itaya, R. (1959). "Behavior of a Continuous Slab Prestressed in Two Directions," *ACI Journal*, 56(6), 441-459.
- Standard Specifications for Construction of Highways, Streets and Bridges*. (1982). Texas State Department of Highways and Public Transportation, Austin, Texas, 423, 429.
- Standard Specifications for Highway Bridges*, fourteenth edition. (1989). American Association of State Highway and Transportation Officials, Washington, D.C., 22.
- Timoshenko, S., and Goodier, J. N. (1951). *Theory of Elasticity*, second edition, McGraw-Hill Book Company, New York, N.Y., 46-54.
- Tiv, M. (1987). "Pickup Point Selection in Structural Panels," thesis presented to The University of Texas at El Paso in partial fulfillment of the requirements for the degree of Master of Science.
- Van Greunen, J. (1979). "Nonlinear Geometric, Material and Time-Dependent Analysis of Reinforced and Prestressed Concrete Slabs and Panels," dissertation presented to University of California, Berkeley, Calif., in partial fulfillment of the requirements for the degree of Doctor of Philosophy.
- Zia, P., White, R. N., and Vanhorn, D. A. (1970). "Principles of Model Analysis," *Models for Concrete Structures*, Amer. Concr. Inst., Detroit, Mich., 19-39.

APPENDIX I - NOTATION

The following symbols are used in this report:

- A = area per unit width of concrete slab;
- A_g = area of gross section;
- A_s = area of reinforcing steel;
- A_t = cross-sectional area of tendon;
- b = perimeter of lifting collar;
- b_o = length of critical section;
- c = distance from centroid;
- D = column diameter;
- DL = amount of dead load;
- d = depth of reinforcement;
- E = modulus of elasticity;
- E_c = initial modulus of elasticity for concrete;
- E_s = modulus of elasticity for reinforcing steel;
- F = force;
- F_{pj} = jacking force;
- F_{ps} = prestress tendon force;
- f'_c = compressive stress capacity of concrete;
- f_{pc} = concrete stress induced by prestressing;
- f_{pu} = ultimate force of prestressing tendon;
- f_y = yield stress of reinforcing steel;
- h = total thickness of the slab;
- I = moment of inertia;
- I_c = moment of inertia for concrete;
- I_g = moment of inertia of the gross column section;
- I_s = moment of inertia for reinforcing steel;
- K = wobble coefficient;
- kl_u = effective length;
- L = length quantity;
- L_M = moment arm;
- L_t = tendon length;
- M = internal moment;

M_x = internal moment per unit width in longitudinal direction;
 M_y = internal moment per unit width in transverse direction;
 n = number of transverse prestress tendons;
 P = total axial force of the tendon;
 P_c = critical load for buckling;
 P_u = ultimate shear force;
 r = radius of gyration;
 S = spacing of reinforcement;
 S_1 = required linear scale factor;
 SF = actual scale factor for quantity under consideration;
 SF_M = scale factor for moment;
 SF_V = scale factor for shear;
 V = shear force;
 V_p = vertical component of prestress force;
 v = shear stress;
 v_c = shear stress in concrete;
 W_c = unit weight of concrete;
 W_p = assumed width of the effective prestress at center line of a slab;
 W_s = width of the slab;
 W_t = width of tendon band;
 α = change in angle between prestress force at the anchorage and the force at a given distance in radians;
 β_c = ratio of long side to short side of concentrated load or reaction area;
 β_d = absolute value of ratio of maximum factored dead load moment to maximum factored total load moment;
 ΔL_t = tendon elongation;
 ϵ = strain;
 ϵ_{max} = maximum linear elastic strain;
 μ = friction coefficient;
 ρ = ratio of cross-sectional steel area to cross-sectional concrete area;
 σ_{max} = allowable concrete stress;
 σ_n = stress in concrete caused by n prestress tendons;
 ϕ = load or resistance factor;
 Ψ = angle of dissipation of prestress; and
 θ = angle of failure surface to slab surface.

APPENDIX II - ELASTICITY PROGRAM

```

DIMENSION STRS(100,100)
REAL*8 PI
OPEN (UNIT=4,FILE='IN.DAT',STATUS='UNKNOWN')
OPEN (UNIT=5,FILE='OUT.DAT',STATUS='UNKNOWN')
PI = 3.141592653582
READ (4,*) Q1, Q2, A, EL, C, E, NU, ST
C   Q1 - CONCRETE STRESS EXERTED BY TRANSVERSE TENDONS
C       AT ANCHOR ENDS
C   Q2 - CONCRETE STRESS EXERTED BY LONGITUDINAL TENDONS
C       AT ANCHOR ENDS
C   A - 1/2 OF TENDON BAND WIDTH
C   EL - 1/2 OF SLAB LENGTH
C   C - 1/2 OF SLAB WIDTH
C   E - CONCRETE MODULUS OF ELASTICITY
C   NU - POISSON'S RATIO OF CONCRETE
C   ST - DISTANCE INCREMENTS
JMAX = C/ST
IMAX = EL/ST
DO 20 J = 0, JMAX
  Y = J * ST
  DO 10 I = 0, IMAX
    X = I * ST
    SIGMA = 0.0
    DO 5 M = 1, 5
      SIH1 = (EXP(M*PI*C/EL) - EXP(-M*PI*C/EL))/2.0
      SIH2 = (EXP(2*M*PI*C/EL) - EXP(-2*M*PI*C/EL))/2.0
      COH = (EXP(M*PI*C/EL) + EXP(-M*PI*C/EL))/2.0
      SIHY = (EXP(M*PI*Y/EL) - EXP(-M*PI*Y/EL))/2.0
      COHY = (EXP(M*PI*Y/EL) + EXP(-M*PI*Y/EL))/2.0
      SIGMA= SIGMA + ((SIN(M*PI*A/EL))/M)*(((M*PI*C/EL*COH +
1          SIH1)*COHY - M*PI*Y/EL*SIHY*SIH1)/(SIH2+2*M*PI*C/
2          EL))*(COS(M*PI*X/EL))
    5    CONTINUE
      STRS(I,J) = -Q1*A/EL - 4*Q1*SIGMA/PI
  10    CONTINUE
  20    CONTINUE
C   OUTPUT STRESS
  DO 30 J = 0, JMAX
  30    WRITE(5,100) (INT(STRS(I,J)), I = 0, IMAX)
      WRITE(5,101)
C   OUTPUT STRAIN
  DO 50 J = 0, JMAX
  50    WRITE(5,100) (INT(STRS(I,J)/E + NU*Q2/E), I = 0, IMAX)
100    FORMAT (1X,10I6,/)
101    FORMAT (/)
END

```


APPENDIX III - TABLES OF ELASTIC LOADING RESULTS

TABLE 5. Laboratory and Computer Predicted Strain and Moment before Hoisting

GAUGE (1)	Laboratory Results						NOPARC Output					
	Strain ($\mu\epsilon$)				Moment (k-in/in)		Strain ($\mu\epsilon$)				Moment (k-in/in)	
	XB (2)	YB (3)	XT (4)	YT (5)	MX (6)	MY (7)	XB (8)	YB (9)	XT (10)	YT (11)	MX (12)	MY (13)
1	-246	40	—	17	—	2.1	-227	35	-131	30	-10.0	0.6
2	-215	35	- 53	12	-15.8	2.1	-228	35	-132	30	-10.0	0.6
3	-135	39	-115	18	- 2.7	2.0	-229	34	-130	30	-10.3	0.5
4	-159	50	-108	28	- 5.6	2.1	-236	31	-129	28	-11.1	0.4
5	-208		-103		-10.7		-218	26	-101	25	-11.8	0.2
6	-229	40	-136	15	- 9.8	2.3	-227	35	-132	30	- 9.9	0.6
7	-189	43	-115	13	- 7.8	2.7	-228	35	-132	30	-10.0	0.6
8	-178	42	-109	23	- 7.3	1.8	-230	34	-130	30	-10.4	0.5
9	-260	55	-110	33	-15.0	2.1	-231	34	-124	31	-11.0	0.4
10	-203		-111		- 9.5		-218	45	-100	42	-11.9	0.5
11	-243	45	-131	23	-11.6	2.1	-227	35	-131	29	-10.0	0.7
12	-225	39	-121	17	-10.7	2.0	-228	36	-131	29	-10.1	0.8
13	-164	55	-128	25	- 4.3	2.8	-230	35	-129	30	-10.5	0.6
14	-278	66	-110	34	-16.7	3.0	-232	35	-125	31	-11.0	0.5
15	-258		- 94		-16.2		-219	45	-100	41	-12.0	0.6
16	-258	47	-137	18	-12.4	2.7	-227	37	-130	27	-10.1	1.0
17	-115	41	-134	20	0.9	2.0	-228	37	-129	27	-10.3	1.0
18	-155	48	-125	24	- 3.7	2.3	-230	37	-128	28	-10.6	1.0
19	-253	57	- 99	21	-15.3	3.3	-233	37	-125	32	-11.1	0.6
20	-257		-114		-14.4		-260	38	-147	35	-11.8	0.5
21	-270	7	-132	24	-14.0	- 1.4	-228	39	-126	24	-10.6	1.5
22	-248	48	-149	26	-10.4	2.1	-228	39	-126	24	-10.6	1.5
23	-255	48	-137	32	-12.2	1.6	-230	39	-124	23	-10.9	1.6
24	-266	51	-147	21	-12.3	2.8	-234	39	-123	23	-11.4	1.6

GAUGE - Gauge Location Number, see Fig. 18

XB - Longitudinal Direction, Bottom Layer

YB - Transverse Direction, Bottom Layer

XT - Longitudinal Direction, Top Layer

YT - Transverse Direction, Top Layer

MX - Moment in Longitudinal Direction

MY - Moment in Transverse Direction

Note: 1 kip-in/in = 4.45 kN-m/m

TABLE 6. Laboratory and Computer Predicted Strain and Moment under Load 0.1

GAUGE (1)	Laboratory Results						NOPARC Output					
	Strain ($\mu\epsilon$)				Moment (k-in/in)		Strain ($\mu\epsilon$)				Moment (k-in/in)	
	XB (2)	YB (3)	XT (4)	YT (5)	MX (6)	MY (7)	XB (8)	YB (9)	XT (10)	YT (11)	MX (12)	MY (13)
1	-282	33	—	26	—	0.8	-260	48	-100	19	-15.9	2.7
2	-258	33	—	21	—	1.2	-263	38	-97	28	-16.4	1.1
3	-204	40	-146	21	-6.5	1.8	-250	29	-110	35	-14.1	-0.3
4	-172	52	-128	35	-5.1	1.7	-250	29	-120	30	-13.2	0.1
5	-239	—	-125	—	-11.7	—	-220	26	-97	25	-12.4	0.2
6	-286	14	-150	35	-14.0	-1.7	-263	38	-97	27	-16.4	1.1
7	-252	—	-112	28	-14.1	—	-273	33	-90	33	-18.0	0.2
8	—	42	-124	13	—	2.6	-250	29	-110	36	-14.1	-0.4
9	-300	69	-127	34	-17.3	3.3	-240	31	-117	34	-12.5	-0.1
10	-233	—	-129	—	-10.8	—	-220	47	-98	39	-12.3	0.9
11	-298	58	-115	3	-18.2	4.9	-250	40	-110	26	-14.1	1.4
12	-263	33	-123	19	-14.2	1.4	-250	41	-110	24	-14.1	1.6
13	-180	64	-113	25	-7.2	3.6	-250	38	-110	27	-14.1	1.1
14	-330	78	-123	49	-20.5	2.9	-240	37	-110	29	-13.1	0.9
15	-304	—	-104	—	-19.7	—	-223	50	-97	36	-12.6	1.5
16	-319	51	-157	15	-16.5	3.3	-250	41	-110	23	-14.1	1.7
17	-109	—	-152	13	3.0	—	-250	42	-110	23	-14.1	1.8
18	-169	45	-142	22	-3.6	2.2	-250	42	-110	23	-14.1	1.8
19	-308	59	-126	17	-18.2	3.8	-250	42	-110	27	-14.1	1.5
20	-299	—	-132	—	-16.8	—	-270	44	-140	29	-13.3	1.5
21	-333	9	-154	22	-18.1	-1.0	-240	42	-110	21	-13.1	2.0
22	-310	46	-168	24	-14.7	2.1	-250	42	-110	21	-14.1	2.0
23	-308	43	-158	33	-15.3	1.1	-240	42	-110	21	-13.1	2.0
24	-324	53	-181	26	-14.8	2.5	-250	41	-110	21	-14.1	1.9

GAUGE - Gauge Location Number, see Fig. 18

XB - Longitudinal Direction, Bottom Layer

YB - Transverse Direction, Bottom Layer

XT - Longitudinal Direction, Top Layer

YT - Transverse Direction, Top Layer

MX - Moment in Longitudinal Direction

MY - Moment in Transverse Direction

Note: 1 kip-in/in = 4.45 kN-m/m

TABLE 7. Laboratory and Computer Predicted Strain and Moment under Load 0.2

GAUGE (1)	Laboratory Results						NOPARC Output					
	Strain ($\mu\epsilon$)				Moment (k-in/in)		Strain ($\mu\epsilon$)				Moment (k-in/in)	
	XB (2)	YB (3)	XT (4)	YT (5)	MX (6)	MY (7)	XB (8)	YB (9)	XT (10)	YT (11)	MX (12)	MY (13)
1	-290	15	—	42	—	- 2.1	-270	41	- 92	25	-17.5	1.6
2	-269	20	—	37	—	- 1.3	-277	30	- 87	36	-18.6	- 0.3
3	-213	28	-147	33	- 7.3	- 0.2	-243	23	-120	42	-12.5	- 1.4
4	-162	45	-131	42	- 3.9	0.5	-247	25	-120	33	-12.9	- 0.5
5	-237		-124		-11.6		-220	23	- 99	28	-12.2	- 0.3
6	-301	2	-138	67	-16.4	- 5.4	-277	28	- 87	38	-18.6	- 0.7
7	-264	—	-101	42	-16.2	—	-283	22	- 82	43	-19.7	- 1.6
8	—	32	-126	28	—	0.5	-243	22	-120	42	-12.5	- 1.5
9	-297	67	-129	42	-16.9	2.5	-240	27	-120	37	-12.2	- 0.7
10	-233		-131		-10.6		-220	44	- 98	42	-12.3	0.4
11	-307	63	-103	4	-20.1	5.3	-260	44	-100	22	-15.9	2.1
12	-271	42	-111	20	-16.0	2.1	-260	43	-100	23	-15.9	1.9
13	-178	71	-114	21	- 6.9	4.6	-250	39	-110	26	-14.1	1.3
14	-336	76	-123	52	-21.1	2.4	-240	36	-110	30	-13.1	0.7
15	-300		-105		-19.3		-223	48	- 97	37	-12.6	1.2
16	-326	57	-151	14	-17.7	3.9	-250	44	-110	21	-14.1	2.2
17	-110	—	-145	12	2.3	—	-250	44	-110	21	-14.1	2.2
18	-170	44	-131	22	- 4.6	2.1	-250	43	-110	23	-14.1	1.9
19	-308	60	-125	22	-18.3	3.5	-250	42	-110	28	-14.1	1.4
20	-299		-133		-16.7		-270	43	-140	30	-13.3	1.3
21	-337	7	-150	23	-18.8	- 1.3	-250	43	-110	20	-14.1	2.2
22	-314	50	-161	22	-15.7	2.6	-250	42	-110	20	-14.1	2.1
23	-311	44	-158	38	-15.6	0.8	-250	42	-110	21	-14.1	2.0
24	-325	55	-180	24	-15.0	2.9	-250	41	-110	21	-14.1	1.9
DEFL	0.0351 in.						0.0044 in.					

GAUGE - Gauge Location Number, see Fig. 18

XB - Longitudinal Direction, Bottom Layer

YB - Transverse Direction, Bottom Layer

XT - Longitudinal Direction, Top Layer

YT - Transverse Direction, Top Layer

DEFL - Average Corner Deflection

MX - Moment in Longitudinal Direction

MY - Moment in Transverse Direction

Note: 1 kip-in/in = 4.45 kN-m/m

TABLE 8. Laboratory and Computer Predicted Strain and Moment under Load 0.3

GAUGE (1)	Laboratory Results						NOPARC Output					
	Strain ($\mu\epsilon$)				Moment (k-in/in)		Strain ($\mu\epsilon$)				Moment (k-in/in)	
	XB (2)	YB (3)	XT (4)	YT (5)	MX (6)	MY (7)	XB (8)	YB (9)	XT (10)	YT (11)	MX (12)	MY (13)
1	-309	13	—	48	—	- 2.8	-297	38	- 70	28	-22.0	1.1
2	-291	17	—	42	—	- 2.0	-303	26	- 65	40	-23.1	- 1.0
3	-210	28	-135	40	- 8.1	- 0.8	-260	17	-100	48	-15.9	- 2.5
4	-164	41	-128	47	- 4.3	- 0.3	-247	19	-120	38	-12.9	- 1.5
5	-235		-127		-11.1		-220	19	-100	31	-12.1	- 0.9
6	-319	- 3	-120	54	-19.7	- 4.7	-303	23	- 66	42	-23.0	- 1.4
7	-281	—	- 83	48	-19.4	—	-310	16	- 58	50	-24.3	- 2.7
8	—	29	-110	30	—	0.1	-257	15	-103	49	-15.3	- 2.7
9	-300	61	-126	47	-17.4	1.5	-240	21	-120	43	-12.2	- 1.7
10	-231		-128		-10.7		-217	41	-100	44	-11.8	0.0
11	-328	58	- 81	4	-24.0	4.8	-280	39	- 82	26	-19.4	1.3
12	-293	37	- 95	23	-19.5	1.4	-280	40	- 82	26	-19.4	1.4
13	-190	66	- 95	28	- 9.7	3.5	-267	38	- 98	29	-16.7	1.0
14	-332	78	-125	56	-20.5	2.3	-240	39	-120	28	-12.2	1.1
15	-296		-100		-19.3		-223	50	- 98	36	-12.6	1.5
16	-342	56	-132	13	-20.9	3.9	-270	46	- 88	19	-17.9	2.5
17	-124	—	-127	10	- 0.6	—	-270	47	- 89	18	-17.8	2.7
18	-181	33	-120	21	- 6.6	1.2	-260	46	- 99	20	-16.0	2.4
19	-309	62	-130	21	-17.9	3.8	-250	42	-110	27	-14.1	1.5
20	-299		-133		-16.7		-270	44	-140	29	-13.3	1.5
21	-354	11	-134	21	-21.8	- 0.8	-267	46	- 92	17	-17.3	2.7
22	-328	49	-143	21	-18.6	2.6	-270	45	- 92	18	-17.5	2.5
23	-322	47	-147	35	-17.6	1.3	-260	43	- 98	19	-16.1	2.2
24	-329	54	-176	26	-15.8	2.6	-250	42	-110	20	-14.1	2.1
DEFL	0.0474 in.						0.0132 in.					

GAUGE - Gauge Location Number, see Fig. 18

XB - Longitudinal Direction, Bottom Layer

YB - Transverse Direction, Bottom Layer

XT - Longitudinal Direction, Top Layer

YT - Transverse Direction, Top Layer

DEFL - Average Corner Deflection

MX - Moment in Longitudinal Direction

MY - Moment in Transverse Direction

Note: 1 kip-in/in = 4.45 kN-m/m

TABLE 9. Laboratory and Computer Predicted Strain and Moment under Load 1.1

GAUGE (1)	Laboratory Results						NOPARC Output					
	Strain ($\mu\epsilon$)				Moment (k-in/in)		Strain ($\mu\epsilon$)				Moment (k-in/in)	
	XB (2)	YB (3)	XT (4)	YT (5)	MX (6)	MY (7)	XB (8)	YB (9)	XT (10)	YT (11)	MX (12)	MY (13)
1	-261	11	—	64	—	- 4.3	-250	29	- 95	1	-15.4	2.5
2	-264	18	—	17	—	0.2	-253	20	- 90	10	-16.1	0.9
3	-184	39	-122	2	- 6.7	3.3	-240	16	-110	22	-13.1	- 0.4
4	-177	46	-131	34	- 5.3	1.3	-247	23	-120	25	-12.9	0.0
5	-255		-127		-13.0		-220	23	- 97	22	-12.4	0.2
6	-349	10	-153	19	-19.7	- 0.7	-253	20	- 90	10	-16.1	0.9
7	-250	—	-106	16	-14.4	—	-267	17	- 82	17	-18.1	0.1
8	—	37	-128	4	—	2.9	-240	18	-110	26	-13.1	- 0.6
9	-319	72	-133	51	-18.6	2.2	-240	26	-114	29	-12.8	- 0.1
10	-250		-135		-11.9		-220	46	- 97	39	-12.4	0.8
11	-310	46	- 94	- 19	-21.2	5.6	-240	19	-100	6	-14.0	1.2
12	-119	8	-118	1	- 0.9	0.6	-243	24	-103	8	-14.0	1.5
13	-189	62	-104	8	- 8.8	4.8	-250	29	-110	19	-14.1	1.0
14	-353	76	-118	53	-23.1	2.4	-240	32	-110	26	-13.1	0.7
15	-320		-111		-20.6		-223	49	- 97	36	-12.6	1.4
16	-333	17	-125	- 12	-20.6	2.5	-240	15	-103	- 2	-13.7	1.5
17	-120	—	-157	- 20	2.4	—	-240	17	-110	- 1	-13.1	1.6
18	-183	—	-145	10	- 4.6	—	-250	31	-110	13	-14.1	1.7
19	-327	53	-127	19	-19.9	3.1	-250	40	-110	26	-14.1	1.4
20	-309		-130		-17.9		-270	43	-140	29	-13.3	1.4
21	-364	4	-178	9	-18.9	- 0.4	-260	30	-120	12	-14.1	1.7
22	-344	33	-136	8	-20.7	2.3	-250	36	-120	17	-13.2	1.8
23	-327	43	-157	38	-17.2	0.7	-250	41	-110	20	-14.1	2.0
24	-341	47	-192	75	-15.5	- 2.0	-247	41	-110	20	-13.8	2.0

GAUGE - Gauge Location Number, see Fig. 18

XB - Longitudinal Direction, Bottom Layer

YB - Transverse Direction, Bottom Layer

XT - Longitudinal Direction, Top Layer

YT - Transverse Direction, Top Layer

MX - Moment in Longitudinal Direction

MY - Moment in Transverse Direction

Note: 1 kip-in/in = 4.45 kN-m/m

TABLE 10. Laboratory and Computer Predicted Strain and Moment under Load 1.2

GAUGE (1)	Laboratory Results						NOPARC Output					
	Strain ($\mu\epsilon$)				Moment (k-in/in)		Strain ($\mu\epsilon$)				Moment (k-in/in)	
	XB (2)	YB (3)	XT (4)	YT (5)	MX (6)	MY (7)	XB (8)	YB (9)	XT (10)	YT (11)	MX (12)	MY (13)
1	-276	- 6	—	77	—	- 6.9	-267	22	- 83	8	-18.1	1.3
2	-279	5	—	29	—	- 2.0	-267	10	- 81	20	-18.2	- 0.8
3	-178	29	-125	13	- 5.9	1.5	-240	9	-110	28	-13.1	- 1.5
4	-175	41	-134	40	- 4.8	0.3	-240	19	-120	29	-12.2	- 0.7
5	-253		-131		-12.5		-220	20	- 98	25	-12.3	- 0.3
6	-366	- 11	-140	38	-22.4	- 4.1	-270	10	- 78	19	-18.8	- 0.7
7	-264	—	- 90	27	-17.2	—	-273	7	- 76	27	-19.2	- 1.6
8	—	25	-132	13	—	1.1	-240	11	-110	32	-13.1	- 1.7
9	-316	63	-137	53	-18.0	1.2	-240	21	-117	33	-12.5	- 0.9
10	-247		-137		-11.4		-220	43	- 98	42	-12.3	0.3
11	-321	50	- 82	- 25	-23.3	6.5	-250	23	- 95	2	-15.4	1.9
12	-126	17	-109	1	- 2.4	1.4	-250	26	- 96	7	-15.3	1.7
13	-190	61	-106	4	- 8.7	5.1	-250	29	-110	18	-14.1	1.1
14	-355	77	-117	55	-23.4	2.3	-240	31	-110	27	-13.1	0.5
15	-320		-106		-21.1		-223	47	- 97	38	-12.6	1.0
16	-342	23	-117	- 15	-22.2	3.3	-250	18	-100	- 5	-14.9	2.0
17	-125	—	-150	- 22	1.3	—	-250	19	-100	- 3	-14.9	1.9
18	-182	—	-144	9	- 4.6	—	-250	32	-110	13	-14.1	1.8
19	-328	51	-128	19	-19.9	2.9	-250	39	-110	26	-14.1	1.3
20	-311		-130		-18.1		-270	42	-140	30	-13.3	1.2
21	-369	3	-174	9	-19.7	- 0.5	-260	30	-120	12	-14.1	1.7
22	-350	31	-130	9	-21.8	2.0	-260	37	-110	17	-15.0	1.9
23	-330	39	-164	38	-16.9	0.3	-250	41	-110	20	-14.1	2.0
24	-341	46	-191	76	-15.6	- 2.2	-250	41	-110	20	-14.1	2.0
DEFL	0.0351 in.						0.0045 in.					

GAUGE - Gauge Location Number, see Fig. 18

XB - Longitudinal Direction, Bottom Layer

YB - Transverse Direction, Bottom Layer

XT - Longitudinal Direction, Top Layer

YT - Transverse Direction, Top Layer

DEFL - Average Corner Deflection

MX - Moment in Longitudinal Direction

MY - Moment in Transverse Direction

Note: 1 kip-in/in = 4.45 kN-m/m

TABLE 11. Laboratory and Computer Predicted Strain and Moment under Load 1.3

GAUGE (1)	Laboratory Results						NOPARC Output					
	Strain ($\mu\epsilon$)				Moment (k-in/in)		Strain ($\mu\epsilon$)				Moment (k-in/in)	
	XB (2)	YB (3)	XT (4)	YT (5)	MX (6)	MY (7)	XB (8)	YB (9)	XT (10)	YT (11)	MX (12)	MY (13)
1	-294	- 9	—	82	—	- 7.6	-287	18	- 63	12	-21.7	0.6
2	-298	1	—	34	—	- 2.7	-293	6	- 56	24	-22.9	- 1.5
3	-188	24	-111	17	- 8.1	0.7	-253	3	- 95	34	-15.7	- 2.5
4	-176	37	-131	44	- 5.2	- 0.4	-240	14	-120	34	-12.2	- 1.6
5	-253		-131		-12.5		-220	16	-100	28	-12.1	- 0.9
6	-381	- 19	-124	35	-25.3	- 4.6	-293	6	- 58	23	-22.7	- 1.4
7	-279	—	- 72	31	-20.2	—	-303	1	- 48	32	-24.5	- 2.6
8	—	21	-115	17	—	0.5	-257	4	- 97	38	-15.9	- 2.8
9	-319	58	-134	54	-18.5	0.7	-237	15	-117	38	-12.2	- 1.8
10	-249		-137		-11.6		-217	40	- 99	44	-11.9	- 0.1
11	-338	47	- 60	- 18	-26.8	5.7	-270	19	- 76	6	-19.0	1.2
12	-146	7	- 90	4	- 5.9	0.3	-270	23	- 76	9	-19.0	1.3
13	-198	53	- 91	8	-10.8	4.0	-260	28	- 94	20	-16.4	0.8
14	-351	83	-118	59	-22.9	2.5	-240	34	-113	24	-12.9	1.0
15	-323		-124		-19.8		-223	49	- 97	36	-12.6	1.4
16	-367	25	-101	- 12	-26.0	3.2	-267	20	- 83	- 6	-18.1	2.3
17	-137	—	-133	- 23	- 1.3	—	-270	22	- 87	- 6	-18.0	2.4
18	-190	—	-133	7	- 6.3	—	-260	35	- 99	10	-16.0	2.3
19	-327	54	-124	21	-20.1	3.0	-250	40	-110	26	-14.1	1.4
20	-311		-132		-17.9		-270	42	-140	29	-13.3	1.3
21	-383	1	-161	5	-22.2	- 0.3	-280	33	-103	9	-17.5	2.2
22	-363	32	-114	5	-24.4	2.4	-270	39	-100	14	-16.8	2.3
23	-336	47	-153	33	-18.4	1.4	-260	43	-100	19	-15.9	2.2
24	-343	48	-187	79	-16.1	- 2.3	-250	42	-110	20	-14.1	2.1
DEFL	0.0474 in.						0.0127 in.					

GAUGE - Gauge Location Number, see Fig. 18

XB - Longitudinal Direction, Bottom Layer

YB - Transverse Direction, Bottom Layer

XT - Longitudinal Direction, Top Layer

YT - Transverse Direction, Top Layer

DEFL - Average Corner Deflection

MX - Moment in Longitudinal Direction

MY - Moment in Transverse Direction

Note: 1 kip-in/in = 4.45 kN-m/m

TABLE 12. Laboratory and Computer Predicted Strain and Moment under Load 3.1

GAUGE (1)	Laboratory Results						NOPARC Output					
	Strain ($\mu\epsilon$)				Moment (k-in/in)		Strain ($\mu\epsilon$)				Moment (k-in/in)	
	XB (2)	YB (3)	XT (4)	YT (5)	MX (6)	MY (7)	XB (8)	YB (9)	XT (10)	YT (11)	MX (12)	MY (13)
1	-248	- 10	—	31	—	- 3.5	-238	- 6	- 82	- 33	-15.4	2.2
2	-251	1	—	- 13	—	1.2	-242	- 15	- 77	- 24	-16.2	0.7
3	-183	28	-114	- 26	- 7.4	4.6	-235	- 11	- 97	- 3	-13.8	- 0.7
4	-174	46	-127	19	- 5.4	2.5	-241	12	-112	16	-13.0	- 0.3
5	-255		-126		-13.1		-219	16	- 95	17	-12.4	0.0
6	-334	- 10	-137	- 12	-19.7	0.1	-242	- 16	- 76	- 24	-16.3	0.6
7	-236	—	- 91	- 12	-14.4	—	-251	- 15	- 69	- 13	-17.8	- 0.3
8	—	23	-118	- 30	—	4.5	-235	- 4	- 98	6	-13.7	- 0.9
9	-319	70	-131	36	-18.8	3.2	-235	14	-108	19	-12.8	- 0.3
10	-250		-134		-12.0		-219	42	- 96	37	-12.4	0.7
11	-291	20	- 78	- 63	-20.8	7.0	-229	- 21	- 89	- 33	-13.9	0.9
12	-107	- 12	-107	- 24	- 0.8	0.9	-231	- 9	- 90	- 24	-14.0	1.2
13	-190	48	- 95	- 15	- 9.7	5.5	-240	9	- 99	1	-14.1	0.7
14	-354	78	-117	45	-23.3	3.2	-240	23	-108	19	-13.3	0.5
15	-323		-121		-20.0		-221	47	- 96	36	-12.5	1.2
16	-327	- 24	-114	- 55	-21.0	2.4	-229	- 35	- 93	- 50	-13.6	1.0
17	-108	—	-145	- 68	2.5	—	-238	- 32	-101	- 48	-13.7	1.1
18	-181	—	-148	- 3	- 4.2	—	-250	8	-114	- 8	-13.7	1.4
19	-328	52	-128	17	-19.9	3.2	-246	34	-114	22	-13.3	1.2
20	-311		-127		-18.4		-270	40	-140	28	-13.3	1.2
21	-377	3	-177	- 44	-20.2	3.9	-262	- 72	-125	- 83	-13.9	0.5
22	-362	- 42	-138	- 52	-22.2	0.6	-262	15	-126	0	-13.8	1.3
23	-330	41	-162	38	-17.1	0.5	-251	39	-119	19	-13.4	1.9
24	-338	47	-190	81	-15.4	- 2.5	-245	41	-113	20	-13.3	2.0

GAUGE - Gauge Location Number, see Fig. 18

XB - Longitudinal Direction, Bottom Layer

YB - Transverse Direction, Bottom Layer

XT - Longitudinal Direction, Top Layer

YT - Transverse Direction, Top Layer

MX - Moment in Longitudinal Direction

MY - Moment in Transverse Direction

Note: 1 kip-in/in = 4.45 kN-m/m

TABLE 13. Laboratory and Computer Predicted Strain and Moment under Load 3.2

GAUGE (1)	Laboratory Results						NOPARC Output					
	Strain ($\mu\epsilon$)				Moment (k-in/in)		Strain ($\mu\epsilon$)				Moment (k-in/in)	
	XB (2)	YB (3)	XT (4)	YT (5)	MX (6)	MY (7)	XB (8)	YB (9)	XT (10)	YT (11)	MX (12)	MY (13)
1	-263	- 27	—	44	—	- 6.0	-249	- 12	- 71	- 27	-17.4	1.2
2	-265	- 13	—	- 1	—	- 1.1	-253	- 23	- 66	- 16	-18.2	- 0.7
3	-181	15	-115	- 16	- 7.1	2.7	-231	- 18	-101	3	-13.1	- 1.8
4	-172	40	-129	25	- 5.0	1.5	-240	8	-113	19	-12.9	- 0.9
5	-253	—	-127	—	-12.9	—	-218	13	- 97	20	-12.2	- 0.5
6	-350	- 29	-128	- 9	-22.0	- 1.8	-252	- 26	- 66	- 14	-18.1	- 1.1
7	-252	—	- 72	- 6	-17.6	—	-259	-26	- 62	- 3	-19.1	- 2.1
8	—	14	-121	- 21	—	3.0	-230	- 10	-102	12	-12.9	- 1.9
9	-315	60	-133	41	-18.2	1.9	-232	10	-110	23	-12.4	- 1.0
10	-249	—	-134	—	-11.9	—	-218	39	- 97	40	-12.2	0.1
11	-306	21	- 64	- 70	-23.4	7.7	-237	- 17	- 82	- 36	-15.3	1.5
12	-122	- 14	- 94	- 26	- 3.3	0.9	-239	- 8	- 83	- 25	-15.4	1.4
13	-185	45	- 95	- 18	- 9.2	5.5	-239	10	-100	0	-13.9	0.9
14	-354	69	-111	47	-23.8	2.2	-240	22	-109	20	-13.2	0.3
15	-319	—	-112	—	-20.4	—	-221	45	- 97	37	-12.5	0.9
16	-333	- 24	-107	- 57	-22.2	2.6	-234	- 32	- 88	- 53	-14.5	1.5
17	-117	—	-138	- 70	1.0	—	-243	- 30	- 97	- 50	-14.5	1.5
18	-179	—	-144	- 4	- 4.3	—	-252	8	-113	- 8	-14.0	1.4
19	-329	53	-130	19	-19.8	3.1	-246	34	-113	23	-13.4	1.1
20	-311	—	-128	—	-18.3	—	-270	39	-140	28	-13.3	1.1
21	-382	4	-176	- 46	-20.8	4.2	-266	- 71	-122	- 84	-14.5	0.7
22	-365	- 44	-134	- 57	-22.9	0.8	-265	15	-123	- 1	-14.3	1.4
23	-324	48	-159	37	-16.8	1.2	-254	39	-117	19	-13.8	1.9
24	-340	45	-188	81	-15.8	- 2.7	-246	41	-112	20	-13.5	2.0
DEFL	0.0351 in.						0.0042 in.					

GAUGE - Gauge Location Number, see Fig. 18

XB - Longitudinal Direction, Bottom Layer

YB - Transverse Direction, Bottom Layer

XT - Longitudinal Direction, Top Layer

YT - Transverse Direction, Top Layer

DEFL - Average Corner Deflection

MX - Moment in Longitudinal Direction

MY - Moment in Transverse Direction

Note: 1 kip-in/in = 4.45 kN-m/m

TABLE 14. Laboratory and Computer Predicted Strain and Moment under Load 3.3

GAUGE (1)	Laboratory Results						NOPARC Output					
	Strain ($\mu\epsilon$)				Moment (k-in/in)		Strain ($\mu\epsilon$)				Moment (k-in/in)	
	XB (2)	YB (3)	XT (4)	YT (5)	MX (6)	MY (7)	XB (8)	YB (9)	XT (10)	YT (11)	MX (12)	MY (13)
1	-280	-31	—	47	—	-6.6	-274	-16	-48	-23	-21.8	0.5
2	-285	-17	—	2	—	-1.7	-277	-29	-45	-10	-22.3	-1.7
3	-193	10	-103	-12	-9.3	1.9	-247	-24	-86	8	-15.9	-2.8
4	-173	35	-128	29	-5.2	0.7	-239	3	-114	24	-12.7	-1.7
5	-253		-127		-12.9		-216	9	-98	23	-11.9	-1.1
6	-366	-38	-116	3	-24.5	-3.6	-279	-29	-42	-11	-22.8	-1.7
7	-267	—	-55	0	-20.5	—	-285	-30	-37	2	-23.8	-2.8
8	—	12	-115	-16	—	2.4	-244	-17	-89	18	-15.3	-3.0
9	-318	53	-130	45	-18.8	1.0	-232	4	-110	28	-12.4	-2.0
10	-247		-134		-11.7		-215	36	-99	42	-11.7	-0.3
11	-326	17	-48	-64	-26.7	6.8	-259	-21	-62	-32	-19.1	0.8
12	-138	-9	-80	-25	-6.1	1.3	-259	-10	-64	-22	-19.0	0.9
13	-195	35	-83	-15	-11.2	4.3	-254	8	-87	2	-16.5	0.5
14	-350	83	-117	49	-22.9	3.3	-237	24	-111	17	-12.7	0.7
15	-317		-110		-20.4		-221	47	-97	36	-12.5	1.2
16	-353	-21	-89	-57	-25.7	2.9	-254	-30	-70	-54	-18.0	1.8
17	-130	—	-121	-71	-1.7	—	-261	-27	-80	-53	-17.7	2.0
18	-192	—	-138	-6	-6.1	—	-264	11	-101	-11	-16.2	1.9
19	-329	55	-126	18	-20.2	3.4	-247	34	-112	22	-13.6	1.2
20	-312		-130		-18.2		-270	40	-140	28	-13.3	1.2
21	-398	2	-161	-48	-23.6	4.1	-282	-68	-108	-87	-17.3	1.2
22	-370	-40	-117	-59	-24.8	1.3	-281	18	-109	-3	-17.1	1.8
23	-338	69	-150	33	-18.9	3.4	-264	41	-108	18	-15.6	2.1
24	-343	50	-184	81	-16.4	-2.3	-251	41	-108	20	-14.3	2.0
DEFL	0.0474 in.						0.0127 in.					

GAUGE - Gauge Location Number, see Fig. 18

XB - Longitudinal Direction, Bottom Layer

YB - Transverse Direction, Bottom Layer

XT - Longitudinal Direction, Top Layer

YT - Transverse Direction, Top Layer

DEFL - Average Corner Deflection

MX - Moment in Longitudinal Direction

MY - Moment in Transverse Direction

Note: 1 kip-in/in = 4.45 kN-m/m

TABLE 15. Laboratory and Computer Predicted Strain and Moment under Load 5.1

GAUGE (1)	Laboratory Results						NOPARC Output					
	Strain ($\mu\epsilon$)				Moment (k-in/in)		Strain ($\mu\epsilon$)				Moment (k-in/in)	
	XB (2)	YB (3)	XT (4)	YT (5)	MX (6)	MY (7)	XB (8)	YB (9)	XT (10)	YT (11)	MX (12)	MY (13)
1	-259	- 29	—	- 6	—	- 2.1	-225	- 39	- 69	- 63	-15.3	1.8
2	-240	- 17	—	- 45	—	2.2	-229	- 48	- 64	- 55	-16.1	0.3
3	- 97	17	-105	- 57	0.0	6.2	-226	- 38	- 88	- 28	-13.7	- 1.1
4	-173	35	-124	0	- 5.5	3.1	-237	- 1	-108	5	-13.0	- 0.5
5	-259		-132		-13.0		-218	7	- 94	11	-12.4	- 0.3
6	-286	- 33	-129	- 48	-15.8	1.0	-229	- 48	- 64	- 55	-16.1	0.3
7	-227	—	- 81	- 42	-14.4	—	-238	- 45	- 56	- 42	-17.7	- 0.5
8	—	10	-121	- 59	—	5.8	-226	- 26	- 89	- 14	-13.6	- 1.1
9	-322	68	-130	17	-19.1	4.6	-230	1	-103	9	-12.8	- 0.7
10	-249		-132		-12.0		-217	37	- 94	35	-12.3	0.4
11	-289	- 12	- 61	-104	-22.1	7.5	-217	- 56	- 77	- 66	-13.8	0.5
12	-102	- 58	- 98	- 49	- 1.1	- 1.1	-219	- 42	- 78	- 54	-13.9	0.7
13	-184	19	- 97	- 44	- 8.9	5.3	-233	- 12	- 92	- 19	-14.0	0.5
14	-364	67	-115	30	-24.4	3.5	-237	12	-105	10	-13.3	0.2
15	-327		-130		-19.6		-220	44	- 95	35	-12.5	1.0
16	-327	- 70	-106	- 91	-21.7	1.3	-220	- 74	- 83	- 88	-13.6	0.7
17	-112	—	-139	-112	1.6	—	-229	- 72	- 92	- 86	-13.7	0.7
18	-181	—	-152	- 27	- 3.8	—	-250	- 20	-113	- 34	-13.8	1.0
19	-337	50	-132	11	-20.4	3.5	-245	27	-113	17	-13.3	1.0
20	-316		-126		-18.9		-270	36	-141	25	-13.2	1.1
21	-399	0	-187	- 72	-21.4	6.0	-268	-112	-129	-119	-14.1	- 0.1
22	-367	- 80	-128	- 95	-23.6	0.8	-262	- 76	-123	- 87	-14.1	0.5
23	-335	37	-165	32	-17.3	0.6	-257	34	-126	16	-13.3	1.7
24	-337	43	-193	83	-15.0	- 3.1	-246	40	-115	20	-13.2	1.9

GAUGE - Gauge Location Number, see Fig. 18

XB - Longitudinal Direction, Bottom Layer

YB - Transverse Direction, Bottom Layer

XT - Longitudinal Direction, Top Layer

YT - Transverse Direction, Top Layer

MX - Moment in Longitudinal Direction

MY - Moment in Transverse Direction

Note: 1 kip-in/in = 4.45 kN-m/m

TABLE 16. Laboratory and Computer Predicted Strain and Moment under Load 5.2

GAUGE (1)	Laboratory Results						NOPARC Output					
	Strain ($\mu\epsilon$)				Moment (k-in/in)		Strain ($\mu\epsilon$)				Moment (k-in/in)	
	XB (2)	YB (3)	XT (4)	YT (5)	MX (6)	MY (7)	XB (8)	YB (9)	XT (10)	YT (11)	MX (12)	MY (13)
1	-273	- 48	—	11	—	- 5.2	-236	- 46	- 59	- 57	-17.2	0.6
2	-252	- 32	—	- 32	—	- 0.2	-241	- 57	- 53	- 46	-18.2	- 1.2
3	-115	5	-106	- 44	- 1.6	4.1	-222	- 45	- 92	- 22	-13.0	- 2.2
4	-166	31	-127	10	- 4.6	1.9	-236	- 5	-109	8	-12.8	- 1.1
5	-254	—	-127	—	-12.9	—	-216	4	- 95	13	-12.2	- 0.7
6	-301	- 47	-114	- 32	-18.6	- 1.5	-239	- 58	- 54	- 46	-17.9	- 1.3
7	-238	—	- 59	- 37	-17.4	—	-247	- 56	- 48	- 32	-19.2	- 2.3
8	—	2	-133	- 47	—	4.1	-222	- 32	- 93	- 8	-12.9	- 2.2
9	-312	60	-130	19	-18.2	3.7	-228	- 3	-105	12	-12.4	- 1.3
10	-244	—	-133	—	-11.5	—	-216	34	- 95	37	-12.2	0.0
11	-299	- 10	- 50	-105	-24.0	7.8	-224	- 52	- 70	- 70	-15.1	1.2
12	-101	- 26	- 83	- 49	- 2.3	1.8	-227	- 40	- 71	- 56	-15.3	1.1
13	-182	27	- 93	- 45	- 9.1	6.1	-232	- 11	- 93	- 19	-13.8	0.6
14	-348	74	-118	31	-22.7	4.0	-236	11	-105	11	-13.2	0.1
15	-325	—	-117	—	-20.6	—	-219	42	- 96	36	-12.4	0.7
16	-331	- 68	- 93	- 92	-23.2	1.6	-225	- 71	- 78	- 90	-14.5	1.2
17	-118	—	-129	-114	0.1	—	-234	- 69	- 88	- 88	-14.5	1.2
18	-180	—	-146	- 27	- 4.3	—	-252	- 20	-112	- 34	-14.1	1.0
19	-330	51	-132	12	-19.7	3.5	-246	26	-113	17	-13.4	0.9
20	-313	—	-127	—	-18.6	—	-270	35	-141	26	-13.2	1.0
21	-405	- 1	-181	- 70	-22.5	5.7	-272	-112	-126	-120	-14.7	0.0
22	-367	- 80	-121	- 92	-24.2	0.5	-266	- 76	-120	- 87	-14.7	0.5
23	-333	41	-174	32	-16.3	1.0	-260	34	-124	16	-13.8	1.7
24	-334	47	-189	84	-15.1	- 2.8	-247	40	-114	20	-13.4	1.9
DEFL	0.0351 in.						0.0043 in.					

GAUGE - Gauge Location Number, see Fig. 18

XB - Longitudinal Direction, Bottom Layer

YB - Transverse Direction, Bottom Layer

XT - Longitudinal Direction, Top Layer

YT - Transverse Direction, Top Layer

DEFL - Average Corner Deflection

MX - Moment in Longitudinal Direction

MY - Moment in Transverse Direction

Note: 1 kip-in/in = 4.45 kN-m/m

TABLE 17. Laboratory and Computer Predicted Strain and Moment under Load 5.3

GAUGE (1)	Laboratory Results						NOPARC Output					
	Strain ($\mu\epsilon$)			Moment (k-in/in)			Strain ($\mu\epsilon$)			Moment (k-in/in)		
	XB (2)	YB (3)	XT (4)	YT (5)	MX (6)	MY (7)	XB (8)	YB (9)	XT (10)	YT (11)	MX (12)	MY (13)
1	-290	- 52	—	16	—	- 5.9	-263	- 51	- 34	- 52	-22.0	- 0.2
2	-270	- 34	—	- 26	—	- 0.9	-263	- 64	- 32	- 40	-22.2	- 2.4
3	-107	1	- 92	- 41	- 2.1	3.5	-237	- 51	- 78	- 16	-15.6	- 3.2
4	-168	27	-123	13	- 5.1	1.3	-235	- 9	-110	12	-12.6	- 1.8
5	-253	—	-131	—	-12.5	—	-214	1	- 97	16	-11.8	- 1.2
6	-318	- 55	- 93	- 22	-22.0	- 3.1	-267	- 60	- 28	- 43	-22.9	- 1.8
7	-253	—	- 38	- 34	-20.7	—	-271	- 59	- 25	- 29	-23.5	- 2.8
8	—	- 4	-109	- 23	—	1.5	-236	- 38	- 80	- 3	-15.4	- 3.1
9	-312	53	-127	31	-18.5	2.1	-228	- 8	-105	17	-12.4	- 2.1
10	-244	—	-135	—	-11.3	—	-214	31	- 97	40	-11.8	- 0.6
11	-320	- 13	- 35	-102	-27.3	7.3	-246	- 56	- 50	- 67	-19.0	0.6
12	-118	- 56	- 67	- 50	- 5.3	- 0.8	-246	- 42	- 53	- 53	-18.7	0.7
13	-189	21	- 80	- 40	-10.9	5.2	-246	- 13	- 79	- 17	-16.4	0.3
14	-349	78	-115	33	-23.0	4.2	-235	12	-106	9	-13.0	0.3
15	-324	—	-108	—	-21.3	—	-219	42	- 96	36	-12.4	0.7
16	-347	- 67	- 76	- 91	-26.3	1.6	-244	- 69	- 61	- 92	-17.8	1.5
17	-126	—	-112	-115	- 2.1	—	-252	- 67	- 72	- 90	-17.6	1.5
18	-190	—	-136	- 28	- 6.1	—	-264	- 18	-100	- 37	-16.3	1.5
19	-331	54	-132	7	-19.8	4.2	-248	26	-111	17	-13.8	0.9
20	-313	—	-128	—	-18.5	—	-271	35	-140	26	-13.4	1.0
21	-430	0	-164	- 69	-26.4	5.7	-288	-109	-112	-123	-17.5	0.5
22	-386	- 81	-106	- 95	-27.3	0.7	-281	- 73	-107	- 89	-17.3	0.9
23	-345	78	-152	30	-19.4	4.4	-270	35	-114	14	-15.6	1.9
24	-341	46	-184	84	-16.2	- 2.9	-252	41	-109	20	-14.3	2.0
DEFL	0.0474 in.						0.0127 in.					

GAUGE - Gauge Location Number, see Fig. 18

XB - Longitudinal Direction, Bottom Layer

YB - Transverse Direction, Bottom Layer

XT - Longitudinal Direction, Top Layer

YT - Transverse Direction, Top Layer

DEFL - Average Corner Deflection

MX - Moment in Longitudinal Direction

MY - Moment in Transverse Direction

Note: 1 kip-in/in = 4.45 kN-m/m

TABLE 18. Laboratory and Computer Predicted Strain and Moment under Load 7.1

GAUGE (1)	Laboratory Results						NOPARC Output					
	Strain ($\mu\epsilon$)				Moment (k-in/in)		Strain ($\mu\epsilon$)				Moment (k-in/in)	
	XB (2)	YB (3)	XT (4)	YT (5)	MX (6)	MY (7)	XB (8)	YB (9)	XT (10)	YT (11)	MX (12)	MY (13)
1	-249	- 38	—	- 31	—	- 0.8	-214	- 67	- 59	- 90	-15.1	1.5
2	-231	- 28	—	- 67	—	3.1	-218	- 76	- 54	- 82	-15.9	0.0
3	- 88	- 10	- 94	- 81	- 0.1	5.8	-217	- 63	- 80	- 52	-13.6	- 1.3
4	-168	34	-117	- 15	- 5.7	4.3	-233	- 15	-103	- 8	-13.1	- 0.7
5	-258	—	-131	—	-13.0	—	-215	- 4	- 91	2	-12.4	- 0.5
6	-278	- 51	-113	- 74	-16.5	1.6	-218	- 77	- 53	- 82	-16.0	0.0
7	-217	—	- 67	- 69	-14.7	—	-226	- 72	- 46	- 68	-17.4	- 0.8
8	—	6	-160	- 94	—	8.3	-217	- 48	- 80	- 35	-13.6	- 1.4
9	-316	57	-120	4	-19.5	4.7	-226	- 13	- 98	- 4	-12.8	- 0.8
10	-253	—	-127	—	-12.9	—	-215	29	- 92	29	-12.3	0.2
11	-280	- 22	- 56	-128	-21.7	8.6	-207	- 85	- 67	- 94	-13.8	0.2
12	- 89	- 44	- 87	- 69	- 0.8	1.8	-209	- 71	- 68	- 82	-13.9	0.5
13	-186	10	- 85	- 67	-10.2	6.4	-225	- 35	- 84	- 40	-14.0	0.2
14	-353	67	-117	16	-23.2	4.6	-233	- 1	-101	- 2	-13.2	0.1
15	-322	—	-105	—	-21.3	—	-218	38	- 93	31	-12.5	0.8
16	-324	- 91	- 97	-107	-22.2	0.8	-214	-101	- 77	-113	-13.5	0.4
17	-109	—	-133	-136	1.3	—	-224	-100	- 86	-112	-13.7	0.4
18	-175	—	-138	- 57	- 4.5	—	-245	- 54	-108	- 65	-13.8	0.6
19	-336	42	-134	4	-20.1	3.4	-244	16	-111	8	-13.4	0.8
20	-317	—	-123	—	-19.3	—	-270	30	-141	21	-13.2	0.9
21	-406	4	-197	- 71	-21.2	6.2	-273	-124	-134	-128	-14.1	- 0.4
22	-379	- 93	-140	- 96	-23.7	- 0.3	-268	-118	-129	-124	-14.1	- 0.2
23	-350	17	-191	8	-16.4	0.8	-261	17	-128	2	-13.5	1.3
24	-333	49	-193	84	-14.6	- 2.6	-248	39	-118	19	-13.2	1.9

GAUGE - Gauge Location Number, see Fig. 18

XB - Longitudinal Direction, Bottom Layer

YB - Transverse Direction, Bottom Layer

XT - Longitudinal Direction, Top Layer

YT - Transverse Direction, Top Layer

MX - Moment in Longitudinal Direction

MY - Moment in Transverse Direction

Note: 1 kip-in/in = 4.45 kN-m/m

TABLE 19. Laboratory and Computer Predicted Strain and Moment under Load 7.2

GAUGE (1)	Laboratory Results						NOPARC Output					
	Strain ($\mu\epsilon$)				Moment (k-in/in)		Strain ($\mu\epsilon$)				Moment (k-in/in)	
	XB (2)	YB (3)	XT (4)	YT (5)	MX (6)	MY (7)	XB (8)	YB (9)	XT (10)	YT (11)	MX (12)	MY (13)
1	-262	- 61	—	- 16	—	- 4.1	-227	- 76	- 47	- 82	-17.4	0.0
2	-245	- 41	—	- 55	—	0.9	-229	- 87	- 43	- 71	-18.0	- 1.8
3	- 87	- 5	- 99	- 69	0.4	5.3	-212	- 71	- 84	- 45	-12.7	- 2.6
4	-164	30	-121	- 9	- 4.9	3.4	-231	- 20	-104	- 4	-12.8	- 1.4
5	-253		-124		-13.1		-214	- 7	- 92	5	-12.2	- 1.0
6	-291	- 58	-100	- 55	-18.8	- 0.6	-229	- 85	- 42	- 74	-18.0	- 1.4
7	-229	—	- 49	- 58	-17.4	—	-235	- 82	- 38	- 58	-19.0	- 2.5
8	—	- 2	-125	- 84	—	6.8	-213	- 54	- 84	- 29	-12.8	- 2.4
9	-307	59	-126	- 26	-18.1	7.4	-223	- 17	-100	0	-12.4	- 1.5
10	-247		-128		-12.2		-214	26	- 93	32	-12.1	- 0.3
11	-285	- 24	- 37	-136	-23.8	9.1	-215	- 81	- 60	- 97	-15.1	0.8
12	-119	- 71	- 75	- 72	- 4.7	- 0.3	-217	- 69	- 61	- 83	-15.2	0.8
13	-181	9	- 80	- 65	-10.2	6.2	-224	- 35	- 84	- 41	-13.9	0.3
14	-339	63	-114	15	-22.2	4.3	-232	- 3	-101	- 1	-13.1	- 0.2
15	-331		-120		-20.9		-218	36	- 94	33	-12.4	0.5
16	-333	- 87	- 87	-108	-24.0	1.2	-219	- 99	- 72	-115	-14.5	0.7
17	-112	—	-125	-138	0.4	—	-228	- 98	- 82	-115	-14.4	0.8
18	-177	—	-138	- 58	- 4.7	—	-246	- 53	-106	- 66	-14.0	0.8
19	-330	49	-129	6	-20.0	3.8	-244	16	-111	9	-13.4	0.7
20	-314		-123		-19.0		-270	29	-141	22	-13.2	0.7
21	-413	- 2	-190	- 78	-22.5	6.3	-277	-123	-131	-129	-14.8	- 0.2
22	-383	- 93	-134	- 97	-24.6	- 0.2	-272	-117	-126	-125	-14.7	0.0
23	-350	17	-173	11	-18.0	0.6	-263	17	-127	2	-13.8	1.3
24	-335	48	-187	82	-15.4	- 2.5	-249	39	-118	19	-13.3	1.9
DEFL	0.0351 in.						0.0043 in.					

GAUGE - Gauge Location Number, see Fig. 18

XB - Longitudinal Direction, Bottom Layer

YB - Transverse Direction, Bottom Layer

XT - Longitudinal Direction, Top Layer

YT - Transverse Direction, Top Layer

DEFL - Average Corner Deflection

MX - Moment in Longitudinal Direction

MY - Moment in Transverse Direction

Note: 1 kip-in/in = 4.45 kN-m/m

TABLE 20. Laboratory and Computer Predicted Strain and Moment under Load 7.3

GAUGE (1)	Laboratory Results						NOPARC Output					
	Strain ($\mu\epsilon$)			Moment (k-in/in)			Strain ($\mu\epsilon$)			Moment (k-in/in)		
	XB (2)	YB (3)	XT (4)	YT (5)	MX (6)	MY (7)	XB (8)	YB (9)	XT (10)	YT (11)	MX (12)	MY (13)
1	-281	- 65	—	- 11	—	- 4.9	-252	- 79	- 24	- 78	-21.8	- 0.5
2	-262	- 47	—	- 52	—	0.1	-253	- 92	- 21	- 67	-22.2	- 2.6
3	- 99	- 8	- 86	- 65	- 1.8	4.7	-229	- 76	- 69	- 40	-15.7	- 3.4
4	-166	23	-119	- 5	- 5.3	2.5	-230	- 24	-105	0	-12.6	- 2.1
5	-252	—	-128	—	-12.7	—	-212	- 10	- 94	8	-11.9	- 1.5
6	-310	- 68	- 82	- 55	-22.2	- 1.5	-255	- 89	- 18	- 70	-22.6	- 2.1
7	-250	—	- 38	- 61	-20.4	—	-261	- 86	- 14	- 54	-23.5	- 3.2
8	—	- 10	-130	- 77	—	5.5	-227	- 60	- 71	- 23	-15.3	- 3.4
9	-310	71	-124	3	-18.5	6.0	-223	- 23	-100	5	-12.4	- 2.5
10	-245	—	-130	—	-11.8	—	-212	23	- 95	34	-11.8	- 0.8
11	-312	- 28	- 20	-132	-27.9	8.4	-237	- 85	- 40	- 94	-19.0	0.2
12	-111	- 48	- 58	- 64	- 5.4	1.0	-237	- 71	- 43	- 81	-18.7	0.4
13	-187	9	- 68	- 65	-11.8	6.2	-238	- 36	- 71	- 39	-16.4	0.0
14	-309	64	-112	20	-19.5	4.0	-231	- 1	-103	- 3	-12.9	0.2
15	-319	—	-116	—	-20.1	—	-217	37	- 94	32	-12.3	0.6
16	-345	- 87	- 71	-111	-26.5	1.5	-238	- 97	- 55	-117	-17.8	1.1
17	-123	—	-108	-139	- 2.2	—	-246	- 95	- 66	-117	-17.6	1.3
18	-184	—	-124	- 59	- 6.6	—	-259	- 51	- 95	- 68	-16.2	1.1
19	-331	49	-128	0	-20.2	4.3	-246	16	-109	8	-13.8	0.8
20	-314	—	-124	—	-18.9	—	-271	29	-141	21	-13.3	0.8
21	-429	3	-170	- 74	-25.8	6.4	-293	-120	-117	-131	-17.5	0.2
22	-404	- 73	-119	- 98	-27.9	1.6	-288	-115	-112	-127	-17.5	0.3
23	-361	10	-166	8	-19.7	0.2	-274	19	-117	1	-15.7	1.6
24	-340	48	-184	87	-16.1	- 2.9	-254	39	-113	19	-14.2	1.9
DEFL	0.0474 in.						0.0125 in.					

GAUGE - Gauge Location Number, see Fig. 18

XB - Longitudinal Direction, Bottom Layer

YB - Transverse Direction, Bottom Layer

XT - Longitudinal Direction, Top Layer

YT - Transverse Direction, Top Layer

DEFL - Average Corner Deflection

MX - Moment in Longitudinal Direction

MY - Moment in Transverse Direction

Note: 1 kip-in/in = 4.45 kN-m/m

TABLE 21. Laboratory and Computer Predicted Strain and Moment under Load 9.1

GAUGE (1)	Laboratory Results						NOPARC Output					
	Strain ($\mu\epsilon$)				Moment (k-in/in)		Strain ($\mu\epsilon$)				Moment (k-in/in)	
	XB (2)	YB (3)	XT (4)	YT (5)	MX (6)	MY (7)	XB (8)	YB (9)	XT (10)	YT (11)	MX (12)	MY (13)
1	-242	- 55	—	- 59	—	0.0	-206	- 91	- 52	-112	-15.0	1.2
2	-225	- 41	—	- 92	—	4.0	-210	-100	- 46	-104	-15.9	- 0.3
3	- 84	- 14	- 89	-106	- 0.1	7.5	-209	- 86	- 72	- 74	-13.5	- 1.5
4	-165	26	-113	- 36	- 5.7	5.3	-227	- 32	- 97	- 23	-13.0	- 0.9
5	-257		-117		-14.1		-213	- 18	- 88	- 10	-12.5	- 0.8
6	-271	- 64	-102	- 90	-16.8	1.8	-209	-100	- 46	-104	-15.8	- 0.3
7	-210	—	- 63	- 89	-14.4	—	-218	- 96	- 38	- 90	-17.4	- 1.1
8	—	- 7	-106	-120	—	9.3	-209	- 70	- 73	- 55	-13.4	- 1.7
9	-309	57	-120	- 11	-18.8	6.0	-220	- 30	- 93	- 19	-12.7	- 1.1
10	-249		-123		-12.8		-213	18	- 88	20	-12.5	- 0.1
11	-276	- 43	- 48	-157	-22.0	9.2	-200	-108	- 61	-114	-13.6	- 0.1
12	- 80	- 85	- 83	- 71	- 0.3	- 1.7	-202	- 95	- 61	-104	-13.8	0.2
13	-163	- 3	- 76	- 95	- 8.8	7.6	-217	- 60	- 76	- 63	-13.9	- 0.1
14	-340	57	-115	- 6	-22.2	5.5	-228	- 18	- 96	- 17	-13.2	- 0.2
15	-324		-112		-20.9		-216	29	- 90	24	-12.6	0.6
16	-327	-106	- 95	-121	-22.7	0.6	-211	-120	- 74	-129	-13.5	0.0
17	-111	—	-132	-153	1.1	—	-222	-120	- 84	-129	-13.7	0.0
18	-165	—	-126	- 99	- 4.6	—	-235	- 85	- 98	- 95	-13.7	0.3
19	-335	38	-154	- 7	-18.3	3.9	-240	1	-107	- 6	-13.4	0.6
20	-318		-116		-20.0		-269	20	-141	13	-13.1	0.7
21	-409	- 2	-197	- 73	-21.5	5.9	-276	-128	-138	-131	-14.1	- 0.5
22	-386	- 78	-142	- 98	-24.2	1.2	-274	-125	-136	-129	-14.1	- 0.4
23	-356	- 38	-141	- 85	-21.4	3.7	-257	- 56	-122	- 67	-13.7	0.6
24	-337	36	-192	87	-15.1	- 4.0	-252	34	-123	17	-13.1	1.6

GAUGE -- Gauge Location Number, see Fig. 18

XB -- Longitudinal Direction, Bottom Layer

YB -- Transverse Direction, Bottom Layer

XT -- Longitudinal Direction, Top Layer

YT -- Transverse Direction, Top Layer

MX -- Moment in Longitudinal Direction

MY -- Moment in Transverse Direction

Note: 1 kip-in/in = 4.45 kN-m/m

TABLE 22. Laboratory and Computer Predicted Strain and Moment under Load 9.2

GAUGE (1)	Laboratory Results						NOPARC Output					
	Strain ($\mu\epsilon$)				Moment (k-in/in)		Strain ($\mu\epsilon$)				Moment (k-in/in)	
	XB (2)	YB (3)	XT (4)	YT (5)	MX (6)	MY (7)	XB (8)	YB (9)	XT (10)	YT (11)	MX (12)	MY (13)
1	-247	- 76	—	- 42	—	- 3.3	-219	- 97	- 40	-106	-17.3	0.2
2	-240	- 53	—	- 77	—	1.7	-219	-109	- 37	- 95	-17.5	- 1.8
3	- 65	- 11	- 93	- 96	2.0	7.0	-205	- 93	- 76	- 68	-12.8	- 2.6
4	-162	21	-115	- 30	- 5.3	4.3	-226	- 36	- 99	- 19	-12.8	- 1.6
5	-252		-120		-13.4		-212	- 21	- 89	- 7	-12.3	- 1.3
6	-319	- 73	- 88	- 83	-22.5	0.4	-221	-110	- 35	- 95	-17.9	- 1.9
7	-227	—	- 38	- 84	-18.2	—	-225	-106	- 32	- 80	-18.5	- 2.8
8	—	- 19	-116	-114	—	7.7	-205	- 76	- 77	- 50	-12.7	- 2.6
9	-306	48	-120	- 7	-18.5	4.8	-218	- 34	- 95	- 15	-12.3	- 1.8
10	-245		-124		-12.4		-211	15	- 90	22	-12.1	- 0.5
11	-287	- 39	- 67	-144	-21.4	8.5	-208	-103	- 54	-118	-15.0	0.6
12	- 99	-106	- 68	- 91	- 3.4	- 1.9	-209	- 93	- 55	-106	-15.0	0.5
13	-169	- 14	- 79	- 94	- 9.1	6.5	-215	- 59	- 77	- 64	-13.6	0.1
14	-346	55	-114	- 3	-22.8	5.1	-227	- 19	- 96	- 16	-13.1	- 0.4
15	-315		-110		-20.2		-216	27	- 91	25	-12.5	0.3
16	-330	- 98	- 86	-120	-23.8	1.2	-216	-117	- 69	-131	-14.4	0.5
17	-110	—	-123	-152	0.4	—	-227	-117	- 80	-131	-14.5	0.5
18	-165	—	-126	- 98	- 4.6	—	-237	- 84	- 97	- 95	-14.0	0.4
19	-328	40	-130	- 12	-19.7	4.5	-240	0	-107	- 5	-13.4	0.4
20	-315		-120		-19.4		-270	19	-141	14	-13.2	0.5
21	-411	5	-193	- 71	-22.1	6.3	-279	-128	-135	-132	-14.6	- 0.4
22	-393	- 83	-136	-100	-25.4	0.9	-278	-125	-133	-129	-14.7	- 0.4
23	-344	- 40	-154	- 85	-19.1	3.5	-260	- 56	-121	- 67	-14.0	0.6
24	-336	48	-196	81	-14.7	- 2.4	-253	34	-122	16	-13.3	1.7
DEFL	0.0351 in.						0.0041 in.					

GAUGE - Gauge Location Number, see Fig. 18

XB - Longitudinal Direction, Bottom Layer

YB - Transverse Direction, Bottom Layer

XT - Longitudinal Direction, Top Layer

YT - Transverse Direction, Top Layer

DEFL - Average Corner Deflection

MX - Moment in Longitudinal Direction

MY - Moment in Transverse Direction

Note: 1 kip-in/in = 4.45 kN-m/m

TABLE 23. Laboratory and Computer Predicted Strain and Moment under Load 9.3

GAUGE (1)	Laboratory Results						NOPARC Output					
	Strain ($\mu\epsilon$)				Moment (k-in/in)		Strain ($\mu\epsilon$)				Moment (k-in/in)	
	XB (2)	YB (3)	XT (4)	YT (5)	MX (6)	MY (7)	XB (8)	YB (9)	XT (10)	YT (11)	MX (12)	MY (13)
1	-268	- 81	—	- 38	—	- 4.0	-245	-105	- 16	- 99	-21.9	- 1.1
2	-259	- 60	—	- 73	—	0.7	-245	-117	- 13	- 87	-22.1	- 3.2
3	- 78	- 51	- 80	- 92	- 0.4	3.1	-220	-100	- 61	- 61	-15.5	- 3.8
4	-163	15	-116	- 25	- 5.3	3.4	-224	- 41	-100	- 15	-12.5	- 2.4
5	-251		-131		-12.3		-210	- 24	- 91	- 4	-11.9	- 1.8
6	-334	- 83	- 83	- 88	-24.4	- 0.1	-248	-111	- 10	- 93	-22.7	- 2.1
7	-239	—	- 27	- 81	-20.3	—	-253	-109	- 6	- 77	-23.5	- 3.3
8	—	- 25	-122	-103	—	6.3	-219	- 82	- 63	- 44	-15.3	- 3.6
9	-309	43	-119	- 13	-18.9	4.9	-218	- 39	- 95	- 10	-12.3	- 2.6
10	-246		-125		-12.4		-209	12	- 92	25	-11.8	- 1.0
11	-303	- 43	- 19	-161	-27.1	9.5	-230	-107	- 34	-115	-18.8	0.0
12	-115	- 87	- 54	- 85	- 6.2	- 0.7	-229	- 95	- 36	-104	-18.6	0.2
13	-188	- 20	- 62	- 92	-12.4	5.8	-230	- 61	- 63	- 62	-16.3	- 0.3
14	-336	59	-113	0	-22.0	5.2	-226	- 18	- 97	- 18	-12.9	- 0.1
15	-318		-109		-20.6		-216	27	- 91	25	-12.5	0.3
16	-349	-101	- 69	- 24	-27.1	- 7.0	-235	-115	- 52	-133	-17.7	0.8
17	-144	—	-107	- 30	- 4.3	—	-244	-115	- 64	-134	-17.5	0.9
18	-175	—	-116	-101	- 6.4	—	-249	- 82	- 86	- 98	-16.1	0.8
19	-329	40	-128	- 35	-20.0	6.4	-242	1	-105	- 6	-13.7	0.6
20	-315		-121		-19.3		-270	19	-141	13	-13.2	0.6
21	-422	- 3	-175	- 73	-24.7	5.8	-295	-125	-121	-134	-17.4	0.0
22	-374	- 71	-122	-103	-24.8	2.2	-293	-122	-120	-131	-17.3	0.0
23	-356	- 41	-143	- 86	-21.2	3.5	-271	- 54	-111	- 68	-16.0	0.8
24	-340	39	-205	85	-14.3	- 3.6	-258	35	-118	16	-14.1	1.8
DEFL	0.0474 in.						0.0129 in.					

GAUGE - Gauge Location Number, see Fig. 18

XB - Longitudinal Direction, Bottom Layer

YB - Transverse Direction, Bottom Layer

XT - Longitudinal Direction, Top Layer

YT - Transverse Direction, Top Layer

DEFL - Average Corner Deflection

MX - Moment in Longitudinal Direction

MY - Moment in Transverse Direction

Note: 1 kip-in/in = 4.45 kN-m/m

TABLE 24. Laboratory and Computer Predicted Differential Strain and Moment under 50-kip Load

GAUGE (1)	Laboratory Results						NOPARC Output					
	Strain ($\mu\epsilon$)			Moment (k-in/in)			Strain ($\mu\epsilon$)			Moment (k-in/in)		
	XB (2)	YB (3)	XT (4)	YT (5)	MX (6)	MY (7)	XB (8)	YB (9)	XT (10)	YT (11)	MX (12)	MY (13)
1	—	- 77	—	59	—	-11.7	- 87	- 44	81	42	-15.4	- 7.4
2	—	- 65	—	71	—	-11.6	- 86	- 51	81	50	-15.3	- 8.7
3	—	- 63	14	63	—	-10.8	- 28	- 48	27	45	- 5.0	- 8.0
4	7	- 68	- 4	54	1.0	-10.5	3	- 40	- 3	35	0.5	- 6.4
5	8	—	—	—	—	—	10	- 34	- 10	30	1.8	- 5.5
6	- 94	- 71	41	87	-12.5	-13.5	- 86	- 52	81	49	-15.3	- 8.7
7	- 53	—	55	56	- 9.9	—	- 83	- 56	77	53	-14.7	- 9.3
8	—	- 62	10	60	—	-10.5	- 23	- 48	23	45	- 4.2	- 8.0
9	10	- 69	—	—	—	—	5	- 41	- 4	37	0.8	- 6.7
10	—	—	—	—	—	—	11	- 33	- 11	- 28	2.0	- 0.6
11	- 60	- 40	88	19	-13.4	- 5.1	- 74	- 9	69	10	-13.1	- 1.6
12	- 70	- 12	96	17	-15.1	- 2.5	- 72	- 13	67	14	-12.7	- 2.3
13	- 10	- 49	40	22	- 4.5	- 6.2	- 31	- 14	29	14	- 5.5	- 2.4
14	5	- 20	- 10	17	1.4	- 3.2	6	- 14	- 4	13	0.9	- 2.3
15	- 1	—	- 1	—	0.0	—	5	- 15	- 6	11	1.0	- 2.2
16	- 64	21	73	- 6	-12.5	2.4	- 64	8	59	- 6	-11.3	1.2
17	—	—	71	- 9	—	—	- 63	10	56	- 9	-10.9	1.6
18	- 25	- 5	32	- 4	- 5.2	- 0.1	- 38	6	33	- 8	- 6.5	1.2
19	8	10	- 9	- 4	1.6	1.2	2	4	- 2	- 5	0.4	0.8
20	0	—	- 6	—	0.5	—	- 1	0	0	- 2	- 0.1	0.2
21	- 74	4	54	- 13	-11.8	1.4	- 55	9	45	- 8	- 9.2	1.5
22	—	26	99	- 8	—	3.0	- 55	9	45	- 5	- 9.2	1.2
23	- 23	- 8	102	- 13	-11.2	0.4	- 37	5	27	- 2	- 5.9	0.6
24	- 6	6	- 3	- 2	- 0.3	0.7	- 14	- 1	9	- 3	- 2.1	0.2

GAUGE - Gauge Location Number, see Fig. 18

XB - Longitudinal Direction, Bottom Layer

YB - Transverse Direction, Bottom Layer

XT - Longitudinal Direction, Top Layer

YT - Transverse Direction, Top Layer

MX - Moment in Longitudinal Direction

MY - Moment in Transverse Direction

Note: 1 kip-in/in = 4.45 kN-m/m

APPENDIX IV - PARTIAL LIST OF SAMPLE INPUT FILE FOR NOPARC

Model One - Load 7.1

```

361  1  1  3  1  1  1  1  1  0  0
    2  0  0  1  0  2  0  1
      0.0    0.0    .005    1.0
    100.00  100.00    10.0    1.0
      128.0   128.0   128.0   128.0   128.0   128.0   128.0   128.0
    1  0  0  0  0  0  10.0000E+000.0000E+000.0000E+00
    2  0  0  0  0  0  10.6000E+010.0000E+000.0000E+00
    3  0  0  0  0  0  10.1200E+020.0000E+000.0000E+00
    .  .  .  .  .  .  .  .  .  .  .
    .  .  .  .  .  .  .  .  .  .  .
    .  .  .  .  .  .  .  .  .  .  .
359  0  0  0  0  0  10.9600E+020.1080E+030.0000E+00
360  0  0  0  0  0  10.1020E+030.1080E+030.0000E+00
361  0  0  1  0  0  10.1080E+030.1080E+030.0000E+00
    1  1  2  1  1
    1  2  2  2  4800.0    .18    .0870    0.0    1.0
   -.0008    6.0    9.0    20.0 .0000055
    1 29000000.    60000.  1000000.    1.0

    1  0    .215  .000100    .2  225000.    10.    4
170520.    .0058  220000.    .01  240000.    .03  253000.    .067

    2  0    .612  .000100    .2  225000.    10.    4
170520.    .0058  220000.    .01  240000.    .03  253000.    .067

    1  10
   -4.5   -3.6   -2.7   -1.8   -0.9   0.0   0.9   1.8
     2.7    3.6    4.75

    1  4  1
    1  1 -3.5625  0.00767    0.0
    2  1 -3.1875  0.01533   90.0
    3  1  3.5625  0.00767    0.0
    4  1  3.1875  0.01533   90.0
    1 648  0  1
      0.0    0.0    -1.0

    1 21 20  1  1  1  1  0  0  0  0.000  0.000-0.000
    2  1  2 21  1  1  1  1  0  0  0  0.000  0.000-0.000
    3 22 21  2  1  1  1  1  0  0  0  0.000  0.000-0.000
    .  .  .  .  .  .  .  .  .  .  .  .
    .  .  .  .  .  .  .  .  .  .  .  .
    .  .  .  .  .  .  .  .  .  .  .  .
646 340 341 360  1  1  1  1  0  0  0  0.000  0.000-0.000
647 361 360 341  1  1  1  1  0  0  0  0.000  0.000-0.000
648 341 342 361  1  1  1  1  0  0  0  0.000  0.000-0.000
    18  36  2  3
    1  0  0  1  36  2  6  7  348  349

```

	0.		0.		0.														
12	11	48	47	84	83	120	119	156	155	192	191	228	227	264	263				
300	299	336	335	372	371	408	407	444	443	480	479	516	515	552	551				
588	587	624	623																
	32.4		0.		0.		0.												
	32.4		108.		0.		0.												
2	0	0	1	36	2	7	8	349	350										
	0.		0.		-38000.														
14	13	50	49	86	85	122	121	158	157	194	193	230	229	266	265				
302	301	338	337	374	373	410	409	446	445	482	481	518	517	554	553				
590	589	626	625																
	37.8		0.		0.		0.												
	37.8		108.		0.		0.												
3	0	0	1	36	2	8	9	350	351										
	0.		0.		-38000.														
16	15	52	51	88	87	124	123	160	159	196	195	232	231	268	267				
304	303	340	339	376	375	412	411	448	447	484	483	520	519	556	555				
592	591	628	627																
	43.2		0.		0.		0.												
	43.2		108.		0.		0.												
4	0	0	1	36	2	9	10	351	352										
	0.		0.		-38000.														
18	17	54	53	90	89	126	125	162	161	198	197	234	233	270	269				
306	305	342	341	378	377	414	413	450	449	486	485	522	521	558	557				
594	593	630	629																
	48.6		0.		0.		0.												
	48.6		108.		0.		0.												
5	1	0	1	18	2	10		352											
	0.		0.		-38000.														
18	54	90	126	162	198	234	270	306	342	378	414	450	486	522	558				
594	630																		
	54.		0.		0.		0.												
	54.		108.		0.		0.												
6	0	0	1	36	2	10	11	352	353										
	0.		0.		-38000.														
20	19	56	55	92	91	128	127	164	163	200	199	236	235	272	271				
308	307	344	343	380	379	416	415	452	451	488	487	524	523	560	559				
596	595	632	631																
	59.4		0.		0.		0.												
	59.4		108.		0.		0.												
7	0	0	1	36	2	11	12	353	354										
	0.		0.		-38000.														
22	21	58	57	94	93	130	129	166	165	202	201	238	237	274	273				
310	309	346	345	382	381	418	417	454	453	490	489	526	525	562	561				
598	597	634	633																
	64.8		0.		0.		0.												
	64.8		108.		0.		0.												
8	0	0	1	36	2	12	13	354	355										
	0.		0.		-38000.														
24	23	60	59	96	95	132	131	168	167	204	203	240	239	276	275				
312	311	348	347	384	383	420	419	456	455	492	491	528	527	564	563				

	108.		78.		- .6		0.										
17	1	0	2	18	2	286		304									
	0.		0.			-84000.											
542	544	546	548	550	552	554	556	558	560	562	564	566	568	570	572		
574	576																
	0.		90.			- .6		0.									
	108.		90.			- .6		0.									
18	1	0	2	18	2	324		342									
	0.		0.			-84000.											
614	616	618	620	622	624	626	628	630	632	634	636	638	640	642	644		
646	648																
	0.		102.			- .6		0.									
	108.		102.			- .6		0.									
1	10	0	1.0	0.0	0.0	1.0	0.0										

APPENDIX V - PARTIAL LIST OF SAMPLE OUTPUT FILE FOR NOPARC

Model One - Load 7.1

NUMBER OF NODAL POINTS	361
NUMBER OF ELEMENT TYPES	1
NUMBER OF TIME STEPS	1
ITERATION TYPE CODE	3
-1 = INITIAL STIFFNESS ONLY	
0 = CONSTANT STIFFNESS IN LOAD STEPS	
N = REFORM STIFFNESS EACH N ITERATIONS	
CODE FOR NONLINEAR GEOMETRY	1
GEOMETRIC STIFFNESS CODE	1
0 = NOT CONSIDERED	
1 = INCLUDED	
CREEP ANALYSIS CODE	1
SHRINKAGE ANALYSIS CODE	1
0 = ANALYSIS NOT REQUIRED	
1 = ANALYSIS REQUIRED	
CONVERGENCE NORM CODE	1
0 = FORCE NORM USED	
1 = DISPLACEMENT NORM USED	
2 = BOTH FORCE AND DISPL NORMS	
CONVERGENCE TOLERANCE TYPE CODE	0
0 = ABSOLUTE VALUES	
1 = FRACTIONS	
PRINCIPAL AXES DIRECTION CODE	0
0 = CALCULATED IN PROGRAM	
1 = COINCIDE WITH ELEMENT LOCAL AXES	
OUTPUT CONTROL CODES	
0 = NO	
1 = YES	
DISPL, UNBAL FORCES + STRESSES FOR EACH ITER	2
2 = ONLY AT END OF TIME STEPS	
NODAL DISPL IN LOCAL COORD SYSTEM	0
STRESS RESULTANTS	0
STRAINS	1
DISPL FOR EACH ITERATION	0
UNBAL FORCES FOR EACH ITERATION	2
CODE TO START STOP PRINTING OF PATRAN OUTPUT	0
CODE TO SUPPRESS STRAIN, STRESS, TENDON FORCE	1

TOLERANCES TO GET CONVERGENCE

FORCES .00000D+00
 MOMENTS .00000D+00
 TRANSLATIONS .50000D-02
 ROTATIONS .10000D+01

UPPER LIMITS ON UNBALANCE

FORCES 0.10D+03
 MOMENTS 0.10D+03
 TRANSLATIONS 0.10D+02
 ROTATIONS 0.10D+01

ANALYSIS REQD. AT FOLLOWING DAYS AFTER CASTING

128.

1STORAGE REQUIRED = 3250

COMPLETE NODAL POINT DATA

NODE NUMBER	BOUNDARY CONDITION CODES						NODAL POINT COORDINATES		
	X	Y	Z	XX	YY	ZZ	X	Y	Z
1	0	0	0	0	0	1	0.000D+00	0.000D+00	0.000D+00
2	0	0	0	0	0	1	6.000D+00	0.000D+00	0.000D+00
3	0	0	0	0	0	1	1.200D+01	0.000D+00	0.000D+00
.
.
.
359	0	0	0	0	0	1	9.600D+01	1.080D+02	0.000D+00
360	0	0	0	0	0	1	1.020D+02	1.080D+02	0.000D+00
361	0	0	1	0	0	1	1.080D+02	1.080D+02	0.000D+00

MATERIAL PROPERTIES - CONCRETE , REINFORCING STEEL AND PRESTRESSING STEEL

NUMBER OF CONCRETE TYPES 1
 NUMBER OF RE STEEL TYPES 1
 NUMBER OF PRE STEEL TYPES 2
 NUMBER OF CONCRETE LAYER SYSTEMS 1
 NUMBER OF RE STEEL LAYER SYSTEMS 1

CONCRETE MATERIAL PROPERTIES

TYPE NO. 1
 ELASTIC MATERIAL DATA INPUT INDICATOR 2
 CREEP DATA INPUT INDICATOR 2
 SHRINKAGE DATA INPUT INDICATOR 2

DATA INPUT INDICATORS - 1 = READ IN VALUES
 2 = USE ACI DATA

COMPRESSIVE STRENGTH AT 28 DAYS 0.48000D+04

POISSONS RATIO 0.18000D+00
 WEIGHT PER UNIT VOLUME 0.87000D-01
 CRACKED SHEAR CONSTANT 0.10000D+01

DAYS AFTER CASTING 128.
 COMPRESSIVE STRENGTH 0.54468D+04
 TENSILE STRENGTH 0.58819D+03
 MODULUS OF ELASTICITY 0.44893D+07
 STRAIN AT COMPRESSIVE STRENGTH 0.24266D-02
 ULTIMATE STRAIN IN COMPRESSION 0.97063D-02
 ULTIMATE STRAIN IN TENSION 0.00000D+00

TENSION STIFFENING MODEL - INCREASED STEEL MODULUS

ULTIMATE SHRINKAGE -0.80000D-03
 SLUMP OF MIX 0.60000D+01
 SIZE OF MEMBER 0.90000D+01
 RELATIVE HUMIDITY 0.20000D+02
 TEMPERATURE COEFFICIENT 0.55000D-05

STEEL MATERIAL PROPERTIES

TYPE	MODULUS	YIELD STRENGTH	BI-MODULUS	ULT STRAIN
1	0.29000D+08	0.60000D+05	0.10000D+07	0.10000D+01

TENSION STIFFENING MODEL - INCREASED STEEL STIFFNESS

FACTORS TO INCREASE STEEL STIFFNESS MULTIPLES OF CONCRETE CRACKING STRAIN
 4.0D+00 2.7D+00 2.0D+00 1.6D+00 1.2D+00 1.1D+00 1.5D+00 3.0D+00 5.0D+00 8.0D+00 1.2D+01 1.8D+01

PRESTRESSING STEEL PROPERTIES

BOND CODE 0 = POST-TENSIONED - UNBONDED
 1 = POST TENSIONED - BONDED
 2 = PRETENSIONED

TYPE NO	BOND CODE	AREA	WOBBLE COEF	FRICTION COEF	0.1 PERC. FY	RELAX COEF
1	0	2.150D-01	1.00000D-04	2.00000D-01	2.25000D+05	1.00D+01
2	0	6.120D-01	1.00000D-04	2.00000D-01	2.25000D+05	1.00D+01

POINTS ON THE STRESS-STRAIN CURVE - TYPE NO 1

SECTION	E-MODULUS	MAX STRESS	MAX STRAIN
1	2.94000D+07	1.70520D+05	5.80000D-03
2	1.17810D+07	2.20000D+05	1.00000D-02
3	1.00000D+06	2.40000D+05	3.00000D-02
4	3.51351D+05	2.53000D+05	6.70000D-02

POINTS ON THE STRESS-STRAIN CURVE - TYPE NO 2

SECTION	E-MODULUS	MAX STRESS	MAX STRAIN
1	2.94000D+07	1.70520D+05	5.80000D-03
2	1.17810D+07	2.20000D+05	1.00000D-02

3	1.00000D+06	2.40000D+05	3.00000D-02
4	3.51351D+05	2.53000D+05	6.70000D-02

CONCRETE LAYER SYSTEMS

TYPE NO. 1

Z-COORDINATES =

-4.50000	-3.60000	-2.70000	-1.80000	-0.90000	0.00000	0.90000	1.80000
2.70000	3.60000	4.75000					

STEEL LAYER SYSTEMS

TYPE NO. 1

NO. OF LAYERS 4

ANGLE CODE 1

LAYER	MATERIAL	Z-COORD.	SMEARED THK.	ANGLE
1	1	-3.56250D+00	7.67000D-03	0.00000D+00
2	1	-3.18750D+00	1.53300D-02	9.00000D+01
3	1	3.56250D+00	7.67000D-03	0.00000D+00
4	1	3.18750D+00	1.53300D-02	9.00000D+01

2STORAGE REQUIRED = 6490

TRIANGULAR SHELL ELEMENT DATA

NUMBER OF ELEMENTS 648

ELEMENT TYPE OPTION 0

0 = SHELL

1 = MEMBRANE (CST)

2 = PLATE BENDING (RAZZAQUE)

OPTION FOR ELEMENT NODAL LOADS 1

0 = CONSISTENT

1 = TRIBUTARY AREA

GRAVITY LOAD MULTIPLIERS

X	Y	Z
0.000	0.000	-1.000

ELEM	NODE I	NODE J	NODE K	CONCR	C	L	S	ST	L	S	LOCO	ANLO	PLAT	PX	PY	PZ	TEMP
1	21	20	1	1	1	1	1	1	0.00	0.00D+00	68.						
2	1	2	21	1	1	1	1	1	0.00	0.00D+00	68.						
3	22	21	2	1	1	1	1	1	0.00	0.00D+00	68.						
.
.
.
646	340	341	360	1	1	1	1	1	0.00	0.00D+00	68.						
647	361	360	341	1	1	1	1	1	0.00	0.00D+00	68.						
648	341	342	361	1	1	1	1	1	0.00	0.00D+00	68.						

PRESTRESSING TENDON DATA

NUMBER OF TENDONS 18
 MAX NO OF ELEMENTS CROSSED BY A TENDON 36
 MAX NO OF INFLEXION POINTS PER TENDON 2
 MAX NO OF TENDONS IN ONE ELEMENT 3

3STORAGE REQUIRED = 50816

TENDON INFORMATION

TCODE - 0 = SLAB TENDON - IN ELEMENTS
 1 = SLAB TENDON - ON NODES
 2 = PANEL TENDON - IN ELEMENTS
 JCODE - 0 = JACKING FROM ONE END OR SEQUENTIAL
 1 = JACKING SYMMETRICALLY

TENDON NO	TCODE	JCODE	TYPE	NO	EL NO	I	P	NODE A	NODE B	NODE Y	NODE Z	ANCH	SLIP	FORCE JS	FORCE JE
1	0	0	1	36	2	6	7	348	349	0.00D+00	0.00D+00	0.00D+00	0.00D+00	0.00D+00	0.00D+00
2	0	0	1	36	2	7	8	349	350	0.00D+00	0.00D+00	-3.80D+04	0.00D+00	0.00D+00	-3.80D+04
3	0	0	1	36	2	8	9	350	351	0.00D+00	0.00D+00	-3.80D+04	0.00D+00	0.00D+00	-3.80D+04
4	0	0	1	36	2	9	10	351	352	0.00D+00	0.00D+00	-3.80D+04	0.00D+00	0.00D+00	-3.80D+04
5	1	0	1	18	2	10	0	352	0	0.00D+00	0.00D+00	-3.80D+04	0.00D+00	0.00D+00	-3.80D+04
6	0	0	1	36	2	10	11	352	353	0.00D+00	0.00D+00	-3.80D+04	0.00D+00	0.00D+00	-3.80D+04
7	0	0	1	36	2	11	12	353	354	0.00D+00	0.00D+00	-3.80D+04	0.00D+00	0.00D+00	-3.80D+04
8	0	0	1	36	2	12	13	354	355	0.00D+00	0.00D+00	-3.80D+04	0.00D+00	0.00D+00	-3.80D+04
9	0	0	1	36	2	13	14	355	356	0.00D+00	0.00D+00	0.00D+00	0.00D+00	0.00D+00	0.00D+00
10	1	0	2	18	2	20	0	38	0	0.00D+00	0.00D+00	-8.40D+04	0.00D+00	0.00D+00	-8.40D+04
11	1	0	2	18	2	58	0	76	0	0.00D+00	0.00D+00	-8.40D+04	0.00D+00	0.00D+00	-8.40D+04
12	1	0	2	18	2	96	0	114	0	0.00D+00	0.00D+00	-8.40D+04	0.00D+00	0.00D+00	-8.40D+04
13	1	0	2	18	2	134	0	152	0	0.00D+00	0.00D+00	-8.40D+04	0.00D+00	0.00D+00	-8.40D+04
14	1	0	2	18	2	172	0	190	0	0.00D+00	0.00D+00	-8.40D+04	0.00D+00	0.00D+00	-8.40D+04
15	1	0	2	18	2	210	0	228	0	0.00D+00	0.00D+00	-8.40D+04	0.00D+00	0.00D+00	-8.40D+04
16	1	0	2	18	2	248	0	266	0	0.00D+00	0.00D+00	-8.40D+04	0.00D+00	0.00D+00	-8.40D+04
17	1	0	2	18	2	286	0	304	0	0.00D+00	0.00D+00	-8.40D+04	0.00D+00	0.00D+00	-8.40D+04
18	1	0	2	18	2	324	0	342	0	0.00D+00	0.00D+00	-8.40D+04	0.00D+00	0.00D+00	-8.40D+04

NUMBERS OF ELEMENTS CROSSED BY -----

TENDON NO 1
 12 11 48 47 84 83 120 119 156 155 192 191 228 227 264 263 300 299 336 335
 372 371 408 407 444 443 480 479 516 515 552 551 588 587 624 623

TENDON NO 2
 14 13 50 49 86 85 122 121 158 157 194 193 230 229 266 265 302 301 338 337
 374 373 410 409 446 445 482 481 518 517 554 553 590 589 626 625

.

TENDON NO 18

614 616 618 620 622 624 626 628 630 632 634 636 638 640 642 644 646 648

TENDON INFLEXION POINT DATA FOR -----

I P NO	X-COORD	Y-COORD	ECCENTR	CURVE TYPE	DISTANCE AA	MAX ECC
TENDON NO 1						
1	0.3240D+02	0.0000D+00	0.0000D+00	0.	0.0000D+00	0.0000D+00
2	0.3240D+02	0.1080D+03	0.0000D+00	0.	0.0000D+00	0.0000D+00
TENDON NO 2						
1	0.3780D+02	0.0000D+00	0.0000D+00	0.	0.0000D+00	0.0000D+00
2	0.3780D+02	0.1080D+03	0.0000D+00	0.	0.0000D+00	0.0000D+00
.
.
.
TENDON NO 18						
1	0.0000D+00	0.1020D+03	-0.6000D+00	0.	0.0000D+00	0.0000D+00
2	0.1080D+03	0.1020D+03	-0.6000D+00	0.	0.0000D+00	0.0000D+00

TENDON PROFILE FOR -----

POINT NO	CUM. DISTANCE	TENDON SLOPE	PRESTRESS CHANGE	TENDON FORCE	TENDON ECCEN	TENDON SLOPE	PLAN ANGLE	NODE P	NODE Q	PART OF LOAD TAKEN BY NODE P	NODE Q
TENDON NO 1 (ANCHOR SLIP DISTANCE =0.00D+00)											
1	0.00D+00	0.0000D+00	0.00D+00	0.0D+00	0.00D+00	9.0D+01	6	7	6.0D-01	4.0D-01	
2	2.40D+00	0.0000D+00	0.00D+00	0.0D+00	0.00D+00	9.0D+01	6	26	6.0D-01	4.0D-01	
3	6.00D+00	0.0000D+00	0.00D+00	0.0D+00	0.00D+00	9.0D+01	26	25	4.0D-01	6.0D-01	
4	8.40D+00	0.0000D+00	0.00D+00	0.0D+00	0.00D+00	9.0D+01	25	45	6.0D-01	4.0D-01	
5	1.20D+01	0.0000D+00	0.00D+00	0.0D+00	0.00D+00	9.0D+01	45	44	4.0D-01	6.0D-01	
6	1.44D+01	0.0000D+00	0.00D+00	0.0D+00	0.00D+00	9.0D+01	44	64	6.0D-01	4.0D-01	
7	1.80D+01	0.0000D+00	0.00D+00	0.0D+00	0.00D+00	9.0D+01	64	63	4.0D-01	6.0D-01	
8	2.04D+01	0.0000D+00	0.00D+00	0.0D+00	0.00D+00	9.0D+01	63	83	6.0D-01	4.0D-01	
9	2.40D+01	0.0000D+00	0.00D+00	0.0D+00	0.00D+00	9.0D+01	83	82	4.0D-01	6.0D-01	
10	2.64D+01	0.0000D+00	0.00D+00	0.0D+00	0.00D+00	9.0D+01	82	102	6.0D-01	4.0D-01	
11	3.00D+01	0.0000D+00	0.00D+00	0.0D+00	0.00D+00	9.0D+01	102	101	4.0D-01	6.0D-01	
12	3.24D+01	0.0000D+00	0.00D+00	0.0D+00	0.00D+00	9.0D+01	101	121	6.0D-01	4.0D-01	
13	3.60D+01	0.0000D+00	0.00D+00	0.0D+00	0.00D+00	9.0D+01	121	120	4.0D-01	6.0D-01	
14	3.84D+01	0.0000D+00	0.00D+00	0.0D+00	0.00D+00	9.0D+01	120	140	6.0D-01	4.0D-01	
15	4.20D+01	0.0000D+00	0.00D+00	0.0D+00	0.00D+00	9.0D+01	140	139	4.0D-01	6.0D-01	
16	4.44D+01	0.0000D+00	0.00D+00	0.0D+00	0.00D+00	9.0D+01	139	159	6.0D-01	4.0D-01	
17	4.80D+01	0.0000D+00	0.00D+00	0.0D+00	0.00D+00	9.0D+01	159	158	4.0D-01	6.0D-01	
18	5.04D+01	0.0000D+00	0.00D+00	0.0D+00	0.00D+00	9.0D+01	158	178	6.0D-01	4.0D-01	
19	5.40D+01	0.0000D+00	0.00D+00	0.0D+00	0.00D+00	9.0D+01	178	177	4.0D-01	6.0D-01	
20	5.64D+01	0.0000D+00	0.00D+00	0.0D+00	0.00D+00	9.0D+01	177	197	6.0D-01	4.0D-01	
21	6.00D+01	0.0000D+00	0.00D+00	0.0D+00	0.00D+00	9.0D+01	197	196	4.0D-01	6.0D-01	
22	6.24D+01	0.0000D+00	0.00D+00	0.0D+00	0.00D+00	9.0D+01	196	216	6.0D-01	4.0D-01	

23	6.60D+01	0.0000D+00	0.00D+00	0.0D+00	0.00D+00	9.0D+01	216	215	4.0D-01	6.0D-01
24	6.84D+01	0.0000D+00	0.00D+00	0.0D+00	0.00D+00	9.0D+01	215	235	6.0D-01	4.0D-01
25	7.20D+01	0.0000D+00	0.00D+00	0.0D+00	0.00D+00	9.0D+01	235	234	4.0D-01	6.0D-01
26	7.44D+01	0.0000D+00	0.00D+00	0.0D+00	0.00D+00	9.0D+01	234	254	6.0D-01	4.0D-01
27	7.80D+01	0.0000D+00	0.00D+00	0.0D+00	0.00D+00	9.0D+01	254	253	4.0D-01	6.0D-01
28	8.04D+01	0.0000D+00	0.00D+00	0.0D+00	0.00D+00	9.0D+01	253	273	6.0D-01	4.0D-01
29	8.40D+01	0.0000D+00	0.00D+00	0.0D+00	0.00D+00	9.0D+01	273	272	4.0D-01	6.0D-01
30	8.64D+01	0.0000D+00	0.00D+00	0.0D+00	0.00D+00	9.0D+01	272	292	6.0D-01	4.0D-01
31	9.00D+01	0.0000D+00	0.00D+00	0.0D+00	0.00D+00	9.0D+01	292	291	4.0D-01	6.0D-01
32	9.24D+01	0.0000D+00	0.00D+00	0.0D+00	0.00D+00	9.0D+01	291	311	6.0D-01	4.0D-01
33	9.60D+01	0.0000D+00	0.00D+00	0.0D+00	0.00D+00	9.0D+01	311	310	4.0D-01	6.0D-01
34	9.84D+01	0.0000D+00	0.00D+00	0.0D+00	0.00D+00	9.0D+01	310	330	6.0D-01	4.0D-01
35	1.02D+02	0.0000D+00	0.00D+00	0.0D+00	0.00D+00	9.0D+01	330	329	4.0D-01	6.0D-01
36	1.04D+02	0.0000D+00	0.00D+00	0.0D+00	0.00D+00	9.0D+01	329	349	6.0D-01	4.0D-01
37	1.08D+02	0.0000D+00	0.00D+00	0.0D+00	0.00D+00	9.0D+01	349	348	4.0D-01	6.0D-01

TENDON NO 2 (ANCHOR SLIP DISTANCE =0.00D+00)

1	0.00D+00	0.0000D+00	3.76D+04	0.0D+00	0.00D+00	9.0D+01	7	8	7.0D-01	3.0D-01
2	1.80D+00	0.0000D+00	3.76D+04	0.0D+00	0.00D+00	9.0D+01	7	27	7.0D-01	3.0D-01
3	6.00D+00	0.0000D+00	3.76D+04	0.0D+00	0.00D+00	9.0D+01	27	26	3.0D-01	7.0D-01
4	7.80D+00	0.0000D+00	3.76D+04	0.0D+00	0.00D+00	9.0D+01	26	46	7.0D-01	3.0D-01
5	1.20D+01	0.0000D+00	3.76D+04	0.0D+00	0.00D+00	9.0D+01	46	45	3.0D-01	7.0D-01
6	1.38D+01	0.0000D+00	3.76D+04	0.0D+00	0.00D+00	9.0D+01	45	65	7.0D-01	3.0D-01
7	1.80D+01	0.0000D+00	3.77D+04	0.0D+00	0.00D+00	9.0D+01	65	64	3.0D-01	7.0D-01
8	1.98D+01	0.0000D+00	3.77D+04	0.0D+00	0.00D+00	9.0D+01	64	84	7.0D-01	3.0D-01
9	2.40D+01	0.0000D+00	3.77D+04	0.0D+00	0.00D+00	9.0D+01	84	83	3.0D-01	7.0D-01
10	2.58D+01	0.0000D+00	3.77D+04	0.0D+00	0.00D+00	9.0D+01	83	103	7.0D-01	3.0D-01
11	3.00D+01	0.0000D+00	3.77D+04	0.0D+00	0.00D+00	9.0D+01	103	102	3.0D-01	7.0D-01
12	3.18D+01	0.0000D+00	3.77D+04	0.0D+00	0.00D+00	9.0D+01	102	122	7.0D-01	3.0D-01
13	3.60D+01	0.0000D+00	3.77D+04	0.0D+00	0.00D+00	9.0D+01	122	121	3.0D-01	7.0D-01
14	3.78D+01	0.0000D+00	3.77D+04	0.0D+00	0.00D+00	9.0D+01	121	141	7.0D-01	3.0D-01
15	4.20D+01	0.0000D+00	3.78D+04	0.0D+00	0.00D+00	9.0D+01	141	140	3.0D-01	7.0D-01
16	4.38D+01	0.0000D+00	3.78D+04	0.0D+00	0.00D+00	9.0D+01	140	160	7.0D-01	3.0D-01
17	4.80D+01	0.0000D+00	3.78D+04	0.0D+00	0.00D+00	9.0D+01	160	159	3.0D-01	7.0D-01
18	4.98D+01	0.0000D+00	3.78D+04	0.0D+00	0.00D+00	9.0D+01	159	179	7.0D-01	3.0D-01
19	5.40D+01	0.0000D+00	3.78D+04	0.0D+00	0.00D+00	9.0D+01	179	178	3.0D-01	7.0D-01
20	5.58D+01	0.0000D+00	3.78D+04	0.0D+00	0.00D+00	9.0D+01	178	198	7.0D-01	3.0D-01
21	6.00D+01	0.0000D+00	3.78D+04	0.0D+00	0.00D+00	9.0D+01	198	197	3.0D-01	7.0D-01
22	6.18D+01	0.0000D+00	3.78D+04	0.0D+00	0.00D+00	9.0D+01	197	217	7.0D-01	3.0D-01
23	6.60D+01	0.0000D+00	3.78D+04	0.0D+00	0.00D+00	9.0D+01	217	216	3.0D-01	7.0D-01
24	6.78D+01	0.0000D+00	3.78D+04	0.0D+00	0.00D+00	9.0D+01	216	236	7.0D-01	3.0D-01
25	7.20D+01	0.0000D+00	3.79D+04	0.0D+00	0.00D+00	9.0D+01	236	235	3.0D-01	7.0D-01
26	7.38D+01	0.0000D+00	3.79D+04	0.0D+00	0.00D+00	9.0D+01	235	255	7.0D-01	3.0D-01
27	7.80D+01	0.0000D+00	3.79D+04	0.0D+00	0.00D+00	9.0D+01	255	254	3.0D-01	7.0D-01
28	7.98D+01	0.0000D+00	3.79D+04	0.0D+00	0.00D+00	9.0D+01	254	274	7.0D-01	3.0D-01
29	8.40D+01	0.0000D+00	3.79D+04	0.0D+00	0.00D+00	9.0D+01	274	273	3.0D-01	7.0D-01
30	8.58D+01	0.0000D+00	3.79D+04	0.0D+00	0.00D+00	9.0D+01	273	293	7.0D-01	3.0D-01
31	9.00D+01	0.0000D+00	3.79D+04	0.0D+00	0.00D+00	9.0D+01	293	292	3.0D-01	7.0D-01
32	9.18D+01	0.0000D+00	3.79D+04	0.0D+00	0.00D+00	9.0D+01	292	312	7.0D-01	3.0D-01
33	9.60D+01	0.0000D+00	3.80D+04	0.0D+00	0.00D+00	9.0D+01	312	311	3.0D-01	7.0D-01

34	9.78D+01	0.0000D+00	3.80D+04	0.0D+00	0.00D+00	9.0D+01	311	331	7.0D-01	3.0D-01
35	1.02D+02	0.0000D+00	3.80D+04	0.0D+00	0.00D+00	9.0D+01	331	330	3.0D-01	7.0D-01
36	1.04D+02	0.0000D+00	3.80D+04	0.0D+00	0.00D+00	9.0D+01	330	350	7.0D-01	3.0D-01
37	1.08D+02	0.0000D+00	3.80D+04	0.0D+00	0.00D+00	9.0D+01	350	349	3.0D-01	7.0D-01

.
.
.

TENDON NO 18 (ANCHOR SLIP DISTANCE =0.00D+00)

1	0.00D+00	0.0000D+00	8.31D+04	-6.0D-01	0.00D+00	0.0D+00	324	0	1.0D+00	0.0D+00
2	6.00D+00	0.0000D+00	8.31D+04	-6.0D-01	0.00D+00	0.0D+00	325	0	1.0D+00	0.0D+00
3	1.20D+01	0.0000D+00	8.32D+04	-6.0D-01	0.00D+00	0.0D+00	326	0	1.0D+00	0.0D+00
4	1.80D+01	0.0000D+00	8.32D+04	-6.0D-01	0.00D+00	0.0D+00	327	0	1.0D+00	0.0D+00
5	2.40D+01	0.0000D+00	8.33D+04	-6.0D-01	0.00D+00	0.0D+00	328	0	1.0D+00	0.0D+00
6	3.00D+01	0.0000D+00	8.33D+04	-6.0D-01	0.00D+00	0.0D+00	329	0	1.0D+00	0.0D+00
7	3.60D+01	0.0000D+00	8.34D+04	-6.0D-01	0.00D+00	0.0D+00	330	0	1.0D+00	0.0D+00
8	4.20D+01	0.0000D+00	8.34D+04	-6.0D-01	0.00D+00	0.0D+00	331	0	1.0D+00	0.0D+00
9	4.80D+01	0.0000D+00	8.35D+04	-6.0D-01	0.00D+00	0.0D+00	332	0	1.0D+00	0.0D+00
10	5.40D+01	0.0000D+00	8.35D+04	-6.0D-01	0.00D+00	0.0D+00	333	0	1.0D+00	0.0D+00
11	6.00D+01	0.0000D+00	8.36D+04	-6.0D-01	0.00D+00	0.0D+00	334	0	1.0D+00	0.0D+00
12	6.60D+01	0.0000D+00	8.36D+04	-6.0D-01	0.00D+00	0.0D+00	335	0	1.0D+00	0.0D+00
13	7.20D+01	0.0000D+00	8.37D+04	-6.0D-01	0.00D+00	0.0D+00	336	0	1.0D+00	0.0D+00
14	7.80D+01	0.0000D+00	8.37D+04	-6.0D-01	0.00D+00	0.0D+00	337	0	1.0D+00	0.0D+00
15	8.40D+01	0.0000D+00	8.38D+04	-6.0D-01	0.00D+00	0.0D+00	338	0	1.0D+00	0.0D+00
16	9.00D+01	0.0000D+00	8.38D+04	-6.0D-01	0.00D+00	0.0D+00	339	0	1.0D+00	0.0D+00
17	9.60D+01	0.0000D+00	8.39D+04	-6.0D-01	0.00D+00	0.0D+00	340	0	1.0D+00	0.0D+00
18	1.02D+02	0.0000D+00	8.40D+04	-6.0D-01	0.00D+00	0.0D+00	341	0	1.0D+00	0.0D+00
19	1.08D+02	0.0000D+00	8.40D+04	-6.0D-01	0.00D+00	0.0D+00	342	0	1.0D+00	0.0D+00

4STORAGE REQUIRED = 7531

NUMBER OF EQUATIONS 1788

BANDWIDTH 105

6STORAGE REQUIRED = 47422

5STORAGE REQUIRED = 7531

LOAD CONTROL DATA

NUMBER OF LOAD STEPS	1
NUMBER OF ITERATIONS PERMITTED	10
NUMBER OF LOADED JOINTS	0
FRACTION OF DEAD LOAD	0.1000D+01
FRACTION OF SURFACE LOAD	0.0000D+00
FRACTION OF SPRING LOAD	0.0000D+00
FRACTION OF PRESTRESS LOAD	0.1000D+01
PRESTRESS - FRACTION OF EL DEF ALLOWED	0.0000D+00
NUMBER OF LOAD STEPS FOR TIME DEP. ANAL.	0

NUMBER OF ITERATIONS FOR TIME DEP. ANAL. 0
 ITERATION TYPE CODE 3
 NUMBER OF ELEMENTS WITH TEMP CHANGE 0

5STORAGE REQUIRED = 7531
 7STORAGE REQUIRED = 189907

ELEMENT AND TOTAL STIFFNESS MATRICES FORMED AND TRIANGULARIZED
 TIME STEP NO 1 LOAD STEP NO 1 ITERATION NO 1

8STORAGE REQUIRED = 191695
 8STORAGE REQUIRED = 191695
 9STORAGE REQUIRED = 52876

CONVERGENCE CRITERIA NOT SATISFIED FOR THIS ITER

8STORAGE REQUIRED = 191695
 9STORAGE REQUIRED = 52876

Model One - Load 7.1

===== RESULTS

TIME STEP NUMBER 1
 LOAD STEP NUMBER 1
 ITERATION NUMBER 2

TOTAL EXTERNAL NODAL FORCES

NODE	PX	PY	PZ	MX	MY	MZ
1	0.00000D+00	0.00000D+00	-9.65700D+00	0.00000D+00	0.00000D+00	0.00000D+00
2	0.00000D+00	0.00000D+00	-1.44855D+01	0.00000D+00	0.00000D+00	0.00000D+00
3	0.00000D+00	0.00000D+00	-1.44855D+01	0.00000D+00	0.00000D+00	0.00000D+00
.
.
.
359	0.00000D+00	0.00000D+00	-1.44855D+01	0.00000D+00	0.00000D+00	0.00000D+00
360	0.00000D+00	0.00000D+00	-1.44855D+01	0.00000D+00	0.00000D+00	0.00000D+00
361	0.00000D+00	0.00000D+00	0.00000D+00	0.00000D+00	0.00000D+00	0.00000D+00

JOINT DISPLACEMENTS

NODE	DISPL-X	DISPL-Y	DISPL-Z	ROTAT-X	ROTAT-Y	ROTAT-Z
1	9.39895D-03	-1.33884D-03	-3.14150D-02	-1.95334D-05	-9.84172D-04	0.00000D+00
2	8.88641D-03	-1.26668D-03	-2.57011D-02	5.68881D-06	-9.15181D-04	0.00000D+00
3	8.14122D-03	-8.95711D-04	-2.05269D-02	3.61895D-06	-8.09161D-04	0.00000D+00
.
.
.

359	-8.15162D-03	8.96260D-04	4.95326D-03	4.13337D-04	3.28692D-04	0.00000D+00
360	-8.90231D-03	1.26517D-03	2.71196D-03	4.48918D-04	4.19811D-04	0.00000D+00
361	-9.41769D-03	1.32834D-03	0.00000D+00	5.19754D-04	4.81070D-04	0.00000D+00

ELEMENT NUMBER 268

STRAINS AT CENTROIDS OF STEEL LAYERS

	INT PT 1			INT PT 2			INT PT 3		
NO	STRAIN-XX	STRAIN-YY	STRAIN-XY	STRAIN-XX	STRAIN-YY	STRAIN-XY	STRAIN-XX	STRAIN-YY	STRAIN-XY
1	-2.18D-04	-7.58D-05	3.78D-05	-2.20D-04	-6.98D-05	2.98D-05	-2.16D-04	-7.55D-05	1.77D-05
2	-2.09D-04	-7.58D-05	3.55D-05	-2.11D-04	-7.04D-05	2.84D-05	-2.07D-04	-7.55D-05	1.75D-05
3	-4.62D-05	-7.53D-05	-5.46D-06	-4.46D-05	-8.13D-05	2.53D-06	-4.86D-05	-7.56D-05	1.47D-05
4	-5.52D-05	-7.53D-05	-3.18D-06	-5.38D-05	-8.07D-05	3.97D-06	-5.74D-05	-7.56D-05	1.48D-05

ELEMENT NUMBER 273

STRAINS AT CENTROIDS OF STEEL LAYERS

	INT PT 1			INT PT 2			INT PT 3		
NO	STRAIN-XX	STRAIN-YY	STRAIN-XY	STRAIN-XX	STRAIN-YY	STRAIN-XY	STRAIN-XX	STRAIN-YY	STRAIN-XY
1	-1.85D-04	-8.36D-05	-1.55D-05	-1.83D-04	-8.18D-05	-1.30D-05	-1.84D-04	-8.52D-05	-1.68D-05
2	-1.80D-04	-8.28D-05	-1.47D-05	-1.77D-04	-8.11D-05	-1.25D-05	-1.78D-04	-8.43D-05	-1.58D-05
3	-7.37D-05	-6.82D-05	2.35D-07	-7.65D-05	-7.00D-05	-2.27D-06	-7.52D-05	-6.65D-05	1.46D-06
4	-7.96D-05	-6.90D-05	-5.94D-07	-8.21D-05	-7.06D-05	-2.84D-06	-8.09D-05	-6.75D-05	5.04D-07

.
.
.

ELEMENT NUMBER 642

STRAINS AT CENTROIDS OF STEEL LAYERS

	INT PT 1			INT PT 2			INT PT 3		
NO	STRAIN-XX	STRAIN-YY	STRAIN-XY	STRAIN-XX	STRAIN-YY	STRAIN-XY	STRAIN-XX	STRAIN-YY	STRAIN-XY
1	-2.25D-04	3.75D-05	-2.24D-05	-2.23D-04	3.70D-05	-2.08D-05	-2.24D-04	3.84D-05	-1.98D-05
2	-2.20D-04	3.65D-05	-1.80D-05	-2.18D-04	3.61D-05	-1.65D-05	-2.19D-04	3.73D-05	-1.57D-05
3	-1.24D-04	1.81D-05	6.15D-05	-1.26D-04	1.86D-05	5.98D-05	-1.25D-04	1.72D-05	5.89D-05
4	-1.29D-04	1.91D-05	5.70D-05	-1.31D-04	1.95D-05	5.56D-05	-1.30D-04	1.83D-05	5.48D-05

